

Alma Mater Studiorum Università di Bologna
Archivio istituzionale della ricerca

TDP-43 Modulation by Tau-Tubulin Kinase 1 Inhibitors: A New Avenue for Future Amyotrophic Lateral Sclerosis Therapy

This is the final peer-reviewed author's accepted manuscript (postprint) of the following publication:

Published Version:

Nozal, V., Martínez-González, L., Gomez-Almeria, M., Gonzalo-Consuegra, C., Santana, P., Chaikuad, A., et al. (2022). TDP-43 Modulation by Tau-Tubulin Kinase 1 Inhibitors: A New Avenue for Future Amyotrophic Lateral Sclerosis Therapy. JOURNAL OF MEDICINAL CHEMISTRY, Online ahead of print., 1-23 [10.1021/acs.jmedchem.1c01942].

Availability:

This version is available at: <https://hdl.handle.net/11585/844967> since: 2022-01-12

Published:

DOI: <http://doi.org/10.1021/acs.jmedchem.1c01942>

Terms of use:

Some rights reserved. The terms and conditions for the reuse of this version of the manuscript are specified in the publishing policy. For all terms of use and more information see the publisher's website.

This item was downloaded from IRIS Università di Bologna (<https://cris.unibo.it/>).
When citing, please refer to the published version.

(Article begins on next page)

This is the final peer-reviewed accepted manuscript of:

[TDP-43 Modulation by Tau-Tubulin Kinase 1 Inhibitors: A New Avenue for Future Amyotrophic Lateral Sclerosis Therapy.](#)

Nozal V, Martínez-González L, Gomez-Almeria M, Gonzalo-Consuegra C, Santana P, Chaikuad A, Pérez-Cuevas E, Knapp S, Lietha D, Ramírez D, Petralla S, **Monti B**, Gil C, Martín-Requero A, Palomo V, de Lago E, Martinez A.

J Med Chem. 2022 Jan 27;65(2):1585-1607.

The final published version is available online at: [doi: 10.1021/acs.jmedchem.1c01942](https://doi.org/10.1021/acs.jmedchem.1c01942)

Rights / License:

The terms and conditions for the reuse of this version of the manuscript are specified in the publishing policy. For all terms of use and more information see the publisher's website.

This item was downloaded from IRIS Università di Bologna (<https://cris.unibo.it/>)

When citing, please refer to the published version.

This document is confidential and is proprietary to the American Chemical Society and its authors. Do not copy or disclose without written permission. If you have received this item in error, notify the sender and delete all copies.

TDP-43 modulation by tau tubuline kinase 1 inhibitors: a new avenue for future amyotrophic lateral sclerosis therapy

Journal:	<i>Journal of Medicinal Chemistry</i>
Manuscript ID	jm-2021-01942r.R1
Manuscript Type:	Article
Date Submitted by the Author:	n/a
Complete List of Authors:	<p>Nozal, Vanesa; Consejo Superior de Investigaciones Cientificas, Centro de Investigaciones Biologicas; Instituto de Salud Carlos III</p> <p>Martinez-Gonzalez, Loreto; Consejo Superior de Investigaciones Cientificas, Centro de Investigaciones Biologicas; Instituto de Salud Carlos III</p> <p>Gomez-Almeria, Marta; Universidad Complutense de Madrid, Facultad de Medicina</p> <p>Gonzalo-Consuegra, Claudia; Universidad Complutense de Madrid, Facultad de Farmacia</p> <p>Santana, Paula; Universidad Autónoma de Chile - Campus El Llano Subercaseaux</p> <p>Chaikuad, Apirat; Goethe-Universitat Frankfurt am Main, Institut für Pharmazeutische Chemie</p> <p>Perez-Cuevas, Eva; Consejo Superior de Investigaciones Cientificas, Centro de Investigaciones Biologicas; Instituto de Salud Carlos III</p> <p>Knapp, Stefan; Goethe University Frankfurt, Institute of Pharmaceutical Chemistry</p> <p>Lietha, Daniel; Consejo Superior de Investigaciones Cientificas, Centro de Investigaciones Biologicas</p> <p>Ramirez, David; Universidad de Concepción Facultad de Ciencias Biológicas</p> <p>Petralla, Sabrina; Alma Mater Studiorum University of Bologna, Pharmacy and Biotechnology</p> <p>Monti, Barbara; University of Bologna, Department of Pharmacy and Biotechnology,</p> <p>Gil, Carmen; Consejo Superior de Investigaciones Cientificas, Centro de Investigaciones Biologicas</p> <p>Martin-Requero, Angeles; Consejo Superior de Investigaciones Cientificas, Centro de Investigaciones Biologicas; Instituto de Salud Carlos III</p> <p>Palomo, Valle; Consejo Superior de Investigaciones Cientificas, Centro de Investigaciones Biologicas; Instituto de Salud Carlos III</p> <p>de Lago, Eva; Universidad Complutense de Madrid, Facultad de Medicina; Instituto de Salud Carlos III</p> <p>Martínez, Ana; Consejo Superior de Investigaciones Cientificas, Centro de Investigaciones Biologicas; Instituto de Salud Carlos III</p>

1
2
3
4
5
6
7
8
9
10
11
12
13
14
15
16
17
18
19
20
21
22
23
24
25
26
27
28
29
30
31
32
33
34
35
36
37
38
39
40
41
42
43
44
45
46
47
48
49
50
51
52
53
54
55
56
57
58
59
60



REVISED 1 14.12.2021

TDP-43 modulation by tau tubulin kinase 1 inhibitors: A new avenue for future amyotrophic lateral sclerosis therapy

Vanesa Nozal,^{1,2} Loreto Martínez-González,^{1,2} Marta Gomez-Almeria,³ Claudia Gonzalo-Consuegra,³ Paula Santana,⁴ Apirat Chaikud,^{5,6} Eva Pérez-Cuevas,^{1,2} Stefan Knapp,^{5,6} Daniel Lietha,¹ David Ramírez,⁷ Sabrina Petralla,⁸ Barbara Monti,⁸ Carmen Gil,¹ Angeles Martín-Requero,^{1,2} Valle Palomo,^{1,2} Eva de Lago,^{2,3} Ana Martinez^{1,2} *

¹Centro de Investigaciones Biológicas Margarita Salas-CSIC, Ramiro de Maeztu 9, 28040 Madrid (Spain)

²Centro de Investigación Biomédica en Red de Enfermedades Neurodegenerativas (CIBERNED), Instituto de Salud Carlos III, 28031 Madrid (Spain)

³Instituto de Investigación en Neuroquímica, Dpto de Bioquímica y Biología Molecular, Facultad de Medicina, Universidad Complutense de Madrid, 28040 Madrid (Spain)

⁴Facultad de Ingeniería, Instituto de Ciencias Químicas Aplicadas, Universidad Autónoma de Chile, el Llano Subercaseaux 2801, San Miguel, Santiago (Chile)

⁵Institute for Pharmaceutical Chemistry, Goethe University Frankfurt, Max von Lauestrasse 9, 60438 Frankfurt (Germany)

⁶Structural Genomics Consortium, Buchmann Institute for Life Sciences, Goethe University Frankfurt, Max von Lauestrasse 15, 60438 Frankfurt (Germany)

⁷Departamento de Farmacología, Facultad de Ciencias Biológicas, Universidad de Concepción. Víctor Lamas 1290, PO Box 160-C, Concepción (Chile)

⁸Department of Pharmacy and Biotechnology, University of Bologna, Via Selmi 3, 40126 Bologna (Italy)

Corresponding author:

Prof. Ana Martinez

e-mail: ana.martinez@csic.es

Abstract.

Amyotrophic Lateral sclerosis (ALS) is a fatal neurodegenerative disease without any effective treatment. Protein TDP-43 is a pathological hallmark of ALS, both in sporadic and familial patients. Post-translational modifications of TDP-43 promote its aggregation in the cytoplasm. Tau tubulin kinase (TTBK1) phosphorylates TDP-43 in cellular and animal models, thus TTBK1 inhibitors emerge as a promising therapeutic strategy for ALS. The design, synthesis, biological evaluation, kinase-ligand complex structure determination and molecular modeling studies confirmed novel pyrrolopyrimidine derivatives as valuable inhibitors for further development. Moreover, compound **29** revealed good brain penetration *in vivo*, and was able to reduce TDP-43 phosphorylation not only in cell cultures but also in spinal cord of transgenic TDP-43 mice. A shift to M2 anti-inflammatory microglia was also demonstrated *in vivo*. Both of these activities led to motor neuron preservation in mice, proposing pyrrolopyrimidine **29** as a valuable lead compound for future ALS therapy.

Keywords: TTBK1 inhibitors, ALS, TDP-43 phosphorylation, drug design, kinase

1. Introduction

Amyotrophic lateral sclerosis (ALS) is a fatal and rare neurodegenerative disease that affects motoneurons causing the death of the patients within three to five years after disease onset due to cardiorespiratory failure. Despite this fatal outcome, disease-modifying agents have not been discovered and current therapeutic options only expand lifespan of the patients up to several months. Multiple pathological mechanisms have been described to occur in the affected motor neurons and among them, deposits of TAR DNA binding protein of 43 kDa (TDP-43), which are present in the 97% of the patients independently from their etiological origin, sporadic or familial.¹ TDP-43 is a highly conserved nuclear protein that plays many different roles in RNA metabolism such as transcription, splicing, transport, stability through recruitment into stress granules and microRNA biosynthesis.² In ALS and other TDP-43-pathies such as the rare Alexander's disease, the frontotemporal dementia (FTD-TDP) or the prevalent limbic-predominant age-related TDP-43 encephalopathy (LATE), nuclear localization of TDP-43 is lost.³ Elevated levels of this protein are present in the cytoplasm of ALS patients which are affected by different post-translational modifications thought to impede the return of the protein to the nucleus.⁴ Among them, aberrant hyperphosphorylation is the most relevant one in TDP-43 inclusions.⁵ Therefore, the recovery of TDP-43 homeostasis is an emergent therapeutic approach for the discovery of new drugs for ALS and other severe diseases.⁶

Only few kinases have been described to participate directly or indirectly in TDP-43 phosphorylation including glycogen synthase kinase 3 β (GSK3 β),⁷ casein kinase 1 (CK1),⁸ cell division cycle kinase 7 (CDC7),⁹ mitogen-activated protein kinases (MAPK/ERK)¹⁰ and tau tubulin kinases (TTBK1/2).¹¹ Consequently, inhibitors of these proteins have thus been considered as an emerging therapeutic option.¹² Several inhibitors of GSK3 β , CK1 and CDC7 have been described and tested in ALS models.^{13,14,15} In addition, despite the fact that inhibitors for TTBK1/2 have been recently disclosed,¹⁶ their role in TDP-43 pathologies has not been explored so far.

TTBKs belong to the superfamily of CK1 which contains two isoforms in human: TTBK1 and TTBK2 with different expression patterns throughout the body and different physiological roles. TTBK2 expression is ubiquitous and mutations in *TTBK2* gene trigger spinocerebellar ataxia 11 (SCA11) since the protein is involved in ciliogenesis. Furthermore, mice that presented truncated TTBK2 show embryonic lethality with strong neural tube and sonic hedgehog signalling defects. These data emphasize the relevance of this kinase in modulating physiological pathways and the challenge to be targeted by small molecules without toxic events.¹⁷⁻¹⁸ On the other hand, TTBK1 is specifically expressed in the central nervous system (CNS) and it is linked to neuronal pathological roles.¹⁹ TTBK1 has been described for the first time in 2006 as a kinase responsible for the phosphorylation and aggregation of tau.²⁰ Since then, multiple studies have demonstrated the role of TTBK1 in the modulation of tau linked with Alzheimer's disease (AD), as it is the main kinase responsible for the phosphorylation of Ser422, a key epitope in the early formation of fibrils prior to neurofibrillary tangles (NFT).²¹⁻²² Regarding TDP-43 pathologies, Liachko *et al.* established a relevant role of TTBK1 in TDP-43 phosphorylation, demonstrating the ability of the kinase to phosphorylate TDP-43 Ser409 and Ser410 both *in vitro* and *in vivo*. siRNA treatment in a *C. elegans* model resulted in different outcomes for the two isoforms where, only depletion of TTBK1 by siRNA resulted in significant reduced phosphorylation of TDP-43.¹¹ Thus, TTBK1 has emerged as a potential drug target for neurodegenerative diseases where the pathology of TDP-43 plays a key role and its inhibitors may play a crucial role in several unmet diseases such as ALS, LATE and FTD.²³

Only few small-molecules have been reported inhibiting TTBK1 (Figure 1). Two chemical diverse compounds, 3-[(6,7-dimethoxyquinazolin-4-yl)amino]phenol (**AZ-1**) and methyl 2-bromo-5-(7*H*-pyrrolo[2,3-*d*]pyrimidin-4-ylamino)benzoate (**AZ-2**), have been identified as binders of TTBK1 using surface plasmon resonance.²⁴ Furthermore, the crystal structure of both compounds in complex with the kinase domain of TTBK1 has been

determined, but neither the IC_{50} values for TTBK1 and TTBK2 nor their selectivity against other kinases has been described but their K_D . The heterocyclic compound 3-{5-[(4-amino-4-methylpiperidin-1-yl)methyl]pyrrolo[2,1-*f*][1,2,4]triazin-4-yl}amino)-5-bromophenol (**2KC**) with equipotent IC_{50} values for TTBK1 and TTBK2 (120 nM and 170 nM, respectively) has been also described in crystallographic complex with the kinase domain of TTBK1.²⁵ However, neither the kinase selectivity profile of these three compounds nor their behavior in cellular models have been reported. During the preparation of this manuscript, the first brain-penetrant TTBK1 inhibitors have been reported, including the azaindazole **TTBK1-IN-1**, and despite their lack of selectivity for TTBK2, target engagement and decrease of tau phosphorylation *in vivo* have been shown.^{16, 26} These data corroborate the therapeutic relevance of TTBK1 inhibitors for tauopathies and especially for Alzheimer's disease.

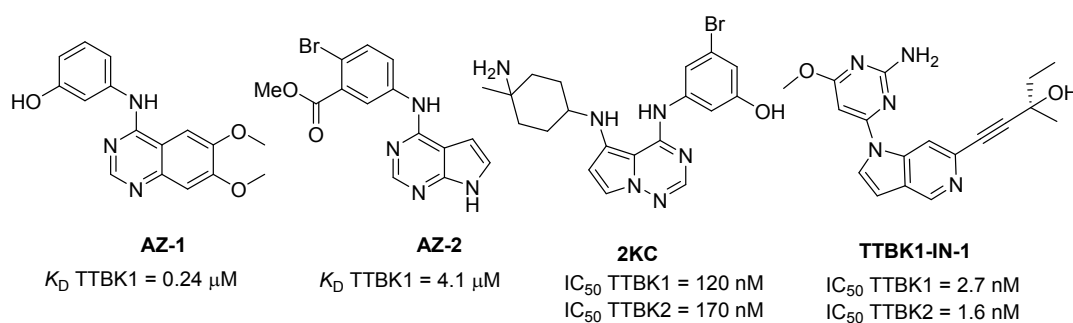


Figure 1. Chemical structure of the few described TTBK1 inhibitors and their reported K_D or IC_{50} values.

In this work we describe the design, synthesis and optimization of new TTBK1 isoform-selective inhibitors for the treatment of TDP-43 proteinopathies. A family of more than sixty heterocyclic compounds was synthesized and their inhibition of TTBK1 and TTBK2 was tested *in vitro*. Their selectivity for TTBK1 isoform, permeability through the blood-brain barrier, crystal structures of the kinase-inhibitor complexes with TTBK1 and TTBK2, molecular dynamics and cellular activity in ALS disease models are presented. Finally, one of the most promising candidates was studied in a TDP-43^{A315T}-transgenic mouse model. Our results confirmed the therapeutic potential of TTBK1 for ALS and other TDP-

43-pathies and the compounds reported represent promising lead structures for the treatment of these diseases.

2. Results and discussion

2.1 Design, synthesis and enzymatic evaluation of TTBK inhibitors

When this medicinal chemistry program began few years ago, the kinase domain of TTBK1 with ATP (PDB id. 4BTJ) together with three small molecules that bind to the adenine binding pocket (PDB id. 4BTM, 4BTK and 4NFN) have been available in the Protein Data Bank.²⁴⁻²⁵ Until very recently, the crystal structure of the catalytic domain of TTBK2 has not been determined.^{22, 27} This body of structural information was considered a starting point for our drug design program. As such, the design of new compounds aimed to study the importance of two hydrogen bonds with Gln108 and Gln110 located in the hinge region and explore the druggability of the hydrophobic pocket around Asp176 and the catalytic Lys63 (Figure 2).

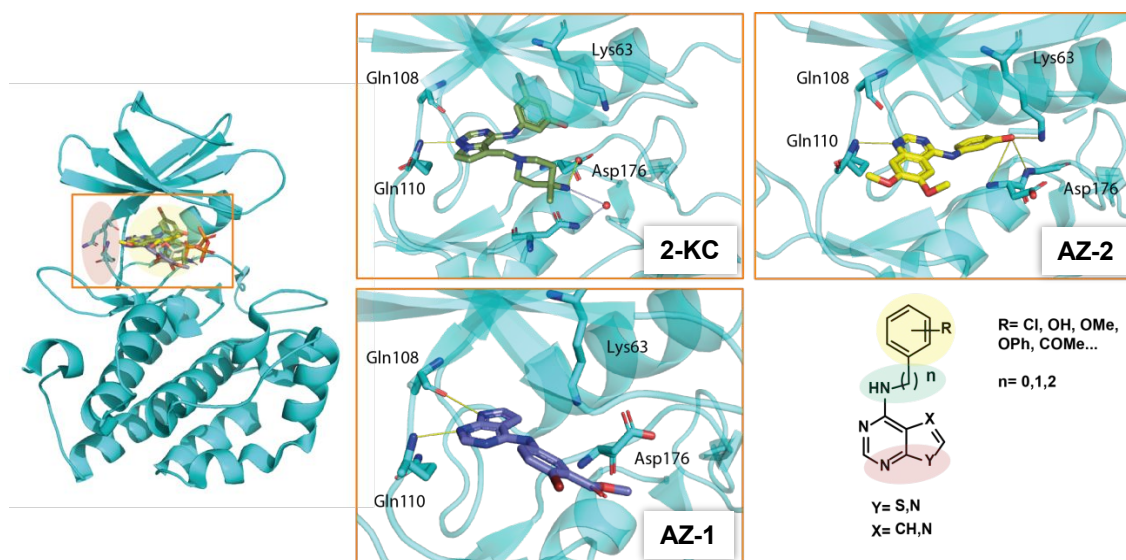
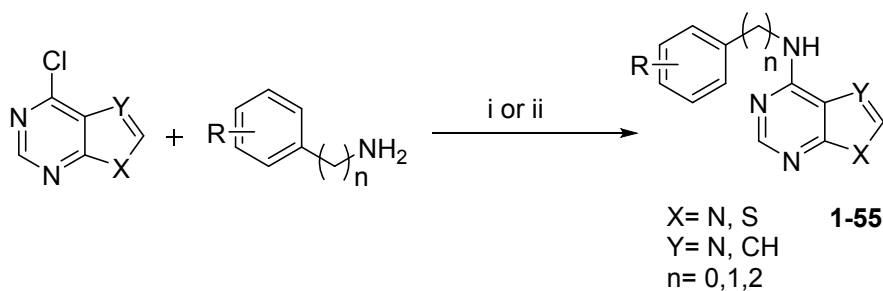


Figure 2. Crystal structure of kinase domain of TTBK1 with compounds AZ-1, AZ-2 and 2KC (PDB id. 4BTM, 4BTK and 4NFN) that lead to the design of the new TTBK1 inhibitors.

Hence, we chose a [6+5] heterocycle as a central core, which is considered as privileged scaffold for protein kinase inhibitors,²⁸ varying the nature of the five-membered ring to

explore the importance of a hydrogen-donor atom for the interaction with Gln110 and Gln108. Furthermore, we linked directly to this heterocycle, a phenyl ring with different substituents: halogens, hydrogen bond donors and acceptors, in different positions. The introduced phenyl ring would presumably establish interactions in the hydrophobic pocket (yellow area in Figure 2). The nature and length of the linker were also varied to explore this hydrophobic region (green area in Figure 2).

Synthesis of the compounds was easily realized implementing a one-step reaction with indium trichloride as a Lewis acid to facilitate the aromatic nucleophilic substitution of pi-deficient heterocycles (Scheme 1).²⁹ In cases where a halogen atom was a substituent in the phenyl ring, we discarded the use of InCl_3 to avoid the polymerisation of the building blocks. Synthesis of these compounds has been achieved using THF as reagents solvent and under microwave irradiation. A first family of 27 compounds (**1-27**) was synthesized following this methodology with moderate to very good yields (Scheme 1 and Table 1). Their chemical structure was confirmed by NMR (^1H and ^{13}C NMR) and other analytical methods as detailed in the experimental section.

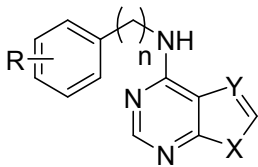


Scheme 1. i) InCl_3 (0.1 eq), MW, MeCN, 100 °C; ii) MW, THF, 100 °C (See Table 1 and 2 for R description)

The inhibitory activities of the new prepared compounds against TTBK isoforms 1 and 2 were evaluated in the Medical Research Council (MRC) Phosphorylation Unit (University of Dundee). Data are shown in Table 1. Initially the compounds were tested at a fixed concentration of 10 μM , and when the inhibition was larger than 50%, a dose-response was conducted to determine IC_{50} values. Overall, the tested compounds showed TTBK1 inhibition in the low micromolar range and were either equipotent inhibiting TTBK2 or

showed approximately up to one order of magnitude lower activity. These results and the calculation of the “TTBK1-selectivity index” defined as $IC_{50} (TTBK1)/IC_{50} (TTBK2)$, allowed us to establish a limited structure-activity relationships for improving TTBK1 activity.

Table 1. Chemical structure, yield and enzymatic inhibition of the synthesized compounds **1-27** against TTBK1 and TTBK2.



Comp.	Y	X	n	R	Yield (%)	A. TTBK1 IC ₅₀ (μM) or %inh@10 μM	B. TTBK2 IC ₅₀ (μM) or %inh@10 μM	Selectivity index A/B
1	N	NH	0	3-OH	29	9.15 μM	13%@10 μM	0.22
2	N	NH	0	4-OH	20	3%@10 μM	1%@10 μM	-
3	N	NH	0	4-morpholine	70	25%@10 μM	12%@10 μM	-
4	N	NH	0	4-Cl	75	8%@10 μM	1%@10 μM	-
5	CH	S	0	4-Cl	50	20%@10 μM	-	-
6	CH	S	0	H	70	17%@10 μM	-	-
7	CH	NH	0	3-OH	87	6.10 μM	6.70 μM	0.90
8	CH	NH	0	4-OH	38	3.00 μM	7.40 μM	0.45
9	CH	NH	0	4-morpholine	24	4.90 μM	15.70 μM	0.30
10	CH	NH	0	4-Cl	92	3.20 μM	20.30 μM	0.15
11	CH	NH	1	4-Cl	55	32%@10 μM	10%@10 μM	-
12	CH	NH	2	4-Cl	25	18.20 μM	86.00 μM	
13	CH	NH	1	4-OH	14	23%@10 μM	10%@10 μM	-
14	CH	NH	2	4-OH	23	12.80 μM	37.70 μM	0.33
15	CH	NH	0	3-Cl	49	15.20 μM	13.90 μM	1.09
16	CH	NH	0	2-Cl	69	21.80 μM	42.10 μM	0.51
17	CH	NH	0	2-OH	20	14%@10 μM	1%@10 μM	-
18	CH	NH	0	[b]cyclohexyl	23	23%@10 μM	10%@10 μM	-
19	CH	NH	0	[b]1,3dioxole	15	1.58 μM	7.58 μM	0.21
20	CH	NH	0	4-COMe	25	4.30 μM	9.30 μM	0.46
21	CH	NH	0	3-morpholine	58	4.70 μM	5.70 μM	0.82
22	CH	NH	0	H	64	0.79 μM	1.68 μM	0.47
23	CH	NH	0	4-OMe	74	0.52 μM	1.32 μM	0.39
24	CH	NH	0	4-OCF ₃	92	1.00 μM	8.80 μM	0.11
25	CH	NH	0	4-OiPr	66	1.50 μM	8.40 μM	0.17

26	CH	NH	0	4-OEt	20	2.30 μ M	13.70 μ M	0.16
27	CH	NH	0	4-OPh	53	0.39 μ M	0.85 μ M	0.45

Considering the main heterocycle, pyrrolopyrimidine-derived compounds were more active than their purine derivative analogues (see compounds **1-4** vs **7-10**) that lacked kinase inhibitory activity. The thienopyrimidine-derived compounds **5** and **6** resulted also in inactive compounds. Altogether, these results highlighted the importance of the presence of a hydrogen-donor atom at position 7 in the five membered-ring and motivated us to choose the pyrrolopyrimidine moiety as the main scaffolding heterocycle.

The length of the connector of the phenyl moiety attached at the exocyclic amino group was also crucial for TTBK1 inhibition. Thus, the presence of only one methylene group in the linker affected negatively activity and resulted in inactive compounds (**11** and **13**). Also the introduction of two methylene groups resulted in less potent compounds than those with the phenyl ring directly attached to the amine (derivatives **8** vs **14**, and **10** vs **12**).

Moreover, the position of substituents in the phenyl ring affects the potency of the inhibitors, highlighting *para*- substitution as the more favourable modification to increase TTBK1 inhibition (i.e. **10**>**15**>**16** or **8**>**7**>**17**). Interestingly, the best IC₅₀ value (in the low micromolar range) was obtained with a compound bearing a second aromatic ring in the *para*- position of the aniline ring (compound **27**).

Finally, we synthesized compound **28** (Figure 3) where the phenyl ring was replaced by the saturated cyclohexyl moiety. The lack of TTBK1 inhibition highlighted the importance of this aromatic ring for compound activity.

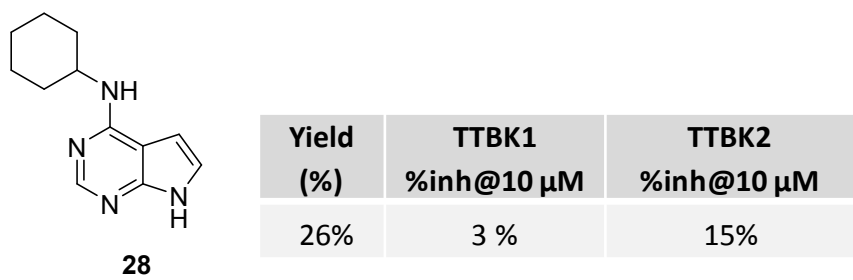
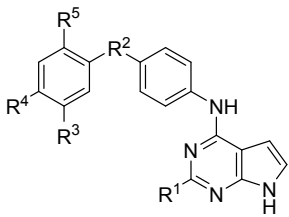


Figure 3. Chemical structure, yield and inhibition of TTBK1/2 of compound **28**.

The discovery of **27** motivated us to further exploit this family of compounds, consequently we designed a second subfamily of ligands harbouring two aromatic rings with different substituents and linkers connected to a pyrrolopyrimidine heterocycle. These compounds (**29-54**) were prepared following the reaction conditions of Scheme 1 and were enzymatically evaluated against TTBK1 and TTBK2 as outlined before. Data are summarized in Table 2, revealing more potent TTBK1 inhibitors in this second set of compounds with IC_{50} values in submicromolar range. Furthermore, and although selectivity in these two isoenzymes is a great challenge, compounds **29** and **39** may be considered as TTBK1 selective inhibitors as a factor of 10 is present in their IC_{50} values.

Table 2. Chemical structure, yield and biological inhibition of the synthesized compounds **29-55** against TTBK1 and TTBK2.



Comp.	R ¹	R ²	R ³	R ⁴	R ⁵	Yield (%)	A. TTBK1 IC ₅₀ (μM) or %inh@10 μM	B. TTBK2 IC ₅₀ (μM) or %inh@10 μM	Selectivity index A/B
29	H	-O-	H	Cl	H	62	0.24 μM	4.22 μM	0.05
30	H	-O-	H	F	H	40	0.77 μM	3.02 μM	0.25
31	H	-O-	H	CN	H	6	0.44 μM	2.14 μM	0.20
32	H	-O-	H	OMe	H	63	0.54 μM	0.97 μM	0.55
33	H	-O-	H	CF ₃	H	74	5.03 μM	5% @ 10 μM	0.06

34	H	-O-	H	Br	H	83	0.75 μ M	1.21 μ M	0.61
35	H	-O-	H	NO ₂	H	83	0.42 μ M	1.24 μ M	0.33
36	H	-O-	H	NH ₂	H	9	0.52 μ M	4.90 μ M	0.10
37	H	-O-	H	Me	H	57	1.02 μ M	8.79 μ M	0.11
38	H	-O-	Me	H	H	80	2.20 μ M	6.40 μ M	0.34
39	H	-O-	Cl	H	H	62	1.55 μ M	1%@10 μ M	0.02
40	H	-O-	CF ₃	H	H	78	5.61 μ M	1%@10 μ M	0.06
41	H	-O-	OMe	H	H	33	0.84 μ M	6.79 μ M	0.12
42	H	-O-	H	H	Cl	79	0.53 μ M	0.49 μ M	1.08
43	H	-O-	H	H	OMe	64	3.56 μ M	9.54 μ M	0.37
44	H	-O-	H	Cl	Cl	63	2.30 μ M	5.72 μ M	0.40
45	NH ₂	-O-	H	Cl	H	70	0.45 μ M	2.70 μ M	0.16
46	NH ₂	-O-	H	CF ₃	H	77	0.58 μ M	4.49 μ M	0.13
47	NH ₂	-O-	Cl	H	H	16	0.37 μ M	3.05 μ M	0.12
48	NH ₂	-O-	CF ₃	H	H	45	1.32 μ M	3.90 μ M	0.33
49	H	-S-	H	NO ₂	H	42	2.72 μ M	22.72 μ M	0.11
50	H	-S-	H	NH ₂	H	69	0.65 μ M	4.94 μ M	0.13
51	H	-OCH ₂ -	H	H	H	28	0.75 μ M	1.21 μ M	0.61
52	H	-CO-	H	H	H	97	1.71 μ M	11.92 μ M	0.14
53	H	-CO-	H	F	H	19	1.50 μ M	5.4 μ M	0.27
54	H	-CO-	Cl	Cl	H	35	9%@10 μ M	-	-

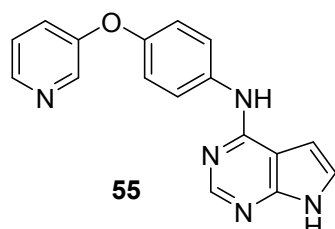
In the light of these biological activities, some conclusions may be drawn: the preferred connector between the two phenyl rings is the ether one (-O-), followed by the thioether (-S-) and the carbonyl moiety (-CO-). In that sense, compounds **52** and **53**, with a carbonyl group linking the phenyl groups, resulted in less potency than their counterparts **27** and **30**, respectively, which have an ether group as linker. At the same time derivatives **35** and **36** were slightly more or equipotent than their thio- analogs **49** and **50**, respectively.

Introduction of an amino group in position 2 of the pyrrolopyrimidine core lead to potent compounds against TTBK1 but less selective (**29**, **33**, **39**, **40** vs **45-48** respectively).

Regarding the substitution in the second phenyl ring, a combination of steric and electrostatic factors may influence the inhibition of the two isoforms. Thus, the most selective TTBK1 inhibitors were derivatives **29**, **33**, **39** and, **40** with chlorine or

trifluoromethyl- substituents in positions *meta*- and *para*-, with compound **29** being identified as the most potent and selective TTBK1 inhibitor.

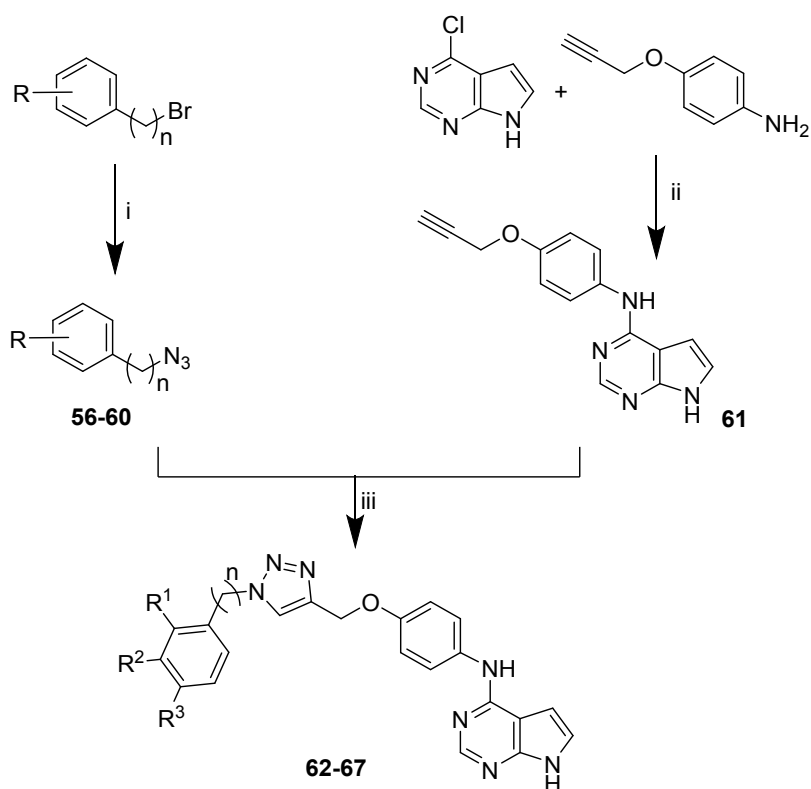
Finally, introduction of the pi-deficient pyridine heterocycle (compound **55**, Figure 4) trends to increase selectivity in comparison to its analog **27**.



Yield (%)	TTBK1 IC ₅₀ (μM)	TTBK2 IC ₅₀ (μM)	Selectivity index
35	0.75	6.05	0.12

Figure 4. Chemical structure, yield and inhibition of TTBK1/2 of compound **55**.

A third subfamily of compounds were synthesized exploring modifications in the second aromatic group. In this series, we prepared a set of different organic azides (**56-60**) and the alkyne **61** and, using the cooper(I)-catalyzed alkyne-azide cycloaddition (CuAAC) methodology,³⁰ new ligands bearing a triazole ring (**62-67**) were synthesized with good yields (Scheme 2, Table 3).



Scheme 2. i) NaN_3 (1.5 eq.), DMF, r.t.; ii) InCl_3 (0.1 eq.), MW, MeCN, 100 °C; iii) CuSO_4 (0.1 eq.), tris(benzyltriazolylmethyl)amine (0.1 eq.), sodium ascorbate (0.2 eq.), DMF, r.t.

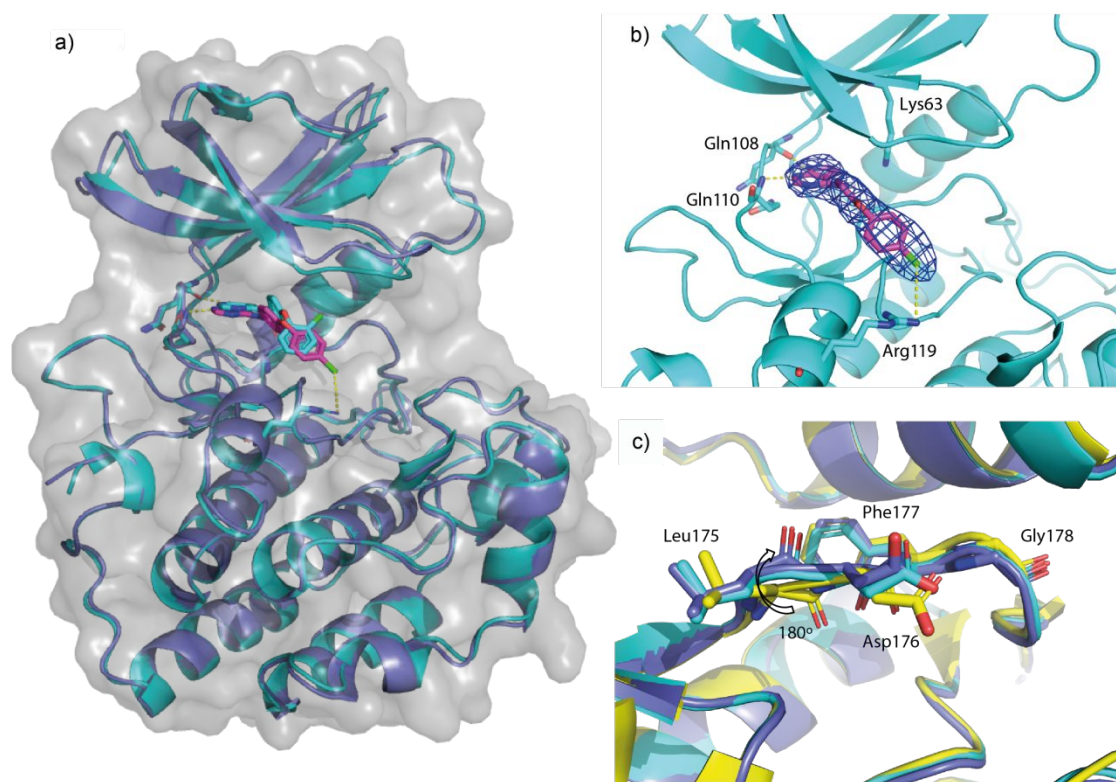
Data on this series are summarized in Table 3. In general, compounds containing a triazole ring resulted in moderate selective TTBK1 inhibitors.

Table 3. Chemical structure, yield and biological inhibition of the synthesized compounds **62-67** against TTBK1 and TTBK2.

Comp.	n	R ¹	R ²	R ³	Yield (%)	A. TTBK1 IC ₅₀ (μM) or %inh@10 μM	B. TTBK2 IC ₅₀ (μM) or %inh@10 μM	Selectivity index A/B
62	0	H	H	H	34	29%@10 μM	1%@10 μM	-
63	1	H	H	Cl	64	0.61 μM	2.87 μM	0.21
64	1	Cl	H	H	31	0.36 μM	2.75 μM	0.13
65	1	H	Cl	H	33	0.48 μM	2.03 μM	0.24
66	2	H	H	H	64	0.39 μM	2.61 μM	0.15
67	1	H	H	CH ₃	73	0.99 μM	1.75 μM	0.57

2.2. Elucidation of ligand-kinase binding modes

Since the homology of kinase domains of the two isoforms is high with 88% identity and 96% similarity, we aimed to crystallize different protein-ligand complexes and computationally study the binding mode of the compounds with the different kinases in order to explain the experimentally-observed selectivity of the synthesized inhibitors. For this purpose, we crystallized the kinase domain of TTBK1 (13-313) and TTBK2 (6-299) (see experimental section for detailed information) with different compounds, including **23**, **27**, **29**, **32** and **42** (Figure S1, Figure 5, Table S1). Among these the derivatives **29** and **42** (Figure 5) were of particular interest as they had different affinities for TTBK1 and TTBK2.



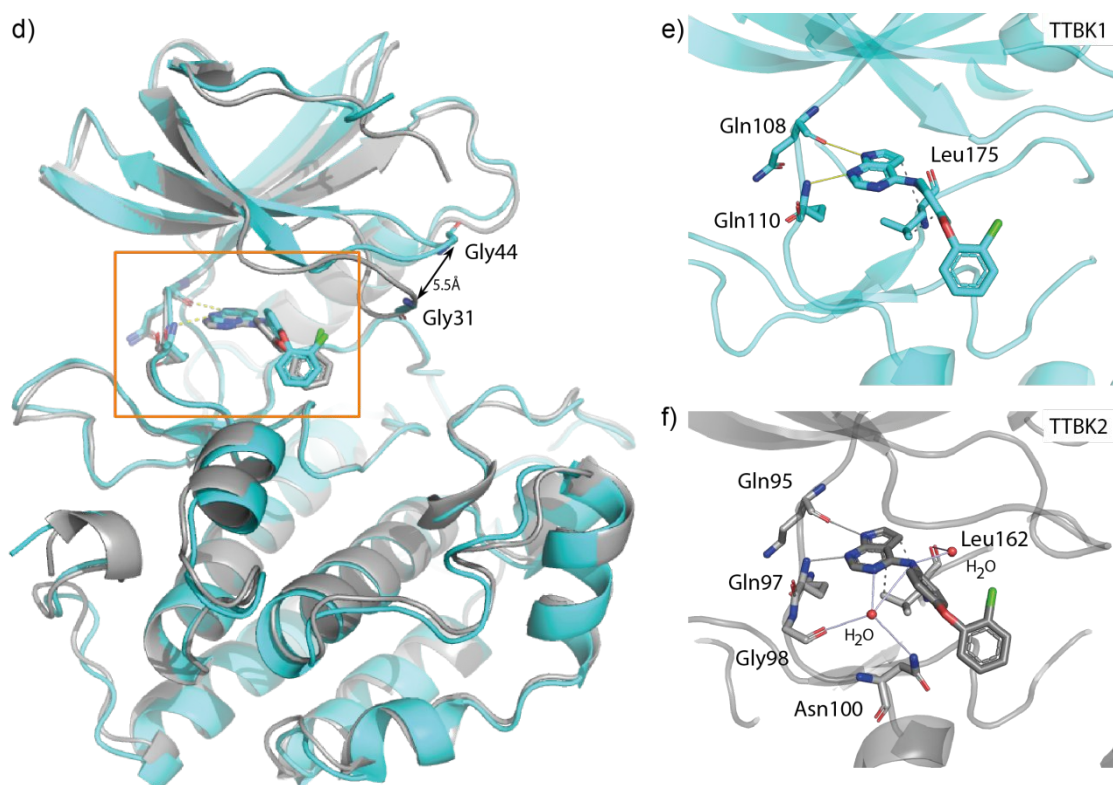


Figure 5. Crystal structures determined by X-ray diffraction of the synthesized compounds with the kinase domain of TTBK: a) Structure of TTBK1 in complex with **29** (in cyan) and **42** (in purple); b) Density map and binding mode of **29** with TTBK1 showing interaction with Arg119; c) TTBK1 bound to pyrrolopyrimidines displays a flipped conformation of the backbone carbonyl in Leu175 previous to the DFG (Asp176 – Phe177 – Gly178) motif, compared to ATP bound TTBK1 (yellow PDB id. 4BTJ); d) Superposition of the structures of TTBK1 (cyan) and TTBK2 (grey) bound to compound **42**; e) f) detail of the interactions of compound **42** with TTBK1 and TTBK2 (respectively).

The structures confirmed that all compounds bound to the ATP pocket forming canonical hydrogen bonds with the hinge region residues Gln108 and Gln110 of TTBK1 and residues Gln95 and Gln97 of TTBK2. Only in TTBK2 a water-mediated hydrogen bond was formed between the nitrogen in the position 1 of the pyrrolopyrimidine ring, Gly98 and Asn100. Crystal structures of TTBK1 with derivatives **29** and **42** were highly similar (Figure 5a, 5c). However, despite the initial hypothesis of interaction with the catalytic lysine located in the hydrophobic pocket, all the compounds displayed their aromatic substituents towards the front pocket. In this binding mode, the interaction between compound **29** and Arg119 in TTBK1, that was not observed in the complex with **42**, seemed to be important for the potency of the compound for TTBK1.

Comparison of the structures of compound **42** bound to both TTBK isoenzymes revealed some interesting points. first, the glycine-rich loop was displaced up to 5.5 Å between the two isoforms which may also be attributed to crystal packing (Figure 5d). In addition, this inhibitor formed two water-mediated hydrogen bonds with TTBK2 that were absent for TTBK1 (Figure 5e, 5f).

A conformational change N-terminal to the DFG motif appeared to be induced by these pyrrolopyrimidines, resulting in flipping of the backbone carbonyl of Leu175 compared to the canonical TTBK1 conformation (Figure 5c). This flip is also observed for TTBK2 allowing the establishment of a water-mediated-hydrogen bond between Leu162 and the exocyclic amine group (Figure 5f). The DFG region has been previously demonstrated to exhibit high plasticity allowing alternative DFG conformations in various kinases.³¹ In addition, such conformational flip allowed Leu175 N-terminal to the DFG motif to form hydrophobic stacking with the pyrrolopyrimidine moiety, a binding mode unique to a subset of kinases that enables an accommodation of kinase inhibitors in the back pocket and may increase inhibitor potency and selectivity.³²

Since all the residues within (5 Å radius to the ligand are 100% conserved in both isoforms, the observed compound selectivity likely resulted from different dynamic behavior. We therefore performed a molecular mechanic experiment to explain the SAR studies and the selectivity of the compounds towards both isoforms. We use the crystal structures that we obtained as a starting point of these studies. Docking using Glide software and subsequent MM-GBSA calculations were performed to obtain a correlation between calculated free binding energies (ΔG_{bind}) and the observed IC_{50} values of the active compounds (**1-55**) against TTBK1. A good correlation coefficient was obtained ($R^2 = 0.7733$), which allowed us to validate these calculations and study the relationship between the predicted free energy values and the experimentally biological activity data (Figure S2).

Taking into an account the particular contribution of the energetic terms to the total ΔG_{bind} , we observed that Coulomb interactions are important to the increased potency of the compounds and penalize those with lower IC_{50} values together with van der Waals energies which were also rather low for those compounds with pIC_{50} s below 5.5 (Table S2). These energetic contributions are also important when comparing the free binding energies for selective and non-selective inhibitors, were differences up to 11 Kcal/mol are found in the solvation contribution term (Table S3).

In order to study the dynamics of the binding with the different isoforms, we next performed molecular dynamic (MD) studies with selected compounds. Thus, we studied complexes of both isoforms with inhibitors **29**, **39** and **42** which present different patterns of substitution in the second aromatic ring and different selectivity profiles. Crystal structures were used as starting point for complex **29**-TTBK1, **42**-TTBK1 and **42**-TTBK2. For those cases where the experimental structure was not available, the binding pose obtained by docking studies was the initial point for the MDs.

It was noticed that all the compounds are stable in the catalytic cavity except for compound **39** (Figure 6a). The root-mean-square deviation of atomic positions (RMSD) value for this compound along the MD study doubles the rest of the compounds which might be directly related to its low potency for TTBK2 inhibition. It was observed that the stability of the modification in compounds within both isoforms was very similar, mainly of pyrrolopyrimidine and phenyl-ether moieties as it can be deduced from the root-mean-square fluctuations of the atoms (RMSF) calculations (Figure 6b). The main difference was the second ring (chloro-phenyl moiety), which was much more mobile in compound **39** (RMSF up to 4.5 Å) reinforcing the hypothesis of weak interaction for this molecule. This compound was only able to establish short hydrophobic interactions; hence the second aromatic ring was not fixed within the front pocket (Figure S3). The potent compounds **29** and **42** remained tightly positioned towards the Arg119, although only compound **29** was able to establish halogen bonds with this residue.

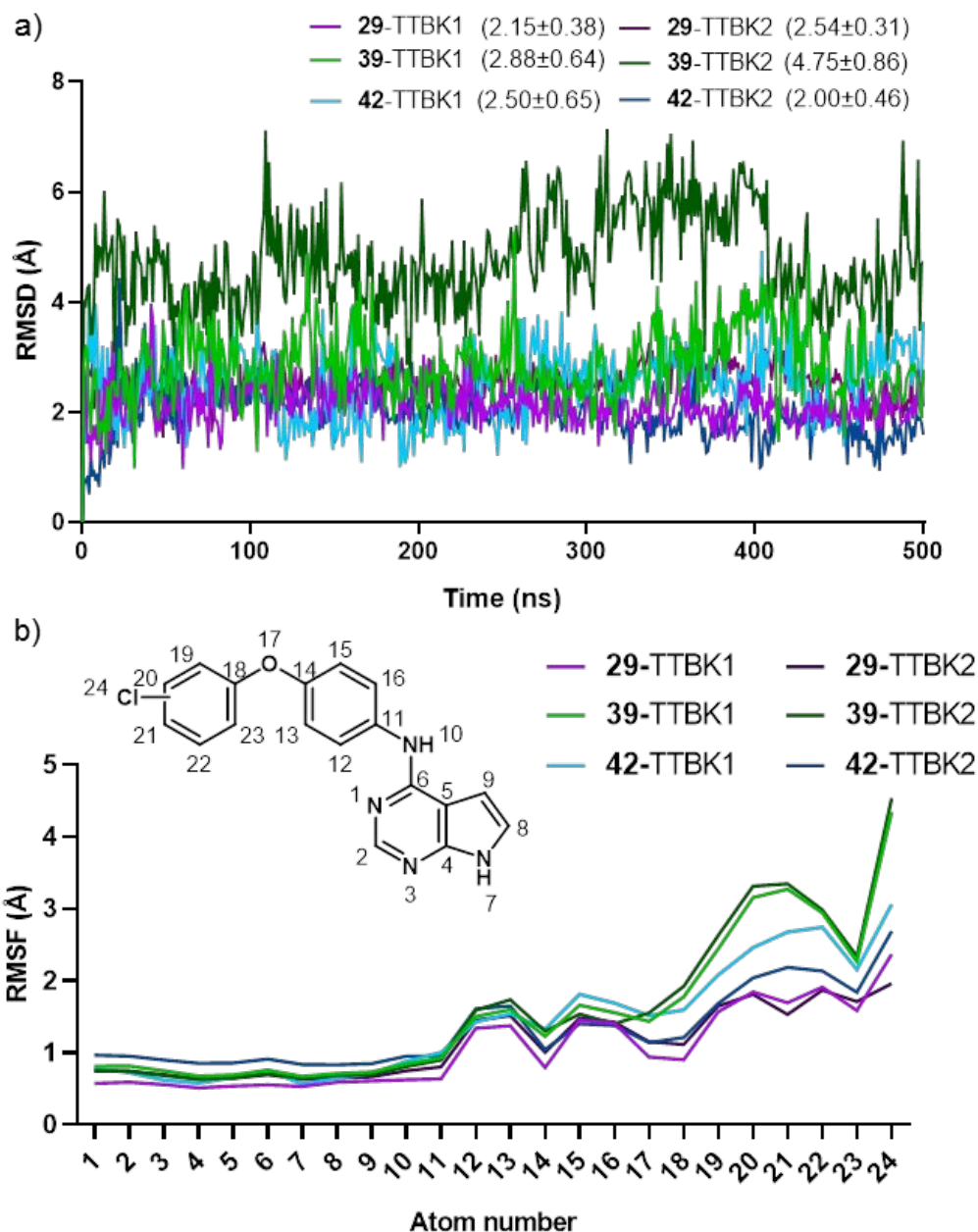


Figure 6. a) RMSD of the MD trajectories for compounds **29**, **39** and **42** in TTBK1 and TTBK2. b) RMSF of the atoms within compound **29**, **39** and **42** during the molecular dynamic studies.

To study carefully how the conformation of the compounds changed during the MD, we clustered every trajectory based on the position of the ligand atoms in each simulation. This allowed us to confirm how stable both compounds **29** and **42** are when interacting with TTBK1 and/or TTBK2. On the contrary, compound **39** presented different conformations where the chlorophenyl moiety flipped, placing the second aromatic ring in different dispositions within the hydrophobic pocket impeding a stable conformation of

the ring and reinforcing the idea of weak interactions related to low potency of the compound (Figure 7).

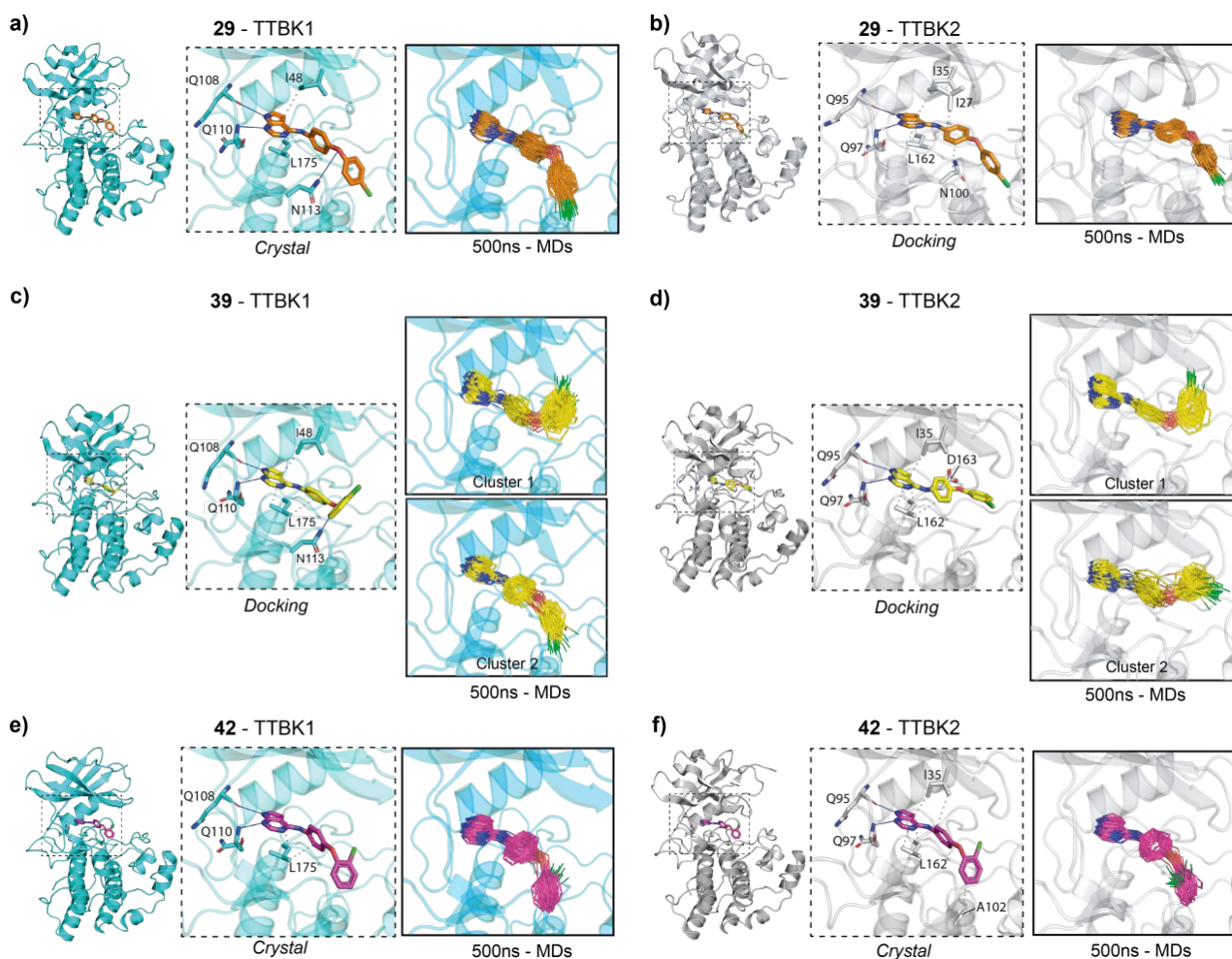


Figure 7. MD simulations of the compounds **29** (a-b), **39** (c-d) and **42** (e-f) with the kinase domain of TTBK1 (a, c, e) and TTBK2 (b, d, f). Middle panel shows a zoom with the interactions identified for each compound. Hydrogen bonds and hydrophobic interactions are shown as blue and gray lines. Right panel shows most populated clusters obtained from the analysis of the 500 ns MD simulation.

Finally, since these TTBK1 inhibitors were ATP-competitive, we performed a kinase profiling for a set of selected kinases from different families of the human kinome. We screened the TTBK1 inhibitor **29** at a fixed concentration of 10 μ M against more than twenty different kinases calculating the selectivity score (Figure 8). In this case, the S_{35} value, which determines the fraction of kinases that are targeted by the compound **29** beyond 35% of residual activity,³³ was 0.04, showing selectivity over similar kinases.

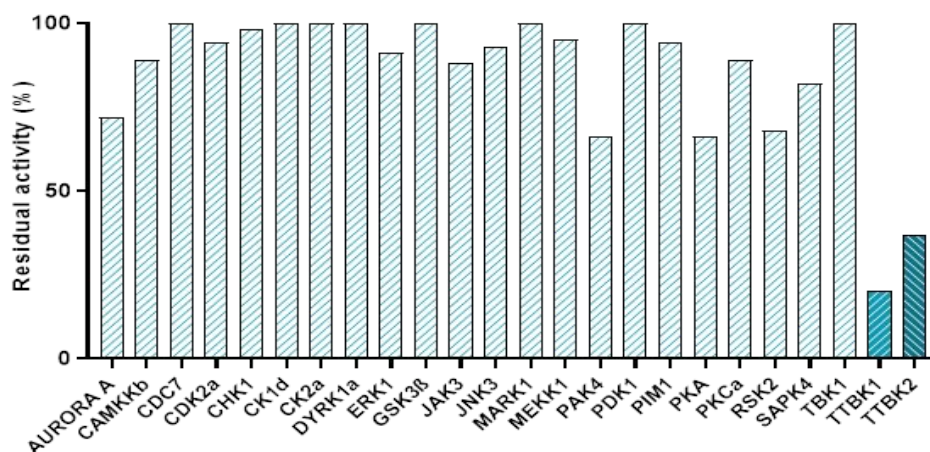
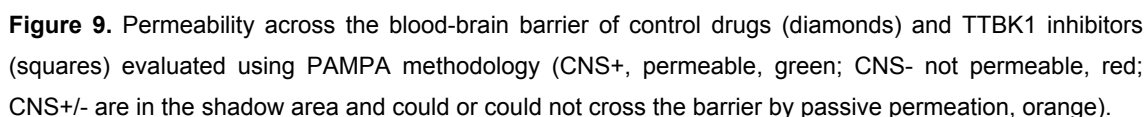


Figure 8. Kinase profiling of TTBK1 inhibitor derivative **29**.

2.3 Blood-Brain Barrier permeability studies

An important property for a drug candidate or chemical probe that is intended to be used for exploring a central nervous system disease, such as ALS, is penetration through the blood-brain barrier (BBB). Using a parallel artificial membrane permeability assay (PAMPA), we determined the predicted brain permeability for all the compounds with adequate potency (TTBK1 IC_{50} below 2.5 μM). Methodology and individual data are found in the experimental section and supplementary material (Table S4, Figure S4), while Figure 9 depicted the results of this assay. Compounds **31** and **36** were not soluble under the experimental conditions and could not be tested. In general, all the compounds are predicted as permeable over the BBB, with the exception of four compounds (**23**, **24**, **26** and **55**) and those ones containing the triazole ring (**63-67**). All these compounds were discarded from subsequent cellular assays.



The potential decrease of TDP-43 phosphorylation in cellular models was studied only for those brain-permeable TTBK1 inhibitors with a selectivity index regarding this isoform (below 0.25). These criteria resulted in 14 compounds that were tested initially in a human neuroblastoma cell-based model of induced TDP-43 phosphorylation. The SH-SY5Y cell line was exposed to the toxic insult of ethacrynic acid (EA) for 24 h which increased phosphorylated TDP-43 levels by glutathione depletion causing cell death.³⁴ In that model, the neuroprotective activity against EA was determined pre-treating the cells with the TTBK1 inhibitors 1 h prior the addition of EA (40 μ M). An initial cell viability study at different compound concentrations (5 and 10 μ M, Figure S5) ruled out derivative **30** and **31** from the assay and fixed the study dose at 5 μ M. As controls, we used a previously reported TTBK1 inhibitor, methyl 2-bromo-5-(7*H*-pyrrolo[2,3-*d*]pyrimidin-4-ylamino) benzoate (**A22**) re-synthesized in our laboratory, and the known GSK3 inhibitor, tideglusib, that showed good results in this cell-based ALS model.¹³ As observed in Figure 10, three compounds (**29**, **37** and **39**) were neuroprotective in this model as they

rescued the cells from the death induced by EA (Figure 10a). The next step was to evaluate if this neuroprotective activity was due to direct modulation of TDP-43. Using Western-blot analysis, we showed that the new synthesized compounds were able to reduce TDP-43 hyperphosphorylation to control levels at the important epitopes Ser409 and Ser410, however the reported TTBK1 inhibitor **AZ2** did not produce such an effect significantly (Figure 10b). We then determined the IC₅₀ of **AZ2**, following the same procedure previously described for the pyrrolopyrimidine compounds, determining values much higher and less selective (TTBK1 IC₅₀ 2.2 μM; TTBK2 IC₅₀ 4.2 μM) than those measured on our derivatives, which may explain the lack of reduction in TDP-43 phosphorylation.

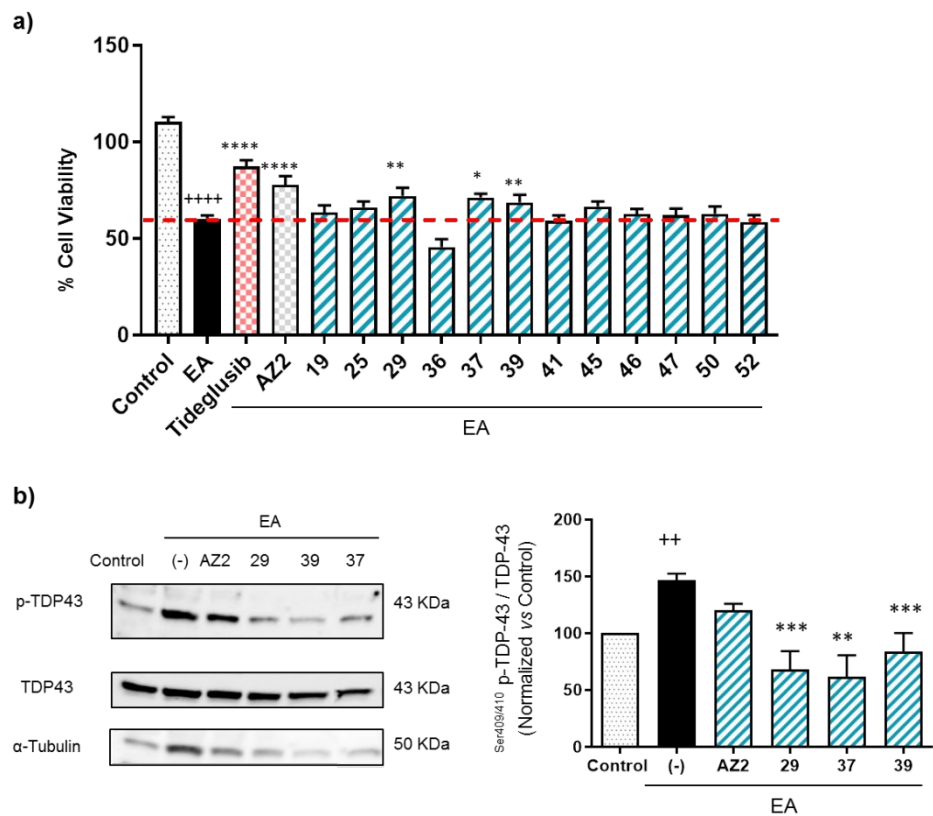


Figure 10. Neuroprotective effect of TTBK1 inhibitors in ethacrynic acid treated SH-SY5Y neuroblastoma cells. a) Cell viability measured by MTT assay after being exposed to EA for 24 h in the presence or absence of drugs treatment (5 μM). b) Representative immunoblot showing TDP-43 phosphorylation levels of SH-SY5Y cells treated with compounds **AZ2**, **29**, **37** and **39** (5 μM). Each data point represents the mean ± SEM of three replications in four different experiments (*p < 0.05; **p < 0.01, ***p < 0.001, ****p < 0.0001 significantly different from EA-treated cells; ++p < 0.01, +++p < 0.0001 significantly different from control cells).

We have previously shown that decreased TDP-43 phosphorylation by other kinase inhibitors such as CDC7, CK1 or GSK3 inhibitors restore the physiological nuclear localization of TDP-43.¹³⁻¹⁵ To test if the decrease of TDP-43 phosphorylation using TTBK1 inhibitors also reestablishes the homeostasis of TDP-43 raising its nuclear localization, we carried out immunofluorescence analyses in EA-treated SH-SY5Y cells. Our findings demonstrated that compound **29** reduced the cytosolic accumulation of TDP-43 in EA-treated cells, restoring its nuclear localization and therefore the homeostasis of the main pathological hallmark of ALS (Figure 11).

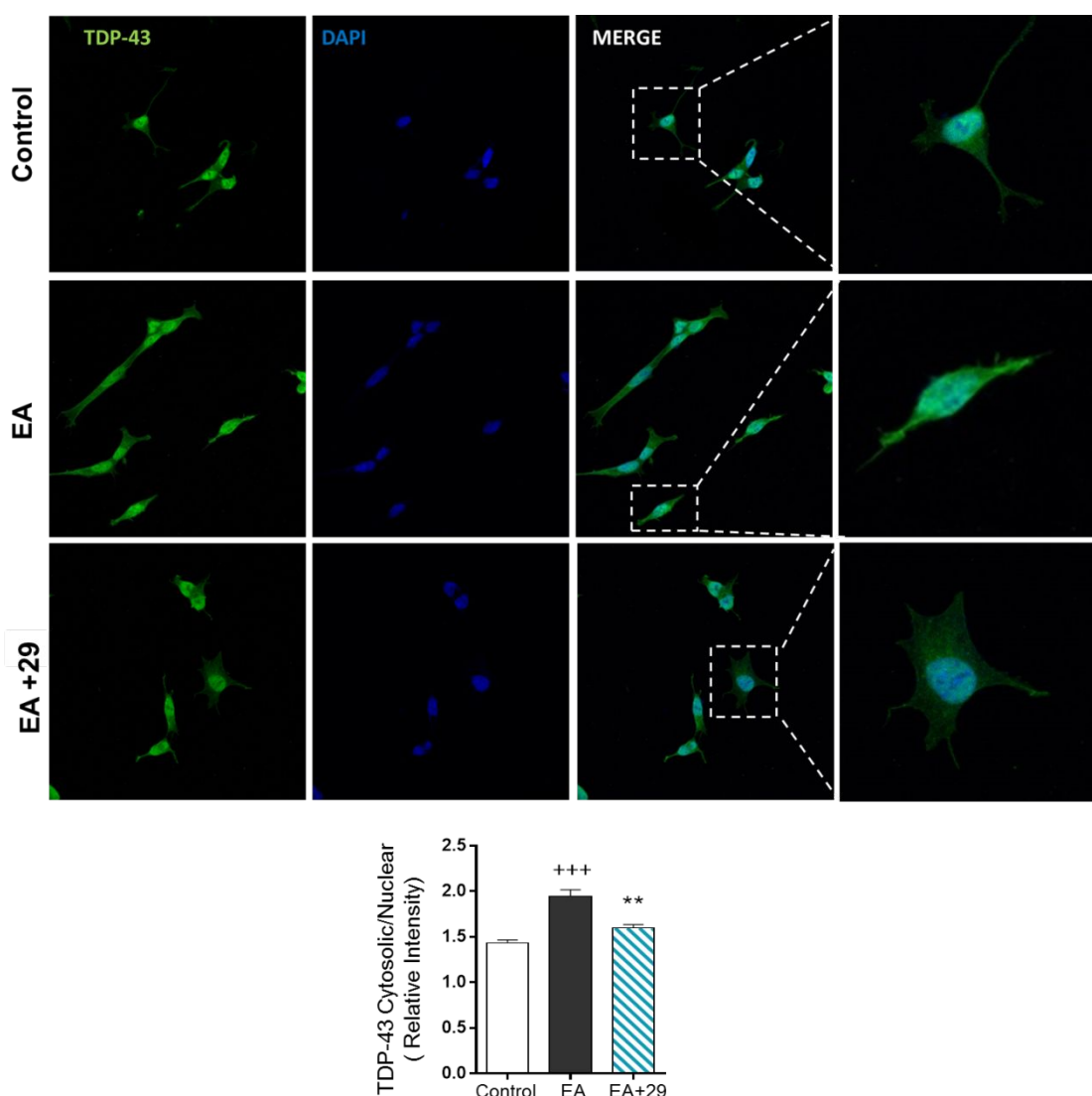


Figure 11. Immunofluorescence analysis of the subcellular localization of TDP-43 in SH-SY5Y cells. Cells were pre-treated with compound **29** (5 μ M) and exposed to EA (40 μ M) for 24 hours. TDP-43 localization was assessed by Confocal Laser Scanning Microscopy. Scale bar: 10 μ m and 20 μ m. Quantification of cytosolic TDP-43 was analysed in at least 50 different cells from 3 separate wells (n=3). Data represent the

mean \pm SEM (magnification 63x). (** $p < 0.005$ significantly different from SH-SY5Y EA-treated cells, +++ $p < 0.001$ significantly different from control).

TTBK1 is an enzyme that has been linked to Alzheimer's disease and hyperphosphorylation of tau, especially at epitope Ser422, important for the pretangle formation. Recently, some non-specific TTBK1/2 inhibitors have shown the ability to reduce tau phosphorylation both in cellular models and *in vivo*.¹⁶ For this reason, the new synthesized TTBK1 ligands were evaluated in a model of tau hyperphosphorylation induced by okadaic acid (OA).³⁵ In that assay, the compounds were able to rescue the SH-SY5Y cells from death induced by OA at two different compound concentrations of 1 and 5 μ M (Figure S6), confirming that our TTBK1 inhibitors in addition to TDP-43, also reduce the toxicity exerted by tau phosphorylation expanding their therapeutic potential for different tauopathies.

2.5 Immunomodulatory effect of TTBK1 inhibition

Chronic inflammation is another common feature observed in ALS, indicating an essential role of microglia in disease development and progression.³⁶ Thus, we decided to study the potential role of TTBK1 inhibition in microglia and its immunomodulatory effects. Therefore, we evaluated the effect of compound **29** on the expression of inducible nitric oxide synthase (iNOS) and of the triggering receptor expressed on myeloid cells 2 (TREM2) in primary cultures of rat microglia after 24 h exposure to the widely used pro-inflammatory stimulus lipopolysaccharide (LPS, 100 ng/mL). iNOS is widely considered a marker of M1 neurotoxic microglia, while TREM2 a marker of M2 neuroprotective microglia. When cells were stimulated with LPS, we observed the expected iNOS induction, which was reduced by the treatment with compound **29**, along with an increase in TREM2 expression (Figure 12) suggesting an immunomodulatory effect of the TTBK1 inhibitor **29**. Compounds that induce microglia switch from

inflammatory M1-type to anti-inflammatory M2-type have been proposed to attenuate neuro-inflammation and bolster neuronal protection and recovery.³⁷

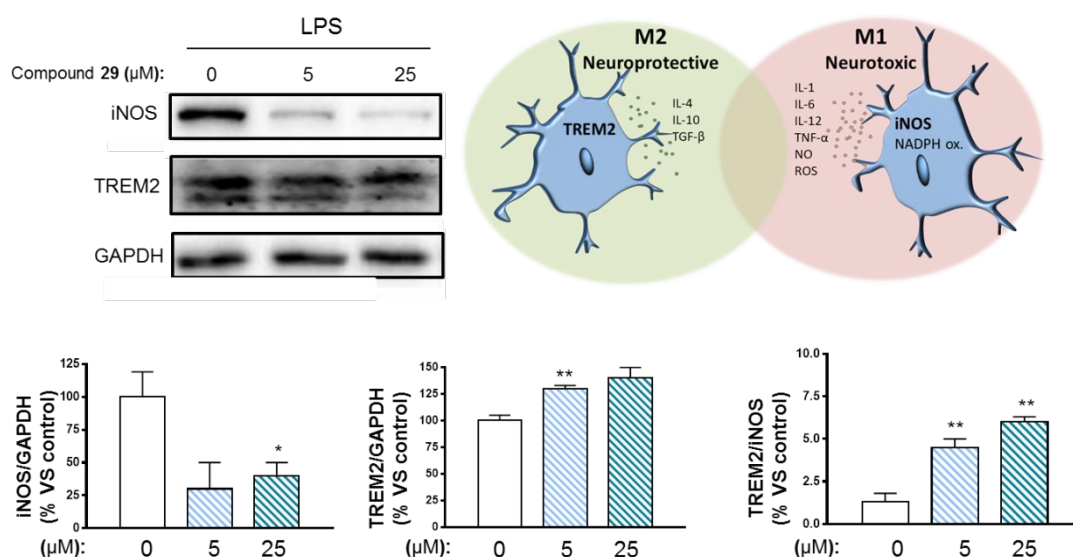


Figure 12. Immunomodulatory effect of compound **29** in primary rat microglial cells. Representative immunoblot showing iNOS and TREM2 protein expression in LPS-treated (100 ng/mL) microglia cells in the presence or absence of compound **29** at increasing concentrations (5 and 25 μ M). GAPDH was used for endogenous normalization. Densitometric data represent the mean \pm SEM of 3 independent experiments. (*p < 0.05; **p < 0.01 significantly different from LPS-treated control cells).

2.6 *In vivo* TDP-43 modulation by a TTBK1 inhibitor

Based in the promising results showed by the new TTBK1 inhibitors in cellular models, we explore the effects of compound **29** in the TDP-43 (A315T) transgenic mouse model, one of the first experimental models of ALS based on mutations in TDP-43 protein.³⁸

Firstly, we investigated the plasma pharmacokinetics and brain distribution of compound **29** in BALB/c wild type mice following a single intraperitoneal dose administration at 5 mg/kg or oral administration at 10 mg/kg. Results are collected in Table 4 and show that compound **29** exhibits the greatest plasma concentration between 1 to 2 h, suggesting prolonged absorption and a high brain penetration in mice by the two routes of administration. Based on these results, we decided to use the intraperitoneal dose of 5 mg/kg in the efficacy study.

Table 4. Pharmacokinetic parameters of compound **29** in plasma and brain following a single intraperitoneal (Dose: 5 mg/kg) and oral (Dose: 10 mg/kg) administration in male BALB/c mice.

Route	Dose	Matrix	T _{max} (h)	C _{max} (ng.mL ⁻¹)	AUC _{last} (h.ng.mL ⁻¹)	T _{1/2} (h)	Brain-Kp (AUClast)
i.p	5 mg/kg	Plasma	1.00	1429.08	5958.82	3.75	2.63
		Brain ^a	1.00	4174.12	15652.49	3.46	
p.o	10 mg/kg	Plasma	2.00	2265.04	18406.33	3.30	2.67
		Brain ^a	2.00	4923.89	49172.57	3.40	

^aBrain concentration and AUC. expressed as ng.g⁻¹ and h.ng.g⁻¹ respectively.

To this end, TDP-43 (A315T) transgenic mice and wild-type animals were daily treated with the TTBK1 inhibitor **29** or vehicle from the age of 65 days up to 95 days. The main goal of our study was to confirm the previously observed TDP-43 phosphorylation decrease and immunomodulatory effect of **29** together with the potential effect of these two relevant biological events in motor neuron preservation in the spinal cord.

We first analysed whether chronic treatment with our TTBK1 inhibitor could prevent enhanced TDP-43 phosphorylation *in vivo*. Immunoblot analyses shown in Figure 13 revealed an increase in TDP-43 phosphorylation levels at the lumbar region in the spinal cord of transgenic mice compared to wild-type animals, which was statistically significantly reduced with compound **29** treatment (Figure 13a). No apparent effect on total levels of TDP-43 was appreciated between transgenic groups (Figure 13b).

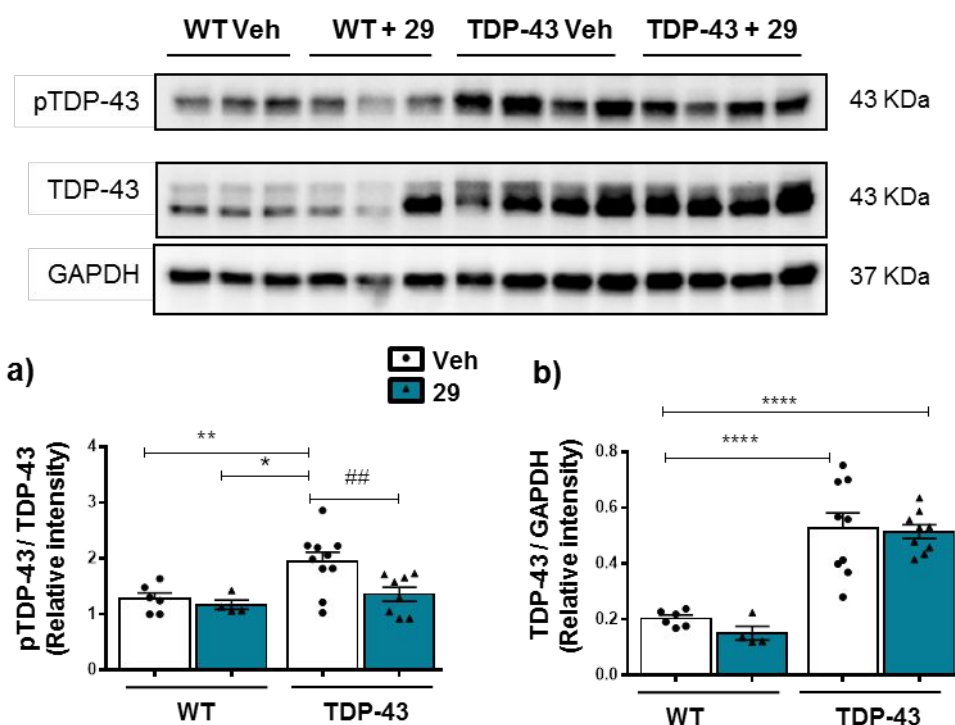


Figure 13. TDP-43 phosphorylated (a) and total TDP-43 (b) levels in the spinal cord of transgenic TDP-43 and wild-type mice treated with compound **29** or vehicle. Representative immunoblots are shown. Data represent the mean \pm SEM of different observations. Data were assessed by one-way ANOVA followed by the Bonferroni test (* $p < 0.05$, ** $p < 0.01$, **** $p < 0.00001$ vs. WT group; ### $p < 0.01$ vs. TDP-43-Veh group).

We have already mentioned the pathogenic role of glial reactivity and related inflammatory processes in ALS neurodegeneration. In order to confirm the immunomodulatory effect of compound **29** *in vivo*, we examined iNOS and TREM2 protein expression in the spinal cord of TDP-43 (A315T) transgenic mice treated with **29** by Western Blot analysis. TDP-43 transgenic mice showed an increased iNOS expression compared to wild type animals, which was significantly reduced in **29**-treated animals (Figure 14a). This effect was accompanied by an increase in the anti-inflammatory microglial marker TREM2 (Figure 14b), confirming the microglia switch from pro-inflammatory M1-type to anti-inflammatory M2-type (Figure 14c) observed in the *in vitro* studies. Similar results were obtained by immunofluorescence analysis, where treatment with TTBK1 inhibitor **29** decreased both microglial (Iba-1) and astrocytes (GFAP) reactivity compared to the controls (Figure S7).

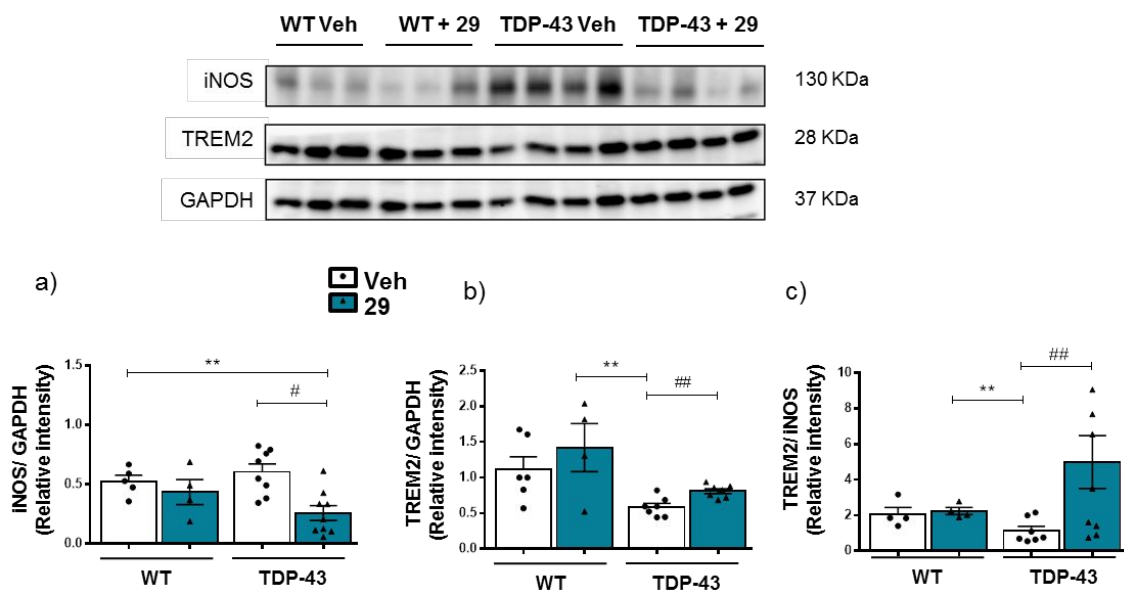


Figure 14. Immunomodulatory effect of compound **29** in the lumbar region of the spinal cord of wild-type and TDP-43 transgenic mice. Protein expression and desintometric data of (a) iNOS (b) TREM2 and (c) the ratio TREM2/iNOS showing microglia switch from inflammatory M1-type to anti-inflammatory M2-type. GAPDH was used for endogenous normalization. Representative immunoblot are shown. Desintometric data represent the mean \pm SEM of different observations. Data were assessed by one-way ANOVA followed by the Bonferroni test (** $p < 0.01$ vs. WT group; # $p < 0.05$, ## $p < 0.01$ vs. TDP-43-Veh group).

Finally, we investigate if the reduction of TDP-43 phosphorylation combined with the anti-inflammatory effect observed in the spinal cord of the transgenic mice treated with compound **29**, contributes to avoid the motor neuron degeneration typical of this TDP-43 transgenic mice at advanced stages of disease progression. The reduction in the number of motor neurons observed in the ventral horn in transgenic animals, measured by two different markers: Nissl staining and choline acetyl transferase (ChAT) immunohistochemistry, was significantly prevented in those animals that received compound **29** as treatment (Figure 15).

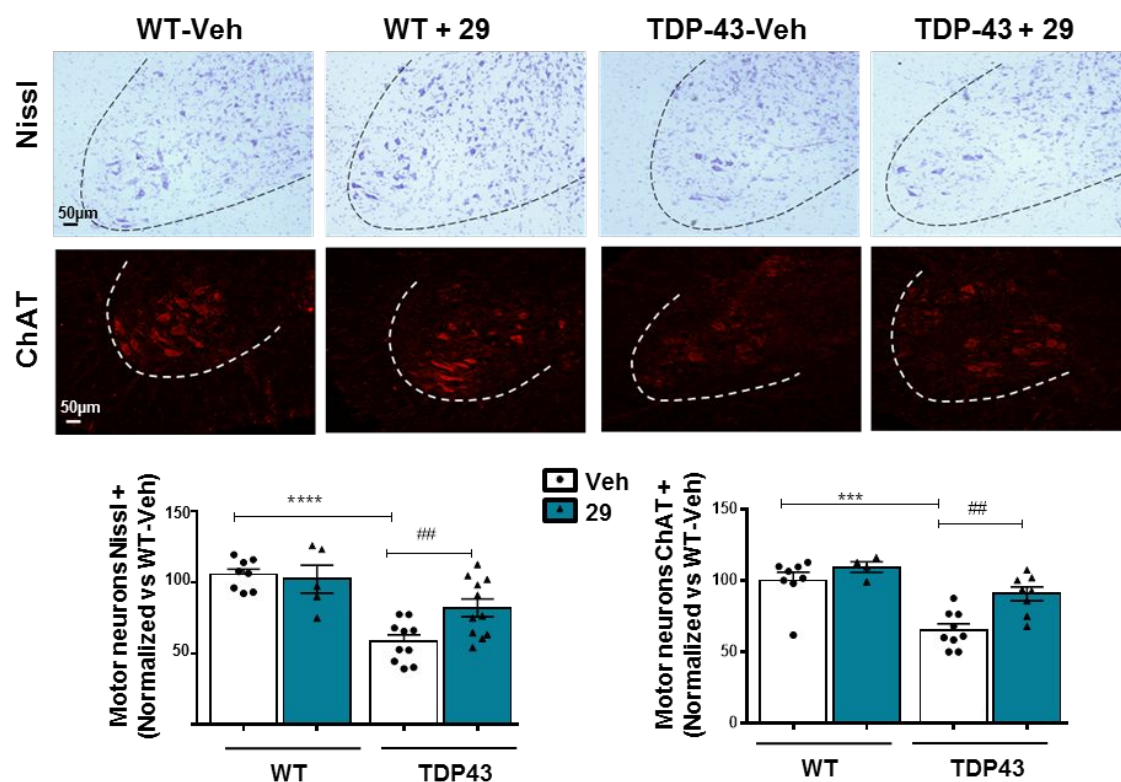


Figure 15. Representative images of Nissl-stained motor neurons and ChAT immunostained sections in the anterior horn of the spinal cord of TDP-43 mice and wild-type treated with compound **29** or vehicle. Quantification of the number of motor neurons Nissl+ and ChAT+ normalized vs WT-Veh is shown. Data were assessed by one-way ANOVA followed by the Bonferroni test (***p < 0.001, ****p < 0.0001 vs. WT-Veh group; ##p < 0.01 vs. TDP-43-Veh).

Taken together, these results demonstrate that TTBK1 inhibition is a potential, effective and viable strategy to protect motor neuron degeneration in ALS and TDP-43 proteinopathies in murine models, and the pyrrolopyrimidine **29** may be a good drug candidate for further development.

2.7 TTBK1 inhibitor modulates TDP-43 pathology in a patient cell-based ALS model

Finally, with the aim to help in the translation of these promising results to the clinical setting, the modulatory effect of compounds **29** and **39** on the TDP-43 homeostasis was tested in a remarkable human cell-based model of the disease recently developed in our group. Cultures of immortalized lymphocytes from ALS patients recapitulate very well TDP-43 pathological features and represent a novel and effective platform to evaluate

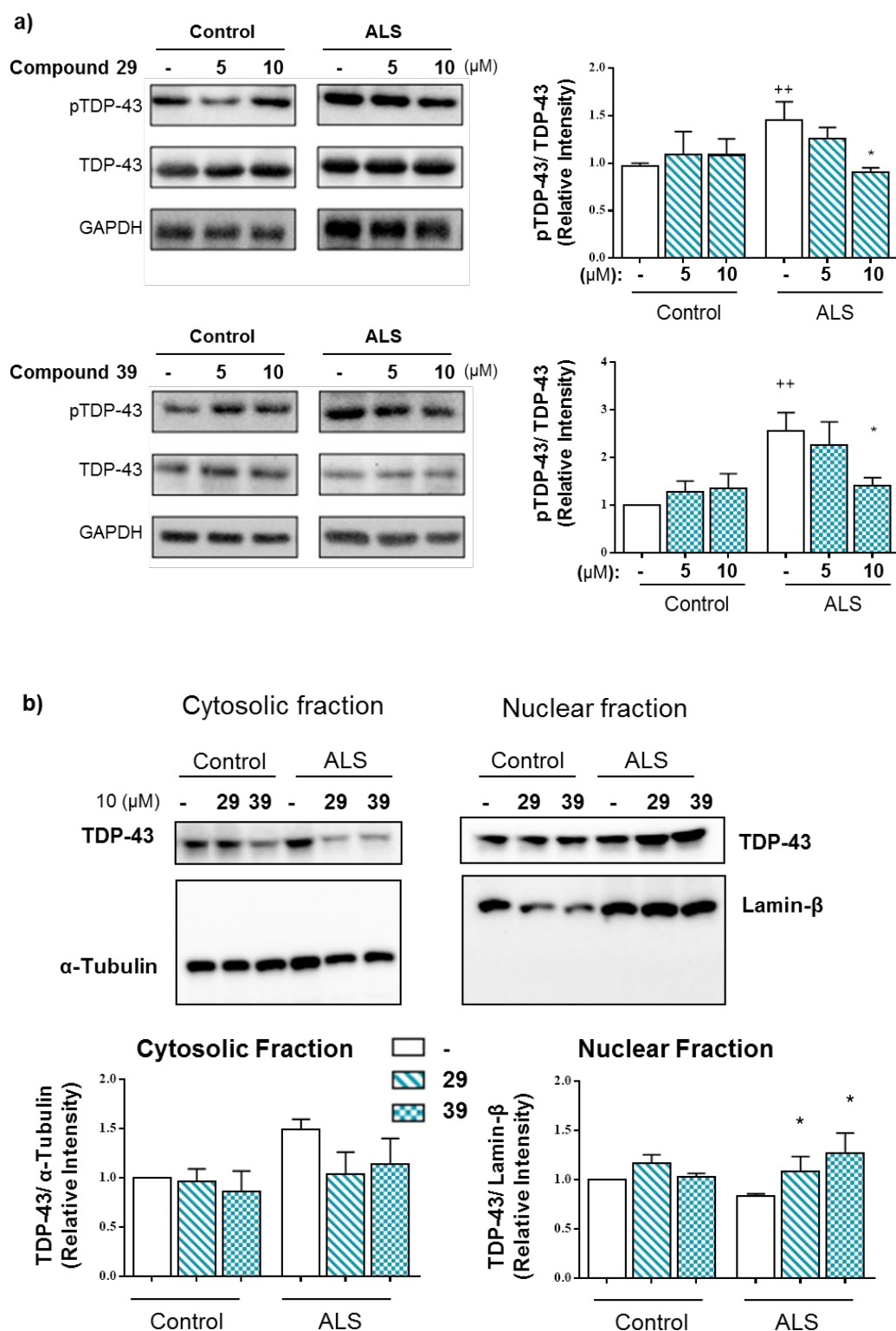
new drugs.³⁹ Lymphocytes were obtained from blood samples of patients or healthy individuals (Table 5) after written informed consent.

Table 5. Demographic and clinical characteristics of subjects included in this study

	Control (n=5)	ALS (n=5)
Gender (M/F)	(2/3)	(2/3)
Age (± SD)	62 ± 7	65 ± 1
Type of onset		
Bulbar	NA	4
Limb	NA	1

Control: Individuals without sing of neurological degeneration; NA: not applicable.
All patients were negative for *SOD1*, *TARDBP* and *C9orf72* mutations.

Thus, to confirm the privileged therapeutic profile of TTBK1 inhibitors in the modulation of TDP-43 proteinopathy, sporadic ALS-patient lymphoblasts were treated with both compounds for 24 h resulting in reduced phosphorylation and cytosolic levels of TDP-43, with simultaneous recovery of nuclear TDP-43 localization (Figure 16). These results highlight and demonstrate the importance of TTBK1 in the modulation of TDP-43 proteinopathy in a human cell-based model of sporadic ALS and reinforce the novelty of TTBK1 inhibition as an interesting approach for the pharmacological treatment of this devastating disease.



respectively. Densitometric analyses represent the mean \pm SEM of different observations carried out in independent cell lines ($n = 5$) from each group ($*p < 0.05$ significantly different from ALS untreated cells).

Conclusions

Overall, we have achieved the design, synthesis and optimization of a new family of small molecules resulting in rather potent and selective TTBK1 inhibitors based on a pyrrolopyrimidine scaffold. These compounds showed ability to decrease TDP-43 phosphorylation both in *in vitro* and in a TDP-43-transgenic mice model, demonstrating their relevance as lead structures for different TDP-43-pathies such as ALS. Moreover, in two different cellular models, including a ALS patient cell-based model, the developed TTBK1 inhibitors were able to recover the nuclear/cytosolic balance of TDP-43 which emphasizes the therapeutic potential of these compounds. Interestingly, experimentally calculated brain permeability predicted a good brain penetration for several compounds that was confirmed experimentally *in vivo* for compound **29** showing a ratio brain-to-plasma of 3:1. In addition, crystal structures of ligand complexes for TTBK1 and TTBK2 can throw some new clues for specific TTBK1 modulation.

Altogether, we reported a new family of TTBK1 inhibitors that for the first time modulate TDP-43 pathology in different models and can be considered new disease modifying drugs for ALS and others TDP-43-pathies such as FTD, LATE or Alexander's syndrome. Only future clinical trials will have the final confirmation of their therapeutic relevance.

Experimental Section

Chemistry

Reagents were obtained from the commercial sources and used without further purification. Purifications of crudes were performed with the indicated solvent as eluent by flash column chromatography carried out at medium pressure using silica gel (E. Merck, Grade 60, particle size 0.040–0.063 mm, 230–240 mesh ASTM) or IsoleraOne

flash purification system from Biotage. ^1H -NMR and ^{13}C -NMR data were obtained from a Bruker AV300 or AV500 MHz spectrometer. Chemical shifts, δ , are expressed in ppm and calculated taking the reference of the appropriated deuterated solvents. Signal multiplicities (bs: broad signal, s: singlet, d: doublet, dd: doublet of doublets, ddd: doublet of doublet of doublets, t: triplet, td: triplet of doublets, q: quartet, m: multiplet) and coupling constants ($J = \text{Hz}$) are indicated for each molecule. Acquired spectroscopic data was analysed with MestreNova 10.2 software. The microwave assisted synthesis was carried out using a Biotage Initiator eight single-mode cavity instrument from Biotage. Experiments were performed with temperature control mode in sealed microwave process vials. The temperature was measured with an IR sensor on the outside of the reaction vessel. Stirring was provided by an in situ magnetic stirrer. High Performance Liquid Chromatography (HPLC) analyses were performed in a Thermo Finnigan Surveyor UV-Vis Plus Detector coupled with FinniganTM LXQ TM. The column used for the analysis was a SunFire[®] C18, 3.5 μm , 4.6x50mm and UV-Vis spectra of the samples were acquired. Melting points were determined in a Büchi Melting Point M-560. High resolution mass spectrometry (HRMS) was done in a spectrometer Agilent 6500 using positive electro spray techniques (ESI). Values are expressed in mass units (m/z). Elemental analyses were performed by the analytical department at CAI-UCM, and the results obtained were within $\pm 0.4\%$ of the theoretical values using the analyzer LECO CHNS-932. All the final compounds have a purity $\geq 95\%$ tested by HPLC.

General procedure for the synthesis of derivatives 1-55: (a) 1 eq of 6-chloro-7-deazapurine, 6-chloropurine or 6-chlorothienopirimidine, 1 eq of the corresponding aniline and 0.1 eq of indium trichloride were dissolved in 2 mL of acetonitrile. The crude is stirred under microwave irradiation at 100 °C until the completeness of the reaction. (b) 1 eq of 6-chloro-7-deazapurine, 6-chloropurine or 6-chlorothienopirimidine and 1 eq of the corresponding aniline were dissolved in 2 mL of tetrahydrofuran. The crude is stirred under microwave irradiation at 100 °C until the completeness of the reaction.

The corresponding crude is extracted using 20 mL of EtOAc and washed with NaHCO₃ and brine, the organic layer is dried over MgSO₄ and evaporated under high vacuum. The corresponding crude is purified using flash chromatography and CH₂Cl₂:MeOH 40:1 as eluent.

3-((9H-purine-6-yl)amino)phenol (1). Yield 29%. M.p. 339-340 °C. ¹H-NMR (500 MHz, DMSO-*d*₆): δ (ppm) 13.16 (s, 1H), 9.61 (s, 1H), 9.31 (s, 1H), 8.36 (s, 1H), 8.26 (s, 1H), 7.55 (s, 1H), 7.32 (m, 1H), 7.08 (m, 1H), 6.42 (m, 1H). ¹³C-NMR (125 MHz, DMSO-*d*₆): δ (ppm) 158.2, 152.8, 150.9, 141.1, 140.0, 128.1, 124.1, 120.0, 112.8, 110.0, 108.3. ESI calcd for C₁₁H₉N₅O [M + H]⁺ 228.0880. Found: 228.0877

(N-(4-phenoxy)-9H-purin-6-amine) (2). Yield 20%. M.p. 336-338 °C. ¹H-NMR (300 MHz, DMSO-*d*₆): δ (ppm) 13.06 (s, 1H), 9.47 (s, 1H), 9.14 (s, 1H), 8.26 (s, 1H), 8.20 (s, 1H), 7.64 (d, *J* = 8.7 Hz, 2H), 6.72 (d, *J* = 8.8 Hz, 2H). ¹³C-NMR (75 MHz, DMSO-*d*₆): δ (ppm) 153.1, 152.1, 151.9, 150.1, 139.3, 131.2, 122.8, 121.1, 119.1, 114.8. ESI calcd for C₁₁H₉N₅O [M + H]⁺ 228.0880. Found: 228.0879

(N-(4-morpholinophenyl)-9H-purin-6-amine) (3) Yield 70%. M.p. 269-270 °C. ¹H-NMR (300 MHz, DMSO-*d*₆): δ (ppm) 13.05 (s, 1H), 9.58 (s, 1H), 8.31 (s, 1H), 8.24 (s, 1H), 7.75 (d, *J* = 9.0 Hz, 2H), 6.92 (d, *J* = 9.1 Hz, 2H), 3.74 (t, *J* = 4.2 Hz, 4H), 3.05 (t, *J* = 4.7 Hz, 4H). ¹³C-NMR (75 MHz, DMSO-*d*₆): δ (ppm) 151.9, 151.6, 150.9, 146.9, 139.9, 132.0, 121.9, 118.4, 115.4, 66.2, 49.1. ESI calcd for C₁₅H₁₆N₆O [M + H]⁺ 297.1458. Found: 297.1457

(N-(4-chlorophenyl)-9H-purin-6-amine) (4) Yield 75%. M.p. 329-330 °C. ¹H-NMR (500 MHz, DMSO-*d*₆): δ (ppm) 13.21 (s, 1H), 9.95 (s, 1H), 8.40 (s, 1H), 8.30 (s, 1H), 8.03 (d, *J* = 8.9 Hz, 2H), 7.37 (d, *J* = 8.9 Hz, 2H). ¹³C-NMR (126 MHz, DMSO-*d*₆): δ (ppm) 151.7, 151.6, 150.6, 140.2, 138.9, 128.2, 125.8, 121.8, 119.5. ESI calcd for C₁₁H₈ClN₅ [M + H]⁺ 246.0541. Found: 246.0542

*N-4-chlorophenylthieno[2,3-*d*]pyrimidin-4-amine (5)* Yield 50%. M.p. 179-180 °C. ¹H-NMR (300 MHz, DMSO-*d*₆): δ (ppm) 9.75 (s, 1H), 8.52 (s, 1H), 7.95-7.84 (m, 3H), 7.75

(d, $J = 6.0$ Hz, 1H), 7.43 (d, $J = 8.9$ Hz, 2H). ^{13}C -NMR (75 MHz, $\text{DMSO}-d_6$): δ (ppm) 166.6, 154.6, 153.0, 138.3, 128.5, 126.8, 124.2, 122.8, 119.4, 117.0. Anal. calcd for $\text{C}_{12}\text{H}_8\text{ClN}_3\text{S}$: C, 49.92; H, 3.84; N, 14.55; S 11.10. Found C, 50.22; H, 3.13; N, 14.09; S 10.76.

N-phenylthieno[2,3-*d*]pyrimidin-4-amine (**6**) Yield 70%. M.p. 175-176 °C. ^1H -NMR (300 MHz, $\text{DMSO}-d_6$): δ (ppm) 9.65 (s, 1H), 8.49 (s, 1H), 7.89 (d, $J = 6.0$ Hz, 1H), 7.86-7.81 (m, 2H), 7.73 (d, $J = 5.9$ Hz, 1H), 7.46-7.31 (m, 2H), 7.16-7.04 (m, 1H). ^{13}C -NMR (75 MHz, $\text{DMSO}-d_6$): δ (ppm) 166.5, 154.8, 153.2, 139.2, 128.5, 123.8, 123.3, 121.5, 119.5, 116.9. Anal. calcd for $\text{C}_{12}\text{H}_9\text{N}_3\text{S}$: C, 63.41; H, 3.99; N, 18.49; S 14.11. Found: C, 63.36; H, 4.16; N, 18.46; S 14.07.

N-(3-phenol)-7H-pyrrolo[2,3-*d*]pyrimidin-4-amine (**7**). Yield 87%. M.p. 253-255 °C. ^1H -NMR (300 MHz, $\text{DMSO}-d_6$): δ (ppm) 11.75 (s, 1H), 9.34 (s, 1H), 9.17 (s, 1H), 8.28 (s, 1H), 7.50 (s, 1H), 7.26 (dd, $J = 2.0, 7.9$ Hz, 1H), 7.22 (dd, $J = 3.5, 1.7$ Hz, 1H), 7.10 (t, $J = 8.0$ Hz, 1H), 6.80 (d, $J = 3.5$ Hz, 1H), 6.43 (dd, $J = 8.0, 2.3$ Hz, 1H). ^{13}C -NMR (75 MHz, $\text{DMSO}-d_6$): δ (ppm) 157.8, 153.9, 151.2, 151.0, 141.8, 129.4, 122.4, 111.5, 109.6, 107.7, 104.1, 99.2. ESI calcd for $\text{C}_{12}\text{H}_{10}\text{N}_4\text{O}$ $[\text{M} + \text{H}]^+$ 227.0927. Found: 227.0929.

N-(4-phenol)-7H-pyrrolo[2,3-*d*]pyrimidin-4-amine (**8**) Yield 38%. M.p. 274-276 °C. ^1H -NMR (300 MHz, $\text{DMSO}-d_6$): δ (ppm) 11.65 (s, 1H), 9.17 (s, 1H), 9.05 (s, 1H), 8.18 (s, 1H), 7.56 (d, $J = 8.8$ Hz, 2H), 7.17 (dd, $J = 3.5, 2.3$ Hz, 1H), 6.77 (d, $J = 8.8$ Hz, 2H), 6.63 (dd, $J = 3.5, 2.1$ Hz, 1H). ^{13}C -NMR (75 MHz, $\text{DMSO}-d_6$): δ (ppm) 154.0, 153.0, 150.9, 150.6, 131.6, 123.0, 121.4, 114.9, 103.0, 98.8. ESI calcd for $\text{C}_{12}\text{H}_{10}\text{N}_4\text{O}$ $[\text{M} + \text{H}]^+$ 227.0927. Found: 227.0925.

N-(4-morpholinophenyl)-7H-pyrrolo[2,3-*d*]pyrimidin-4-amine (**9**) Yield 24%. M.p. 254-255 °C. ^1H -NMR (300 MHz, $\text{DMSO}-d_6$): δ (ppm) 11.65 (s, 1H), 9.10 (s, 1H), 8.20 (s, 1H), 7.67 (d, $J = 7.2$ Hz, 2H), 7.17 (dd, $J = 3.5, 2.3$ Hz, 1H), 6.94 (d, $J = 6.9$ Hz, 2H), 6.67 (dd, $J = 3.5, 1.8$ Hz, 1H), 3.74 (t, $J = 9.4, 4.9$ Hz, 4H), 3.06 (t, $J = 9.2, 4.7$ Hz, 4H). ^{13}C -NMR (75 MHz, $\text{DMSO}-d_6$): δ (ppm) 153.8, 150.9, 150.7, 146.7, 132.5, 122.0, 121.6, 115.4, 103.2, 98.8, 66.1, 49.1. ESI calcd for $\text{C}_{16}\text{H}_{17}\text{N}_5\text{O}$ $[\text{M} + \text{H}]^+$ 296.1506. Found: 296.1496.

N-(4-chlorophenyl)-7*H*-pyrrolo[2,3-*d*]pyrimidin-4-amine (**10**). Yield 92%. M.p. 259-260 °C. ¹H-NMR (300 MHz, DMSO-*d*₆): δ (ppm) 11.82 (s, 1H), 9.43 (s, 1H), 8.30 (s, 1H), 7.97 (dt, *J* = 8.9, 2.0 Hz, 2H), 7.38 (dt, 2H), 7.26 (dd, *J* = 3.5, 2.3 Hz, 1H), 6.80 (dd, *J* = 3.5, 1.9 Hz, 1H). ¹³C-NMR (75 MHz, DMSO-*d*₆): δ (ppm) 153.2, 150.9, 150.6, 139.5, 128.3, 125.3, 122.4, 121.4, 103.8, 98.7. Anal. calcd for C₁₂H₉ClN₄: C, 58.91; H, 3.71; N, 22.90. Found: C, 58.66; H, 3.78; N, 22.83.

N-(4-chlorobenzyl)-7*H*-pyrrolo[2,3-*d*]pyrimidin-4-amine (**11**). Yield 55%. M.p. 208-209 °C. ¹H-NMR (300 MHz, DMSO-*d*₆): δ (ppm) 11.53 (s, 1H), 8.08 (s, 1H), 7.97 (t, *J* = 6.1 Hz, 1H), 7.36 (s, 4H), 7.08 (dd, *J* = 3.4, 2.3 Hz, 1H), 6.56 (dd, *J* = 3.4, 1.9 Hz, 1H), 4.69 (d, *J* = 6.1 Hz, 2H). ¹³C-NMR (75 MHz, DMSO-*d*₆): δ (ppm) 156.2, 151.7, 150.5, 139.9, 131.4, 129.4, 129.4, 128.5, 121.4, 102.9, 98.9, 42.8. Anal. calcd for C₁₃H₁₁ClN₄: C, 60.35; H, 4.29; N, 21.66. Found: C, 60.35; H, 4.24; N, 21.47.

N-(4-chloroethylphenyl)-7*H*-pyrrolo[2,3-*d*]pyrimidin-4-amine (**12**). Yield 25%. M.p. 207-208 °C. ¹H-NMR (300 MHz, DMSO-*d*₆): δ (ppm) 11.48 (s, 1H), 8.12 (s, 1H), 7.47 (t, *J* = 5.7 Hz, 1H), 7.43-7.18 (m, 4H), 7.05 (dd, *J* = 3.4, 2.2 Hz, 1H), 6.51 (dd, *J* = 3.4, 1.7 Hz, 1H), 3.67 (q, *J* = 7.2, 5.8 Hz, 2H), 2.91 (t, *J* = 7.3 Hz, 2H). ¹³C-NMR (75 MHz, DMSO-*d*₆): δ (ppm) 156.0, 151.5, 150.1, 138.9, 130.7, 130.6, 128.2, 120.8, 102.6, 98.5, 41.4, 34.6. ESI calcd for C₁₄H₁₄ClN₄ [M + H]⁺ 273.0902. Found: 273.0895.

4-(((7*H*-pyrrolo[2,3-*d*]pyrimidin-4-yl)amino)methyl)phenol (**13**). Yield 14%. M.p. 206-207 °C. ¹H-NMR (300 MHz, DMSO-*d*₆): δ (ppm) 11.49 (s, 1H), 9.27 (s, 1H), 8.10 (s, 1H), 7.81 (t, 1H), 7.15 (d, *J* = 8.3 Hz, 2H), 7.05 (t, *J* = 2.7 Hz, 1H), 6.69 (d, *J* = 8.5 Hz, 2H), 6.57 (dd, *J* = 3.5, 1.7 Hz, 1H), 4.58 (d, *J* = 5.8 Hz, 2H). ¹³C-NMR (75 MHz, DMSO-*d*₆): δ (ppm) 156.2, 156.0, 151.5, 150.2, 130.5, 128.7, 120.8, 115.0, 102.5, 98.7, 42.7. ESI calcd for C₁₃H₁₂N₄O [M + H]⁺ 241.1084. Found: 241.1079

4-(2-((7*H*-pyrrolo[2,3-*d*]pyrimidin-4-yl)amino)ethyl)phenol (**14**). Yield 23%. M.p. 246-247 °C. ¹H-NMR (300 MHz, DMSO-*d*₆): δ (ppm) 11.47 (s, 1H), 9.18 (s, 1H), 8.11 (s, 1H), 7.45 (t, *J* = 5.7 Hz, 1H), 7.09-7.01 (m, 3H), 6.68 (d, *J* = 8.4 Hz, 2H), 6.52 (dd, *J* = 3.4, 1.7 Hz,

1H), 3.68-3.48 (m, 2H), 2.79 (t, $J = 7.6$ Hz, 2H). ^{13}C -NMR (75 MHz, $\text{DMSO}-d_6$): δ (ppm) 156.0, 155.6, 151.5, 150.1, 129.8, 129.5, 120.7, 115.1, 102.5, 98.6, 42.1, 34.6. ESI calcd for $\text{C}_{14}\text{H}_{14}\text{N}_4\text{O}$ $[\text{M} + \text{H}]^+$ 255.1240. Found: 255.1239

N-(3-chlorophenyl)-7H-pyrrolo[2,3-*d*]pyrimidin-4-amine (**15**). Yield 49%. M.p. 234-235 °C. (lit⁴⁰ 227-228 °C). ^1H -NMR (500 MHz, $\text{DMSO}-d_6$): δ (ppm) 12.81 (s, 1H), 11.42 (s, 1H), 8.45 (s, 1H), 7.90 (s, 1H), 7.66 (m, 1H), 7.50 (m, 1H), 7.45 (m, 1H), 7.34 (m, 1H), 7.26 (m, 1H). ^{13}C -NMR (125 MHz, $\text{DMSO}-d_6$): δ (ppm) 151.4, 146.1, 144.7, 138.7, 133.7, 131.2, 125.9, 125.0, 123.7, 122.6, 102.37, 102.3. ESI calcd for $\text{C}_{12}\text{H}_9\text{ClN}_4$ $[\text{M} + \text{H}]^+$ 245.0589. Found: 245.0587

N-(2-chlorophenyl)-7H-pyrrolo[2,3-*d*]pyrimidin-4-amine (**16**). Yield 69%. M.p. 220-221 °C. ^1H -NMR (300 MHz, $\text{DMSO}-d_6$): δ (ppm) 11.73 (s, 1H), 9.07 (s, 1H), 8.13 (s, 1H), 7.69 (dd, $J = 8.0, 1.6$ Hz, 1H), 7.54 (dd, $J = 8.0, 1.6$ Hz, 1H), 7.37 (dt, $J = 7.7, 1.6$ Hz, 1H), 7.24 (dt, $J = 7.6, 1.7$ Hz, 1H), 7.14 (dd, $J = 3.5, 2.3$ Hz, 1H), 6.51 (dd, $J = 3.5, 1.8$ Hz, 1H). ^{13}C -NMR (75 MHz, $\text{DMSO}-d_6$): δ (ppm) 154.3, 151.1, 150.9, 136.4, 129.5, 129.4, 128.5, 127.3, 126.4, 122.2, 103.1, 98.7. Anal. calcd for $\text{C}_{12}\text{H}_9\text{ClN}_4$: C, 58.91; H, 3.71; N, 22.90. Found: C, 58.77; H, 3.79; N, 22.90.

N-(2-phenyloxy)-7H-pyrrolo[2,3-*d*]pyrimidin-4-amine (**17**). Yield 20%. M.p. 233-235 °C. ^1H -NMR (300 MHz, $\text{DMSO}-d_6$): δ (ppm) 11.82 (s, 1H), 10.61 (s, 1H), 8.91 (s, 1H), 8.22 (s, 1H), 7.56 (dd, $J = 7.9, 1.6$ Hz, 1H), 7.22 (dd, $J = 3.5, 2.3$ Hz, 1H), 7.02 (ddd, $J = 8.0, 7.1, 1.6$ Hz, 1H), 6.92 (dd, $J = 8.0, 1.6$ Hz, 1H), 6.84 (ddd, $J = 7.9, 7.2, 1.6$ Hz, 1H), 6.70 (dd, $J = 3.5, 1.8$ Hz, 1H). ^{13}C -NMR (75 MHz, $\text{DMSO}-d_6$): δ (ppm) 153.8, 150.6, 150.2, 149.6, 127.8, 125.0, 124.3, 122.2, 119.1, 117.4, 103.2, 99.1. ESI calcd for $\text{C}_{12}\text{H}_{10}\text{N}_4\text{O}$ $[\text{M} + \text{H}]^+$ 227.0927. Found: 227.0926

N-(5,6,7,8-tetrahydronaphthalen-1-yl)-7H-pyrrolo[2,3-*d*]pyrimidin-4-amine (**18**). Yield 23%. M.p. 239-240 °C. ^1H -NMR (300 MHz, $\text{DMSO}-d_6$): δ (ppm) 11.58 (s, 1H), 8.74 (s, 1H), 8.06 (s, 1H), 7.20- 7.05 (m, 3H), 6.99 (dd, $J = 7.3, 1.7$ Hz, 1H), 6.22 (dd, $J = 3.2, 1.5$ Hz, 1H), 2.78 (t, $J = 5.3$ Hz, 2H), 2.61 (t, $J = 5.3$ Hz, 2H), 1.68 (t, $J = 3.4$ Hz, 4H). ^{13}C -

NMR (75 MHz, DMSO- d_6): δ (ppm) 155.7, 151.6, 151.5, 138.0, 137.9, 134.0, 127.0, 125.6, 125.2, 121.9, 103.0, 99.4, 29.7, 25.0, 22.9 (C-18-19). Anal. calcd for $C_{16}H_{16}N_4$: C, 72.70; H, 6.10; N, 21.70. Found: C, 72.50; H, 6.05; N, 21.22.

N-(benzo[d][1,3]dioxol-5-yl)-7H-pyrrolo[2,3-d]pyrimidin-4-amine (**19**). Yield 15%. M.p. 282-283 °C. ^1H -NMR (300 MHz, DMSO- d_6): δ (ppm) 11.69 (s, 1H), 9.17 (s, 1H), 8.22 (s, 1H), 7.58 (d, J = 2.1 Hz, 1H), 7.23-7.15 (m, 2H), 6.89 (d, J = 8.4 Hz, 1H), 6.70 (dd, J = 3.5, 1.9 Hz, 1H), 6.00 (s, 2H). ^{13}C -NMR (75 MHz, DMSO- d_6): δ (ppm) 153.6, 150.77, 150.72, 146.9, 142.3, 134.7, 121.9, 113.3, 107.8, 103.3, 103.0, 100.8, 98.7. ESI calcd for $C_{13}H_{10}N_4O_2$ $[M + H]^+$ 255.0877. Found: 255.0877.

1-(4-((7H-pyrrolo[2,3-d]pyrimidin-4-yl)amino)phenyl)ethan-1-one (**20**). Yield 25%. M.p. 279-280 °C. ^1H -NMR (300 MHz, DMSO- d_6): δ (ppm) 11.87 (s, 1H), 9.67 (s, 1H), 8.38 (s, 1H), 8.11 (d, J = 8.8 Hz, 2H), 7.96 (d, J = 8.8 Hz, 2H), 7.31 (dd, J = 3.5, 2.3 Hz, 1H), 6.87 (dd, J = 3.5, 1.9 Hz, 1H). ^{13}C -NMR (75 MHz, DMSO- d_6): δ (ppm) 196.6, 153.2, 151.5, 150.9, 145.5, 130.5, 129.7, 123.3, 119.0, 104.7, 99.1, 26.7. Anal. calcd for $C_{14}H_{12}N_4O$: C, 65.07; H, 5.80; N, 23.71. Found: C, 64.88; H, 5.68; N, 23.20

N-(3-morpholinophenyl)-7H-pyrrolo[2,3-d]pyrimidin-4-amine (**21**). Yield 58%. M.p. 258-259 °C. ^1H -NMR (300 MHz, DMSO- d_6): δ (ppm) 11.65 (s, 1H), 9.10 (s, 1H), 8.20 (s, 1H), 7.67 (dd, J = 7.2, 2.2 Hz, 2H), 7.17 (dd, J = 3.5, 2.3 Hz, 1H), 6.94 (dd, J = 6.9, 2.1 Hz, 2H), 6.67 (dd, J = 3.5, 1.8 Hz, 1H), 3.74 (t, J = 9.4, 4.9 Hz, 4H), 3.06 (t, J = 9.2, 4.7 Hz, 4H). ^{13}C -NMR (75 MHz, DMSO- d_6): δ (ppm) 153.6, 151.4, 150.8, 150.8, 141.1, 128.8, 122.0, 111.7, 109.4, 107.2, 103.6, 98.7, 66.1, 48.7. Anal. calcd for $C_{16}H_{17}N_5O$ C, 65.07; H, 5.80; N, 23.71. Found: C, 64.88; H, 5.68; N, 23.20.

N-phenyl-7H-pyrrolo[2,3-d]pyrimidin-4-amine (**22**). Yield 64%. M.p. 239-240 °C. ^1H -NMR (300 MHz, DMSO- d_6): δ (ppm) 11.75 (s, 1H), 9.29 (s, 1H), 8.28 (s, 1H), 7.89 (dd, J = 7.5, 1.0 Hz, 2H), 7.33 (td, J = 8.7, 2.1 Hz, 2H), 7.23 (dd, J = 3.5, 2.3 Hz, 1H), 7.01 (tt, J = 7.2, 2.4, 1.1 Hz, 1H), 6.79 (dd, J = 3.5, 1.8 Hz, 1H). ^{13}C -NMR (75 MHz, DMSO- d_6): δ (ppm)

153.5, 150.8, 150.7, 140.4, 128.4, 122.1, 122.0, 120.2, 103.6, 98.8. ESI calcd for $C_{12}H_{10}N_4$ $[M + H]^+$ 211.0978 hallado 211.0979.

N-(4-methoxyphenyl)-7*H*-pyrrolo[2,3-*d*]pyrimidin-4-amine (**23**). Yield 74%, M.p. 229-230 °C. 1H -NMR (300 MHz, DMSO- d_6): δ (ppm) 11.66 (s, 1H), 9.14 (s, 1H), 8.20 (s, 1H), 7.71 (d, J = 9.0 Hz, 2H), 7.18 (dd, J = 3.5, 2.3 Hz, 1H), 6.92 (d, J = 9.0 Hz, 2H), 6.67 (dd, J = 3.5, 1.9 Hz, 1H), 3.75 (s, 3H). ^{13}C -NMR (75 MHz, DMSO- d_6): δ (ppm) 156.2, 156.0, 151.5, 150.2, 130.5, 128.7, 120.8, 115.0, 102.5, 98.7, 42.7. Anal. calcd for $C_{13}H_{12}N_4O$: C, 64.99; H, 5.03; N, 23.32. Found: C, 64.59; H, 5.03; N, 23.03.

N-(4-(trifluoromethoxy)phenyl)-7*H*-pyrrolo[2,3-*d*]pyrimidine-4-amine (**24**). Yield 92%, M.p. 202-203 °C. 1H -NMR (300 MHz, DMSO- d_6): δ (ppm) 11.81 (s, 1H), 9.47 (s, 1H), 8.29 (s, 1H), 8.02 (d, J = 9.1 Hz, 2H), 7.34 (dd, J = 9.2, 1.0 Hz, 2H), 7.26 (dd, J = 3.5, 2.3 Hz, 1H), 6.80 (dd, J = 3.5, 1.9 Hz, 1H). ^{13}C -NMR (75 MHz, DMSO- d_6): δ (ppm) 153.2, 151.0, 150.6, 142.6 (d, J = 1.9 Hz), 139.7, 122.5, 121.4, 121.2, 120.2 (d, J = 255.3 Hz), 103.8, 98.7. Anal. calcd for $C_{13}H_9F_3N_4O$: C, 53.07; H, 3.08; N, 19.04. Found: C, 52.81; H, 3.16; N, 18.99.

N-(4-isopropoxyphenyl)-7*H*-pyrrolo[2,3-*d*]pyrimidin-4-amine (**25**). Yield 66%. M.p. 218-219 °C. 1H -NMR (300 MHz, DMSO- d_6): δ (ppm) 11.66 (s, 1H), 9.13 (s, 1H), 8.20 (s, 1H), 7.69 (d, J = 9.0 Hz, 2H), 7.17 (dd, J = 3.5, 2.3 Hz, 1H), 6.89 (d, J = 9.0 Hz, 2H), 6.68 (dd, J = 3.5, 1.8 Hz, 1H), 4.54 (hept, J = 6.0, 1H), 1.26 (d, J = 6.0, 6H). ^{13}C -NMR (75 MHz, DMSO- d_6): δ (ppm) 153.8, 150.9, 150.7, 133.2, 122.4, 121.7, 115.7, 103.2, 98.8, 69.4, 21.9 ESI calcd for $C_{15}H_{16}N_4O$ $[M + H]^+$ 269.1397. Found: 269.1393.

N-(4-etoxyphenyl)-7*H*-pyrrolo[2,3-*d*]pyrimidin-4-amine (**26**). Yield 20%. M.p. 241-242 °C. 1H -NMR (300 MHz, DMSO- d_6): δ (ppm) 11.66 (s, 1H), 9.13 (s, 1H), 8.20 (s, 1H), 7.70 (d, J = 9.1 Hz, 2H), 7.17 (dd, J = 3.4, 2.3 Hz, 1H), 6.91 (d, J = 9.1 Hz, 2H), 6.67 (dd, J = 3.5, 1.9 Hz, 1H), 4.00 (q, J = 7.0, 2H), 1.33 (d, J = 7.0, 3H). ^{13}C -NMR (75 MHz, DMSO- d_6): δ (ppm) 154.0, 153.8, 150.9, 150.7, 133.2, 122.4, 121.7, 114.2, 103.2, 98.8, 63.1, 14.8. ESI calcd for $C_{14}H_{14}N_4O$ $[M + H]^+$ 255.1240. Found: 255.1236.

N-(4-phenoxyphenyl)-7*H*-pyrrolo[2,3-*d*]pyrimidin-4-amine (**27**). Yield 53%. M.p. 250-251 °C. ¹H-NMR (300 MHz, DMSO-*d*₆): δ (ppm) 11.75 (s, 1H), 9.34 (s, 1H), 8.26 (s, 1H), 7.89 (d, *J* = 9.0 Hz, 2H), 7.37 (dd, *J* = 8.6, 7.3 Hz, 2H), 7.23 (dd, *J* = 3.5, 2.3 Hz, 1H), 7.13-6.96 (m, 5H), 6.77 (dd, *J* = 3.5, 1.9 Hz, 1H). ¹³C-NMR (75 MHz, DMSO-*d*₆): δ (ppm) 157.6, 153.5, 150.8, 150.75, 150.7, 136.3, 129.9, 122.7, 122.1, 122.0, 119.4, 117.6, 103.5, 98.7. Anal. calcd for C₁₈H₁₄N₄O: C, 71.51; H, 7.67; N, 18.53. Found: C, 71.04; H, 4.70; N, 18.38.

N-cyclohexyl-7*H*-pyrrolo[2,3-*d*]pyrimidin-4-amine (**28**). Yield 26%. M.p. 146-147 °C. ¹H-NMR (300 MHz, DMSO-*d*₆): δ (ppm) 11.41 (s, 1H), 8.06 (s, 1H), 7.09 (d, *J* = 7.9 Hz, 1H), 7.03 (dd, *J* = 3.4, 2.2 Hz, 1H), 6.57 (dd, *J* = 3.4, 1.8 Hz, 1H), 4.12-3.95 (m, 1H), 2.00-1.87 (m, 2H), 1.82-1.74 (m, 2H), 1.74-1.56 (m, 2H), 1.44-1.22 (m, 4H). ¹³C-NMR (75 MHz, DMSO-*d*₆): δ (ppm) 155.3, 151.4, 150.2, 120.4, 102.3, 98.7, 48.5, 32.8, 25.5, 25.0. ESI calcd for C₁₂H₁₆N₄ [M + H]⁺ 217.1448. Found: 217.1439.

N-(4-(4-chlorophenoxy)phenyl)-7*H*-pyrrolo[2,3-*d*]pyrimidin-4-amine (**29**). Yield 62%. M.p. 250-251 °C. ¹H-NMR (300 MHz, DMSO-*d*₆): δ (ppm) 11.77 (s, 1H), 9.36 (s, 1H), 8.26 (s, 1H), 7.92 (d, *J* = 9.0 Hz, 2H), 7.41 (d, *J* = 9.0 Hz, 2H), 7.24 (dd, *J* = 3.4, 2.3 Hz, 1H), 7.06 (d, *J* = 9.0 Hz, 2H), 7.00 (d, *J* = 9.0 Hz, 2H), 6.77 (dd, *J* = 3.5, 1.9 Hz, 1H). ¹³C-NMR (75 MHz, DMSO-*d*₆): δ (ppm) 156.7, 153.4, 150.8, 150.7, 150.2, 136.8, 129.7, 126.4, 122.1, 121.9, 119.7, 119.2, 103.5, 98.7. Anal. calcd for C₁₈H₁₃ClN₄O: C, 64.20; H, 3.89; N, 16.64. Found: C, 65.15; H, 3.96; N, 16.69.

N-(4-(4-fluorophenoxy)phenyl)-7*H*-pyrrolo[2,3-*d*]pyrimidin-4-amine (**30**). Yield 40%. M.p. 227-228 °C. ¹H-NMR (300 MHz, DMSO-*d*₆): δ (ppm) 11.75 (s, 1H), 9.33 (s, 1H), 8.25 (s, 1H), 7.88 (d, *J* = 9.0 Hz, 2H), 7.26-7.15 (m, 3H), 7.08-6.95 (m, 4H), 6.76 (dd, *J* = 3.5, 1.9 Hz, 1H). ¹³C-NMR (75 MHz, DMSO-*d*₆): δ (ppm) 159.4 (d, *J* = 238.1 Hz), 153.6 (d, *J* = 2.3 Hz), 153.5, 151.3, 150.8, 136.3, 122.1, 122.0, 119.6 (d, *J* = 8.4 Hz), 119.0, 116.4 (d, *J* = 23.3 Hz), 103.5, 98.7. Anal. calcd for C₁₈H₁₃FN₄O: C, 67.49; H, 4.09; N, 17.49. Found: C, 67.09; H, 4.09; N, 17.38.

N-(4-(4-cyanophenoxy)phenyl)-7H-pyrrolo[2,3-d]pyrimidin-4-amine (**31**). Yield 6%. M.p. 259-260 °C. ¹H-NMR (300 MHz, DMSO-*d*₆): δ (ppm) 11.77 (s, 1H), 9.41 (s, 1H), 8.28 (s, 1H), 7.99 (d, *J* = 9.0 Hz, 2H), 7.83 (d, *J* = 8.9 Hz, 2H), 7.25 (dd, *J* = 3.5, 2.3 Hz, 1H), 7.15 (d, *J* = 9.0 Hz, 2H), 7.09 (d, *J* = 8.9 Hz, 2H), 6.79 (dd, *J* = 3.5, 1.8 Hz, 1H). ¹³C-NMR (75 MHz, DMSO-*d*₆): δ (ppm) 161.9, 153.3, 150.8, 150.7, 148.4, 137.8, 134.6, 122.2, 121.8, 120.7, 118.8, 117.3, 104.5, 103.6, 98.7. Anal. calcd for C₁₉H₁₃N₅O: C, 69.71; H, 4.00; N, 21.39. Found: C, 69.33; H, 4.15; N, 21.01.

N-(4-(4-methoxyphenoxy)phenyl)-7H-pyrrolo[2,3-d]pyrimidin-4-amine (**32**). Yield 63%. M.p. 202-203 °C. ¹H-NMR (300 MHz, DMSO-*d*₆): δ (ppm) 11.74 (s, 1H), 9.30 (s, 1H), 8.25 (s, 1H), 7.84 (d, *J* = 9.0 Hz, 2H), 7.23 (dd, *J* = 3.5, 2.3 Hz, 1H), 7.04-6.94 (m, 6H), 6.76 (dd, *J* = 3.1, 1.9 Hz, 1H), 3.76 (s, 3H). ¹³C-NMR (75 MHz, DMSO-*d*₆): δ (ppm) 155.2, 153.5, 152.4, 150.8, 150.7, 150.4, 135.5, 122.0, 121.9, 119.8, 118.0, 115.0, 103.4, 98.7, 55.4. Anal. calcd for C₁₉H₁₆N₄O₂: C, 68.66; H, 4.85; N, 16.86. Found: C, 67.97; H, 4.91; N, 16.64.

N-(4-(4-trifluoromethylphenoxy)phenyl)-7H-pyrrolo[2,3-d]pyrimidin-4-amine (**33**). Yield 74%. M.p. 233-234 °C. ¹H-NMR (300 MHz, DMSO-*d*₆): δ (ppm) 11.77 (s, 1H), 9.40 (s, 1H), 8.28 (s, 1H), 7.98 (d, *J* = 9.0 Hz, 2H), 7.72 (d, *J* = 8.7 Hz, 2H), 7.24 (dd, *J* = 3.5, 2.3 Hz, 1H), 7.14 (t, *J* = 9.1 Hz, 4H), 6.79 (dd, *J* = 3.5, 1.9 Hz, 1H). ¹³C-NMR (75 MHz, DMSO-*d*₆): δ (ppm) 162.1, 154.3, 151.7, 151.6, 149.9, 138.4, 128.3 (q, *J* = 3.6 Hz, C-20-22), 125.2 (q, *J* = 271.7 Hz), 123.6 (q, *J* = 32.1 Hz, 123.1, 122.7, 121.4, 118.0, 104.5, 99.6. Anal. calcd for C₁₉H₁₃F₃N₄O: C, 61.62; H, 3.54; N, 15.13. Found: C, 61.55; H, 3.51; N, 15.04.

N-(4-(4-bromophenoxy)phenyl)-7H-pyrrolo[2,3-d]pyrimidin-4-amine (**34**). Yield 83%. M.p. 257-258 °C. ¹H-NMR (300 MHz, DMSO-*d*₆): δ (ppm) 11.75 (s, 1H), 9.35 (s, 1H), 8.27 (s, 1H), 7.93 (d, *J* = 9.0 Hz, 2H), 7.54 (d, *J* = 9.0 Hz, 2H), 7.24 (dd, *J* = 3.5, 2.3 Hz, 1H), 7.08 (d, *J* = 9.0 Hz, 2H), 6.96 (d, *J* = 8.9 Hz, 2H), 6.78 (dd, *J* = 3.5, 1.9 Hz, 1H). ¹³C-NMR (75 MHz, DMSO-*d*₆): δ (ppm) 157.7, 153.9, 151.3, 151.2, 150.6, 137.3, 133.1,

122.6, 122.4, 120.2, 120.1, 114.7, 104.0, 99.2. Anal. calcd for $C_{18}H_{13}BrN_4O$: C, 56.71; H, 3.44; N, 14.70. Found: C, 56.21; H, 3.51; N, 14.43.

N-(4-((4-nitrophenoxy)phenyl)-7*H*-pyrrolo[2,3-*d*]pyrimidin-4-amine (**35**). Yield 83%. M.p. 270-271 °C. 1H -NMR (300 MHz, DMSO- d_6): δ (ppm) 11.86 (s, 1H), 9.63 (s, 1H), 8.35-8.16 (m, 3H), 8.00 (d, J = 9.0 Hz, 2H), 7.29-7.24 (m, 1H), 7.20 (d, J = 9.0 Hz, 2H), 7.14 (d, J = 9.3 Hz, 2H), 6.84 (dd, J = 3.5, 1.9 Hz, 1H). ^{13}C -NMR (75 MHz, DMSO- d_6): δ (ppm) 163.6, 153.1, 150.5, 150.1, 148.7, 142.0, 137.7, 126.2, 122.5, 122.3, 120.9, 116.9, 103.6, 99.1. ESI calcd for $C_{18}H_{13}N_5O_3$ [$M + H$] $^+$ 348.1091. Found: 348.1088

N-(4-((4-aminophenoxy)phenyl)-7*H*-pyrrolo[2,3-*d*]pyrimidin-4-amine (**36**). Reduction of derivative **35** (1 eq) using $SnCl_2$ (5.5 eq) in EtOH (12 mL) at 100 °C for 20 min under microwave irradiation. Yield 9%. M.p. 242-243 °C. 1H -NMR (300 MHz, DMSO- d_6): δ (ppm) 11.68 (s, 1H), 9.21 (s, 1H), 8.21 (s, 1H), 7.75 (d, J = 9.0 Hz, 2H), 7.19 (dd, J = 3.5, 2.3 Hz, 1H), 6.87 (d, J = 9.0 Hz, 2H), 6.76 (d, J = 8.8 Hz, 2H), 6.71 (dd, J = 3.5, 1.9 Hz, 1H), 6.58 (d, J = 8.8 Hz, 2H), 4.92 (s, 2H). ^{13}C -NMR (75 MHz, DMSO- d_6): δ (ppm) 153.74, 153.64, 150.8, 150.7, 146.5, 145.1, 134.7, 122.1, 121.9, 120.3, 117.0, 114.8, 103.3, 98.7. ESI calcd for $C_{18}H_{15}N_5O$ [$M + H$] $^+$ 318.1349. Found: 318.1348

N-(4-(*p*-tolylloxy)phenyl)-7*H*-pyrrolo[2,3-*d*]pyrimidin-4-amine (**37**). Yield 57%. M.p. 229 °C. 1H -NMR (300 MHz, DMSO- d_6): δ (ppm) 11.72 (s, 1H), 9.29 (s, 1H), 8.24 (s, 1H), 7.85 (d, J = 9.0 Hz, 2H), 7.22 (dd, J = 3.5, 2.4 Hz, 1H), 7.17 (dd, J = 8.8, 0.7 Hz, 2H), 6.99 (d, J = 9 Hz, 2H), 6.89 (d, J = 8.5 Hz, 2H), 6.75 (dd, J = 3.5, 1.9 Hz, 1H), 2.28 (s, 3H). ^{13}C -NMR (75 MHz, DMSO- d_6): δ (ppm) 155.2, 153.5, 151.5, 150.8, 136.0, 131.9, 130.3, 122.03, 121.98, 118.9, 117.9, 103.5, 98.7, 20.2. Anal. calcd for $C_{19}H_{16}N_4O$: C, 72.13; H, 5.10; N, 17.71. Found: C, 71.84; H, 5.15; N, 17.96.

(4-(*m*-tolylloxy)phenyl)-7*H*-pyrrolo[2,3-*d*]pyrimidine-2,4-diamine (**38**). Yield 80%. M.p. 212-213 °C. 1H -NMR (300 MHz, DMSO- d_6): δ (ppm) 11.73 (s, 1H), 9.31 (s, 1H), 8.25 (s, 1H), 7.88 (d, J = 9.0 Hz, 2H), 7.28-7.20 (m, 2H), 7.02 (d, J = 9.0 Hz, 2H), 6.91 (ddt, J = 7.5, 1.7, 0.8 Hz, 1H), 6.82-6.78 (m, 3H), 2.28 (s, 3H). ^{13}C -NMR (75 MHz, DMSO- d_6): δ (ppm) 157.7, 153.5, 150.9, 150.79, 150.76, 139.6, 136.3, 129.6, 123.5, 122.1, 121.9,

119.4, 118.1, 114.7, 103.5, 98.7, 21.0. ESI calcd for $C_{19}H_{16}N_4O$ $[M + H]^+$ 317.1397.
Found: 317.1393

N-(4-(3-chlorophenoxy)phenyl)-7*H*-pyrrolo[2,3-*d*]pyrimidin-4-amine (**39**). Yield 62%.
M.p. 224-225 °C. 1H -NMR (300 MHz, DMSO- d_6): δ (ppm) 11.79 (s, 1H), 9.39 (s, 1H),
8.29 (s, 1H), 7.96 (d, J = 9.0 Hz, 2H), 7.41 (t, J = 8.1 Hz, 1H), 7.26 (dd, J = 3.5, 2.2 Hz,
1H), 7.17 (ddd, J = 8.0, 2.0, 0.9 Hz, 1H), 7.12 (d, J = 9.0 Hz, 2H), 7.03 (t, J = 2.2 Hz, 1H),
6.97 (ddd, J = 8.3, 2.3, 0.8 Hz, 1H), 6.80 (dd, J = 3.5, 1.8 Hz, 1H). ^{13}C -NMR (75 MHz,
DMSO- d_6): δ (ppm) 158.9, 153.4, 150.8, 150.8, 149.7, 137.1, 133.9, 131.4, 122.5, 122.2,
121.9, 120.0, 117.2, 116.0, 103.5, 98.7. Anal. calcd for $C_{18}H_{13}ClN_4O$: C, 64.20; H, 3.89;
N, 16.64. Found: C, 64.06; H, 3.91; N, 16.75.

N-(4-(3-trifluoromethylphenoxy)phenyl)-7*H*-pyrrolo[2,3-*d*]pyrimidin-4-amine (**40**). Yield
78%. M.p. 176-177 °C. 1H -NMR (300 MHz, DMSO- d_6): δ (ppm) 11.75 (s, 1H), 9.37 (s,
1H), 8.27 (s, 1H), 7.96 (d, J = 9.0 Hz, 2H), 7.61 (t, J = 7.8 Hz, 1H), 7.44 (d, J = 7.9 Hz,
1H), 7.32 - 7.19 (m, 3H), 7.13 (d, J = 8.9 Hz, 2H), 6.78 (dd, J = 3.5, 1.9 Hz, 1H). ^{13}C -
NMR (75 MHz, DMSO- d_6): δ (ppm) 158.8, 153.8, 151.2, 151.1, 149.9, 137.6, 131.6,
130.95 (q, J = 32 Hz), 127.7 (d, J = 272.5 Hz), 122.5, 122.3, 121.5, 120.5, 119.5 (d, J =
3.9 Hz), 113.9 (d, J = 4.0 Hz), 103.9, 99.1. Anal. calcd for $C_{19}H_{13}F_3N_4O$: C, 61.62; H,
3.54; N, 15.13. Found: C, 61.06; H, 3.47; N, 15.22.

N-(4-(3-methoxyphenoxy)phenyl)-7*H*-pyrrolo[2,3-*d*]pyrimidin-4-amine (**41**). Yield 33%.
M.p. 206-207 °C. 1H -NMR (300 MHz, DMSO- d_6): δ (ppm) 11.73 (s, 1H), 9.32 (s, 1H),
8.25 (s, 1H), 7.89 (d, J = 9.0 Hz, 2H), 7.31-7.20 (m, 2H), 7.05 (d, J = 9.0 Hz, 2H), 6.76
(dd, J = 3.5, 1.8 Hz, 1H), 6.67 (ddd, J = 8.3, 2.4, 0.9 Hz, 1H), 6.59-6.48 (m, 2H), 3.73 (s,
3H). ^{13}C -NMR (75 MHz, DMSO- d_6): δ (ppm) 160.6, 158.9, 153.5, 150.80, 150.75, 150.5,
136.5, 130.4, 122.1, 121.9, 119.6, 109.5, 108.4, 103.7, 103.5, 98.7, 55.2. ESI calcd for
 $C_{19}H_{16}N_4O_2$ $[M + H]^+$ 333.1346. Found: 333.1342.

N-(4-(2-chlorophenoxy)phenyl)-7*H*-pyrrolo[2,3-*d*]pyrimidin-4-amine (**42**). Yield 79%.
M.p. 214-215 °C. 1H -NMR (300 MHz, DMSO- d_6): δ (ppm) 11.73 (s, 1H), 9.33 (s, 1H),
8.25 (s, 1H), 7.89 (d, J = 9.0 Hz, 2H), 7.58 (dd, J = 8.0, 1.6 Hz, 1H), 7.34 (ddd, J = 8.2,

7.4, 1.6 Hz, 1H), 7.22 (dd, $J = 3.5, 2.4$ Hz, 1H), 7.17 (ddd, $J = 8.0, 7.4, 1.5$ Hz, 1H), 7.05-6.95 (m, 3H), 6.76 (dd, $J = 3.5, 1.9$ Hz, 1H). ^{13}C -NMR (75 MHz, DMSO- d_6): δ (ppm) 153.5, 152.6, 150.80, 150.74, 150.71, 136.5, 130.6, 128.7, 124.6, 123.8, 122.1, 122.0, 119.8, 118.4, 103.5, 98.7. Anal. calcd for $\text{C}_{18}\text{H}_{13}\text{ClN}_4\text{O}$: C, 64.20; H, 3.89; N, 16.64. Found: C, 64.11; H, 3.96; N, 16.63.

N-(4-(2-methoxyphenoxy)phenyl)-7H-pyrrolo[2,3-*d*]pyrimidin-4-amine (**43**). Yield 64%. M.p. 214-215 °C. ^1H -NMR (300 MHz, DMSO- d_6): δ (ppm) 11.69 (s, 1H), 9.23 (s, 1H), 8.21 (s, 1H), 7.76 (d, $J = 9.0$ Hz, 2H), 7.20 (dd, $J = 3.5, 2.3$ Hz, 1H), 7.18-7.14 (m, 2H), 7.02-6.92 (m, 2H), 6.86 (d, $J = 9.1$ Hz, 2H), 6.71 (dd, $J = 3.5, 1.9$ Hz, 1H), 3.77 (s, 3H). ^{13}C -NMR (75 MHz, DMSO- d_6): δ (ppm) 153.6, 152.6, 151.1, 150.8, 150.7, 144.6, 135.0, 124.9, 122.1, 121.9, 121.0, 120.7, 116.7, 113.3, 103.3, 98.7, 55.6. Anal. calcd for $\text{C}_{19}\text{H}_{16}\text{N}_4\text{O}_2$: C, 68.66; H, 4.85; N, 16.96. Found: C, 68.60; H, 4.82; N, 16.97.

N-(4-(2,4-chlorophenoxy)phenyl)-7H-pyrrolo[2,3-*d*]pyrimidin-4-amine (**44**). Yield 63%. M.p. 252-253 °C. ^1H -NMR (300 MHz, DMSO- d_6): δ (ppm) 11.72 (s, 1H), 9.37 (s, 1H), 8.24 (s, 1H), 7.89 (d, $J = 9.1$ Hz, 2H), 7.72 (d, $J = 2.5$ Hz, 1H), 7.39 (dd, $J = 8.8, 2.6$ Hz, 1H), 7.22 (dd, $J = 3.5, 2.3$ Hz, 1H), 7.02 (dd, $J = 8.9, 2.1$ Hz, 3H), 6.75 (dd, $J = 3.5, 1.9$ Hz, 1H). ^{13}C -NMR (75 MHz, DMSO- d_6): δ (ppm) 153.6, 152.0, 150.9, 150.5, 136.9, 130.1, 128.8, 127.7, 124.9, 122.4, 122.2, 120.9, 118.8, 103.7, 98.9. Anal. calcd for $\text{C}_{18}\text{H}_{12}\text{Cl}_2\text{N}_4\text{O}$: C, 58.24; H, 3.26; N, 15.09. Found: C, 58.13; H, 3.33; N, 15.17.

*N*4-(4-(4-chlorophenoxy)phenyl)-7H-pyrrolo[2,3-*d*]pyrimidine-2,4-diamine (**45**). Yield 70%. M.p. 232-233 °C. ^1H -NMR (300 MHz, DMSO- d_6): δ (ppm) 10.83 (s, 1H), 8.94 (s, 1H), 7.98 (d, $J = 9.1$ Hz, 2H), 7.41 (d, $J = 9.0$ Hz, 2H), 6.99 (m, 4H), 6.76 (dd, $J = 3.5, 2.1$ Hz, 1H), 6.53 (dd, $J = 3.5, 1.9$ Hz, 1H), 5.70 (s, 2H). ^{13}C -NMR (75 MHz, DMSO- d_6): δ (ppm) 159.4, 156.8, 154.0, 153.5, 149.7, 137.5, 129.7, 126.3, 121.3, 119.5, 119.1, 117.8, 98.8, 96.9. ESI calcd for $\text{C}_{18}\text{H}_{14}\text{ClN}_5\text{O}$ $[\text{M} + \text{H}]^+$ 352.0960. Found: 352.0956.

*N*4-(4-(4-(trifluoromethyl)phenoxy)phenyl)-7H-pyrrolo[2,3-*d*]pyrimidine-2,4-diamine (**46**). Yield 77%. M.p. 201-202 °C. ^1H -NMR (300 MHz, DMSO- d_6): δ (ppm) 10.85 (s, 1H), 8.99 (s, 1H), 8.03 (d, $J = 9.0$ Hz, 2H), 7.72 (d, $J = 9.0$ Hz, 2H), 7.11 (dd, $J = 9.0, 0.8$ Hz, 2H),

7.07 (d, J = 9.0 Hz, 2H), 6.77 (dd, J = 3.5, 2.2 Hz, 1H), 6.55 (dd, J = 3.5, 1.9 Hz, 1H), 5.72 (s, 2H). ^{13}C -NMR (75 MHz, DMSO- d_6): δ (ppm) 161.3, 159.4, 153.9, 153.5, 148.5, 138.2, 127.4 (q, J = 3.7 Hz), 124.4 (d, J = 271.1 Hz), 122.7 (d, J = 32 Hz), 121.2, 120.4, 117.9, 117.1, 108.5, 98.8, 96.9. ESI calcd for $\text{C}_{19}\text{H}_{14}\text{F}_3\text{N}_5\text{O}$ [$\text{M} + \text{H}$] $^+$ 386.1223. Found: 386.1220.

*N*4-(4-(3-chlorophenoxy)phenyl)-7H-pyrrolo[2,3-*d*]pyrimidine-2,4-diamine (**47**). Yield 16%. M.p. 177-178 °C. ^1H -NMR (300 MHz, DMSO- d_6): δ (ppm) 10.84 (s, 1H), 8.97 (s, 1H), 8.00 (d, J = 9.0 Hz, 2H), 7.39 (t, J = 8.1 Hz, 1H), 7.14 (ddd, J = 8.0, 2.0, 0.9 Hz, 1H), 7.03 (d, J = 9.0 Hz, 2H), 6.99 (t, J = 2.2 Hz, 1H), 6.94 (ddd, J = 8.3, 2.4, 0.9 Hz, 1H), 6.76 (dd, J = 3.5, 2.2 Hz, 1H), 6.54 (dd, J = 3.5, 1.9 Hz, 1H), 5.71 (s, 2H). ^{13}C -NMR (75 MHz, DMSO- d_6): δ (ppm) 159.4, 159.1, 153.9, 153.5, 149.1, 137.8, 133.9, 131.3, 122.5, 121.3, 119.9, 117.8, 117.1, 116.0, 98.8, 96.9. ESI calcd for $\text{C}_{18}\text{H}_{14}\text{ClN}_5\text{O}$ [$\text{M} + \text{H}$] $^+$ 352.0960. Found: 352.0955

*N*4-(4-(3-(trifluoromethyl)phenoxy)phenyl)-7H-pyrrolo[2,3-*d*]pyrimidine-2,4-diamine (**48**). Yield 45%. M.p. 179-180 °C. ^1H -NMR (300 MHz, DMSO- d_6): δ (ppm) 10.84 (s, 1H), 8.98 (s, 1H), 8.02 (d, J = 9.1 Hz, 2H), 7.60 (t, J = 7.9 Hz, 1H), 7.44 (ddt, J = 7.7, 1.7, 0.9 Hz, 1H), 7.32-7.20 (m, 2H), 7.06 (d, J = 9.0 Hz, 2H), 6.76 (dd, J = 3.5, 2.2 Hz, 1H), 6.54 (dd, J = 3.5, 2.0 Hz, 1H), 5.72 (s, 2H). ^{13}C -NMR (75 MHz, DMSO- d_6): δ (ppm) 159.4, 158.6, 153.9, 153.5, 148.9, 138.0, 131.3, 130.6 (d, J = 31.9 Hz), 123.8 (d, J = 272.5 Hz), 121.3, 121.1, 120.0, 119.0 (d, J = 4.1 Hz), 117.9, 113.4 (d, J = 4.0 Hz), 98.8, 96.9. ESI calcd for $\text{C}_{19}\text{H}_{14}\text{F}_3\text{N}_5\text{O}$ [$\text{M} + \text{H}$] $^+$ 386.1223. Found: 386.1219

N-(4-((4-nitrophenyl)thio)phenyl)-7H-pyrrolo[2,3-*d*]pyrimidin-4-amine (**49**). Yield 42%. M.p. 265-266 °C. ^1H -NMR (300 MHz, DMSO- d_6): δ (ppm) 12.46 (s, 1H), 10.72 (s, 1H), 8.43 (s, 1H), 8.17 (d, J = 8.6 Hz, 2H), 8.00 (d, J = 8.1 Hz, 2H), 7.67 (d, J = 8.2 Hz, 2H), 7.44 (t, J = 2.6 Hz, 1H), 7.33 (d, J = 8.6 Hz, 2H), 7.03 (t, J = 2.4 Hz, 1H). ^{13}C -NMR (75 MHz, DMSO- d_6): δ (ppm) 151.7, 148.3, 147.6, 146.6, 144.9, 139.9, 135.7, 126.4, 124.3, 124.1, 123.7, 123.5, 103.7, 100.7. Anal. calcd for $\text{C}_{18}\text{H}_{13}\text{N}_5\text{O}_2\text{S}$: C, 59.49; H, 3.61; N, 19.27; S, 8.82. Found: C, 59.42; H, 3.78; N, 19.14; S, 8.74.

N-(4-((4-aminophenyl)thio)phenyl)-7H-pyrrolo[2,3-*d*]pyrimidin-4-amine (**50**). Reduction of derivative **49** (1 eq) using SnCl₂ (5.5 eq) in EtOH (12 mL) at 100 °C for 20 min under microwave irradiation. Yield 69%. M.p. 200-201 °C. ¹H-NMR (300 MHz, DMSO-*d*₆): δ (ppm) 11.73 (s, 1H), 9.30 (s, 1H), 8.24 (s, 1H), 7.80 (d, *J* = 8.8 Hz, 2H), 7.23 (dd, *J* = 3.5, 2.3 Hz, 1H), 7.22 (dd, *J* = 3.5, 2.3 Hz, 1H), 7.14 (dd, *J* = 16.7, 8.6 Hz, 4H), 6.84 (dd, *J* = 3.5, 1.9 Hz, 1H), 6.61 (d, *J* = 8.5 Hz, 2H), 5.48 (s, 1H). ¹³C-NMR (75 MHz, DMSO-*d*₆): δ (ppm) 153.3, 150.8, 150.6, 149.3, 138.5, 135.0, 131.3, 128.2, 122.1, 120.9, 117.1, 114.7, 103.6, 98.7. Anal. calcd for C₁₈H₁₅N₅S: C, 59.49; H, 3.61; N, 19.27; S, 8.82. Found: C, 59.26; H, 3.70; N, 19.37; S, 8.95.

N-(4-(benzyloxy)phenyl)-7H-pyrrolo[2,3-*d*]pyrimidin-4-amine (**51**). Yield 28%. M.p. 238-239 °C. ¹H-NMR (300 MHz, DMSO-*d*₆): δ (ppm) 11.66 (s, 1H), 9.15 (s, 1H), 8.20 (s, 1H), 7.71 (d, *J* = 9.1 Hz, 2H), 7.50-7.29 (m, 5H), 7.18 (dd, *J* = 3.5, 2.4 Hz, 1H), 7.00 (d, *J* = 9.1 Hz, 2H), 6.67 (dd, *J* = 3.5, 1.9 Hz, 1H), 5.09 (s, 2H). ¹³C-NMR (75 MHz, DMSO-*d*₆): δ (ppm) 153.80, 153.76, 150.9, 150.7, 137.3, 133.5, 128.4, 127.74, 127.66, 122.3, 122.0, 114.7, 103.2, 98.7, 69.4. ESI calcd for C₁₉H₁₆N₄O [M + H]⁺ 317.1397. Found: 317.1395.

(4-((7H-pyrrolo[2,3-*d*]pyrimidin-4-yl)amino)phenyl)(phenyl)methanone (**52**). Yield 97%. M.p. 247-248 °C. ¹H-NMR (300 MHz, DMSO-*d*₆): δ (ppm) 11.91 (s, 1H), 9.76 (s, 1H), 8.38 (s, 1H), 8.16 (d, *J* = 8.9 Hz, 2H), 7.79 (d, *J* = 8.8 Hz, 2H), 7.77-7.53 (m, 5H), 7.32 (dd, *J* = 3.5, 2.3 Hz, 1H), 6.89 (dd, *J* = 3.5, 1.9 Hz, 1H). ¹³C-NMR (75 MHz, DMSO-*d*₆): δ (ppm) 194.4, 152.8, 151.2, 150.5, 145.1, 137.9, 132.0, 131.1, 129.6, 129.3, 128.4, 123.0, 118.6, 104.4, 98.7. ESI calcd for C₁₉H₁₄N₄O [M + H]⁺ 315.1240. Found: 315.1238.

(4-((7H-pyrrolo[2,3-*d*]pyrimidin-4-yl)amino)phenyl)(4-fluorophenyl)methanone (**53**). Yield 19%. M.p. 275-276 °C. ¹H-NMR (300 MHz, DMSO-*d*₆): δ (ppm) 11.89 (s, 1H), 9.75 (s, 1H), 8.38 (s, 1H), 8.16 (d, *J* = 8.9 Hz, 2H), 7.93-7.72 (m, 4H), 7.39 (t, *J* = 8.9 Hz, 2H), 7.32 (dd, *J* = 3.5, 2.3 Hz, 1H), 6.88 (dd, *J* = 3.5, 2.3, 1H). ¹³C-NMR (75 MHz, DMSO-*d*₆): δ (ppm) 193.1, 164.3 (d, *J* = 250.3 Hz, 152.9, 151.2, 150.5, 145.2, 134.5 (d, *J* = 3.2 Hz), 132.2 (d, *J* = 9.2 Hz), 131.1, 129.5, 123.0, 118.7, 115.5 (d, *J* = 22.0 Hz), 104.4, 98.8.

Anal. calcd for $C_{19}H_{13}FN_4O$: C, 68.67; H, 3.94; N, 16.86. Found: C, 68.32; H, 3.90; N, 16.72.

(4-((7H-pyrrolo[2,3-d]pyrimidin-4-yl)amino)phenyl)(3,4-dichlorophenyl)methanone (54).

Yield 35%. M.p. 274-275 °C. 1H -NMR (300 MHz, DMSO- d_6): δ (ppm) 11.91 (s, 1H), 9.78 (s, 1H), 8.39 (s, 1H), 8.18 (d, J = 8.9 Hz, 2H), 7.91 (d, J = 1.9 Hz, 1H), 7.82 (dd, J = 8.5, 6.3 Hz, 3H), 7.68 (dd, J = 8.3, 2.0 Hz, 1H), 7.33 (dd, J = 3.5, 2.3 Hz, 1H), 6.88 (dd, J = 3.5, 1.9 Hz, 1H). ^{13}C -NMR (75 MHz, DMSO- d_6): δ (ppm) 192.0, 152.8, 151.2, 150.5, 145.6, 138.4, 134.6, 131.5, 131.3, 130.9, 130.8, 129.3, 128.7, 123.1, 118.7, 104.5, 98.7. ESI calcd for $C_{19}H_{12}Cl_2N_4O$ $[M + H]^+$ 383.0461. Found: 383.0457

N-(4-(pyridin-3-yloxy)phenyl)-7H-pyrrolo[2,3-d]pyrimidin-4-amine (55). Yield 35%. M.p. 203-204 °C. 1H -NMR (300 MHz, DMSO- d_6): δ (ppm) 11.75 (s, 1H), 9.36 (s, 1H), 8.40-8.36 (m, 1H), 8.35-8.31 (m, 1H), 8.26 (s, 1H), 7.93 (d, J = 9.0 Hz, 2H), 7.45-7.36 (m, 2H), 7.23 (dd, J = 3.5, 2.3 Hz, 1H), 7.10 (d, J = 9.0 Hz, 2H), 6.77 (dd, J = 3.5, 1.9 Hz, 1H). ^{13}C -NMR (75 MHz, DMSO- d_6): δ (ppm) 154.2, 153.5, 150.82, 150.74, 150.1, 143.9, 140.2, 137.0, 124.60, 124.55, 122.2, 121.9, 119.5, 103.6, 98.7. ESI calcd for $C_{17}H_{13}N_5O$ $[M + H]^+$ 304.11193. Found: 304.1191.

Procedure for the synthesis of azides derivatives 56-60: 1 eq. of 1-(bromomethyl) or 1-(bromoethyl)benzene and 1.5 eq. of sodium azide were dissolved in 2 mL of DMF. The reaction mixture was stirred overnight. The organic phase (AcOEt, 10 mL) was washed with 10x3 mL of iced H_2O . The organic phase was dried over Na_2SO_4 and the crude was used in the following reaction without further purification.

1-(azydomethyl)-4-chlorobenzene (56). Yield 74%. 1H -NMR (300 MHz, DMSO- d_6): δ (ppm) 7.47 (d, J = 8.6 Hz, 2H), 7.42 (d, J = 8.7 Hz, 2H), 4.47 (s, 2H). ^{13}C -NMR (75 MHz, DMSO- d_6): δ (ppm) 135.2, 133.2, 130.8, 129.2, 53.2.

1-(azydomethyl)-2-chlorobenzene (57). Yield 65%. 1H -NMR (300 MHz, DMSO- d_6): δ (ppm) 7.46-7.35 (m, 2H), 7.33-7.24 (m, 2H), 4.50 (s, 2H). ^{13}C -NMR (75 MHz, DMSO- d_6): δ (ppm) 133.8, 133.3, 130.0, 129.8, 129.6, 127.2, 52.3.

1
2
3 *1-(azydomethyl)-3-chlorobenzene (58)*. Yield 84%. ¹H-NMR (300 MHz, DMSO-*d*₆): δ
4 (ppm) 7.32 (dd, *J* = 3.8, 0.8 Hz, 3H), 7.25-7.12 (m, 1H), 4.33 (s, 2H). ¹³C-NMR (75 MHz,
5 DMSO-*d*₆): δ (ppm) 137.5, 134.9, 130.3, 128.6, 128.3, 126.3, 54.3.
6
7

8
9 *2-azydoethylbenzene (59)*. Yield 53%. ¹H-NMR (300 MHz, DMSO-*d*₆): δ (ppm) 7.35-7.18
10 (m, 5H), 3.56 (t, *J* = 7.1 Hz, 2H), 2.85 (t, *J* = 7.1 Hz, 2H). ¹³C-NMR (75 MHz, DMSO-*d*₆):
11 δ (ppm) 138.8, 129.3, 128.9, 126.9, 52.0, 34.9.
12
13

14
15 *1-(azidomethyl)-4-methylbenzene (60)*. Yield 56%. ¹H-NMR (300 MHz, DMSO-*d*₆): δ
16 (ppm) 7.34-7.15 (m, 4H), 4.38 (s, 2H), 2.31 (s, 3H). ¹³C-NMR (75 MHz, DMSO-*d*₆): δ
17 (ppm) 137.2, 133.0, 129.8, 128.0, 52.2, 21.6.
18
19

20
21 *N-(4-(prop-2-yn-1-yloxy)phenyl)-7H-pyrrolo[2,3-*d*]pyrimidin-4-amine (61)*. [Synthesized
22 following procedure (a)] Yield 69%. M.p. 217-218 °C. ¹H-NMR (300 MHz, DMSO-*d*₆): δ
23 (ppm) 11.70 (s, 1H), 9.19 (s, 1H), 8.21 (s, 1H), 7.74 (dt, *J* = 9.5, 3.4 Hz, 2H) 7.19 (dd, *J*
24 = 3.5, 2.3 Hz, 1H), 6.98 (dd, *J* = 9.0, 3.4 Hz, 2H), 6.70 (dd, *J* = 3.5, 1.9 Hz, 1H), 4.77 (d,
25 *J* = 2.4 Hz, 2H), 3.57 (t, *J* = 2.3 Hz, 1H). ¹³C-NMR (75 MHz, DMSO-*d*₆): δ (ppm) 153.7,
26 152.6, 150.8, 150.7, 134.0, 122.1, 121.8, 114.8, 103.2, 98.7, 79.5, 78.1, 55.6. Anal. calcd
27 for C₁₅H₁₂N₄O: C, 68.17; H, 4.58; N, 21.20. Found: C, 67.86; H, 4.63; N, 21.23.
28
29
30
31
32
33
34
35

36
37 *Procedure for the synthesis of triazol derivatives 62-67*: A mixture of compound **61** (1
38 eq.) and the corresponding azide (1 eq.) in DMF was reacted overnight at r.t. in presence
39 of copper sulfate (CuSO₄·5H₂O) (0.1 eq.), tris(benzyltriazolylmethyl)amine (TBTA) (0.1
40 eq.) and sodium ascorbate (0.2 eq.). The reaction mixture was poured onto water,
41 extracted with CH₂Cl₂:MeOH (9:1), washed with saturated sodium chloride solution, dried
42 over magnesium sulfate (MgSO₄), concentrated and purified using flash chromatography
43 on silica gel (CH₂Cl₂:MeOH mixture).
44
45
46
47
48
49

50
51 *N-(4-((1-phenyl-1*H*-1,2,3-triazol-4-yl)methoxy)phenyl)-7H-pyrrolo[2,3-*d*]pyrimidin-4-*
52 *amine (62)*. Yield 34%. M.p. 267-268 °C. ¹H-NMR (500 MHz, DMSO-*d*₆): δ (ppm) 11.68
53 (s, 1H), 9.18 (s, 1H), 8.97 (s, 1H), 8.22 (s, 1H), 7.92 (dd, *J* = 7.0, 1.5 Hz, 2H), 7.76 (d, *J*
54 = 9.0 Hz, 2H), 7.61 (t, *J* = 7.9 Hz, 2H), 7.50 (t, *J* = 7.5, 1.0 Hz, 1H), 7.19 (dd, *J* = 3.5, 2.2
55 Hz, 1H), 7.08 (d, *J* = 9.1, 2H), 6.70 (dd, *J* = 3.5, 1.8 Hz, 1H), 5.23 (s, 2H). ¹³C-NMR (125
56
57
58
59
60

MHz, DMSO-*d*₆): δ (ppm) 153.7, 153.4, 150.9, 150.7, 144.1, 136.6, 133.8, 129.9, 122.8, 122.2, 121.8, 120.1, 114.7, 103.3, 98.8, 61.3. ESI calcd for C₂₁H₁₇N₇O [M + H]⁺ 384.1567. Found: 384.1564.

N-(4-((1-(4-chlorobenzyl)-1*H*-1,2,3-triazol-4-yl)methoxy)phenyl)-7*H*-pyrrolo[2,3-*d*]pyrimidin-4-amine (**63**). Yield 64%. M.p. 207-208 °C. ¹H-NMR (300 MHz, DMSO-*d*₆): δ (ppm) 11.67 (s, 1H), 9.16 (s, 1H), 8.29 (s, 1H), 8.20 (s, 1H), 7.73 (d, *J* = 9.1 Hz, 2H), 7.45 (d, *J* = 8.5 Hz, 2H), 7.35 (d, *J* = 8.5 Hz, 2H), 7.18 (dd, *J* = 3.5, 2.3 Hz, 1H), 7.01 (d, *J* = 9.1 Hz, 2H), 6.68 (dd, *J* = 3.5, 1.8 Hz, 1H), 5.62 (s, 2H), 5.12 (s, 2H). ¹³C-NMR (75 MHz, DMSO-*d*₆): δ (ppm) 153.7, 153.4, 150.9, 150.7, 143.3, 135.0, 133.7, 132.9, 129.9, 128.8, 124.7, 122.2, 121.8, 114.7, 112.2, 98.8, 61.3, 52.0. ESI calcd for C₂₂H₁₈N₇O [M + H]⁺ 432.1334. Found: 432.1320.

N-(4-((1-(2-chlorobenzyl)-1*H*-1,2,3-triazol-4-yl)methoxy)phenyl)-7*H*-pyrrolo[2,3-*d*]pyrimidin-4-amine (**64**). Yield 31%. M.p. 173-174 °C. ¹H-NMR (500 MHz, DMSO-*d*₆): δ (ppm) 11.67 (s, 1H), 9.16 (s, 1H), 8.27 (s, 1H), 8.21 (s, 1H), 7.73 (d, *J* = 9.0 Hz, 2H), 7.53 (dd, *J* = 7.5, 1.7 Hz, 1H), 7.39 (dd, *J* = 7.4, 1.7 Hz, 2H), 7.22 (dd, *J* = 7.3, 2.1 Hz, 1H), 7.18 (dd, *J* = 3.4, 2.3 Hz, 1H), 7.02 (d, *J* = 9.0 Hz, 2H), 6.68 (dd, *J* = 3.4, 1.9 Hz, 1H), 5.73 (s, 2H), 5.13 (s, 2H). ¹³C-NMR (125 MHz, DMSO-*d*₆): δ (ppm) 153.7, 153.4, 150.9, 150.7, 143.0, 133.7, 133.3, 132.6, 130.5, 130.2, 129.6, 127.7, 125.0, 122.2, 121.8, 114.7, 103.2, 98.7, 61.3, 50.6. ESI calcd for C₂₂H₁₈N₇O [M + H]⁺ 432.1334. Found: 432.1337.

N-(4-((1-(3-chlorobenzyl)-1*H*-1,2,3-triazol-4-yl)methoxy)phenyl)-7*H*-pyrrolo[2,3-*d*]pyrimidin-4-amine (**65**). Yield 33%. mp 177-178 °C. ¹H-NMR (500 MHz, DMSO-*d*₆): δ (ppm) 11.67 (s, 1H), 9.15 (s, 1H), 8.33 (s, 1H), 8.20 (s, 1H), 7.73 (d, *J* = 9.1 Hz, 2H), 7.41 (d, *J* = 3.1 Hz, 3H), 7.32-7.25 (m, 1H), 7.18 (dd, *J* = 3.4, 2.3 Hz, 1H), 7.02 (d, *J* = 9.0 Hz, 2H), 6.68 (dd, *J* = 3.5, 1.9 Hz, 1H), 5.64 (s, 2H), 5.33 (s, 2H). ¹³C-NMR (125 MHz, DMSO-*d*₆): δ (ppm) 153.7, 53.4, 150.9, 150.7, 143.3, 138.4, 133.7, 133.3, 130.7, 128.1, 127.9, 126.7, 124.8, 122.2, 121.8, 114.7, 103.2, 98.7. ESI calcd for C₂₂H₁₈N₇O [M + H]⁺ 432.1334. Found: 432.1328.

N-(4-((1-phenethyl-1*H*-1,2,3-triazol-4-yl)methoxy)phenyl)-7*H*-pyrrolo[2,3-*d*]pyrimidin-4-amine (**66**). Yield 64%. M.p. 206-207 °C. ¹H-NMR (500 MHz, DMSO-*d*₆): δ (ppm) 11.67 (s, 1H), 9.16 (s, 1H), 8.21 (s, 1H), 8.16 (s, 1H), 7.73 (d, *J* = 9.1 Hz, 2H), 7.30-7.16 (m, 6H), 7.00 (d, *J* = 9.1 Hz, 2H), 6.69 (dd, *J* = 3.5, 2.1 Hz, 1H), 5.10 (s, 2H), 4.62 (t, *J* = 7.4 Hz, 2H), 3.17 (t, *J* = 7.4 Hz, 2H). ¹³C-NMR (125 MHz, DMSO-*d*₆): δ (ppm) 153.7, 153.4, 150.9, 150.7, 142.7, 142.7, 133.7, 128.7, 128.4, 126.6, 124.4, 122.2, 121.8, 114.7, 103.2, 98.7, 62.3, 50.5, 35.7. ESI calcd for C₂₃H₂₁N₇O [M + H]⁺ 412.1880. Found: 412.1873.

N-(4-((1-(4-methylbenzyl)-1*H*-1,2,3-triazol-4-yl)methoxy)phenyl)-7*H*-pyrrolo[2,3-*d*]pyrimidin-4-amine (**67**). Yield 73%. M.p. 215-216 °C. ¹H-NMR (500 MHz, DMSO-*d*₆): δ (ppm) 11.67 (s, 1H), 9.15 (s, 1H), 8.24 (s, 1H), 8.20 (s, 1H), 7.72 (d, *J* = 9.0 Hz, 2H), 7.22 (d, *J* = 8.0 Hz, 2H), 7.20-7.15 (m, 3H), 7.00 (d, *J* = 9.0 Hz, 2H), 6.68 (d, *J* = 3.3 Hz, 1H), 5.55 (s, 2H), 5.11 (s, 2H), 2.27 (s, 3H). ¹³C-NMR (125 MHz, DMSO-*d*₆): δ (ppm) 153.7, 153.4, 150.9, 150.7, 143.1, 137.5, 133.7, 133.0, 129.3, 128.0, 124.6, 122.2, 121.8, 114.7, 103.2, 98.7, 61.3, 52.6, 20.7 ESI calcd for C₂₃H₂₁N₇O [M + H]⁺ 412.1880. Found: 412.1876

X-Ray diffraction studies

Protein expression and purification. The protein was expressed following the protocol by Xue et. al.²⁴ In brief, the gene of human TTBK1 coding for the catalytic domain, residues from 14 to 313 (GeneScrip hTTBK_coli_pET-28a(+)-TEV) was expressed in *E. coli* (BL21DE3). A pre-culture was grown overnight in LB medium, diluted 1:25 in fresh LB medium and incubated at 37 °C with shaking until an OD600 0.6 was reached. Induction was carried out using 1 mM IPTG at 20 °C overnight.

Harvested cells were resuspended in buffer A (20 mM Tris, pH 8.0, 5 mM MgCl₂, 300 mM NaCl, 5% (v/v) glycerol, 0.05% (w/v) CHAPS, 1 mM tris(2-carboxyethyl)phosphine (TCEP), 10 mM imidazole) with EDTA-free Protease Inhibitor Cocktail (Roche) and lysed with a single passage through a cell disruptor (MIXONIX Inc.). Lysate was clarified by centrifugation, and the supernatant loaded onto a 1 mL HiTrap Crude column (GE

Healthcare). After washing with buffer A with 30 column volumes (CV), the protein was eluted with increasing concentrations of buffer A supplemented with 250 mM imidazole. Fractions containing TTBK1 were pooled and diluted 3-fold with buffer C (20 mM HEPES, pH 7.0, 5% (v/v) glycerol) and loaded onto a pre-equilibrated 10 mL Resource S column (GE Healthcare). The column was washed with 5 CV of buffer C, and the bound protein was eluted by a salt gradient with buffer C containing 1 M NaCl. Fractions containing TTBK1 were then loaded onto a Hiloal 16/60 Superdex 200 pre-equilibrated with buffer D (20 mM Tris, pH 8.0, 0.5 mM MgCl₂, 300 mM NaCl, 5% (v/v) glycerol, 0.05% (w/v) CHAPS, 2 mM TCEP). Finally, fractions containing TTBK1 were concentrated in Amicon Ultra centrifugal units (10 K MWCO) and snap frozen in liquid nitrogen. This protein was used for the 29-complexed crystallization.

For the other crystal structures, TTBK1 (aa 13-320) and TTBK2 (aa 1-299) were recombinantly co-expressed with lambda phosphatase in E. coli Rosetta as a His-Sumo- and His-tagged proteins, respectively. Both proteins were initially purified by Ni²⁺-affinity chromatography, and the tags were cleaved either by SENP1 protease (TTBK1) or TEV (TTBK2). The cleaved proteins were further purified by size exclusion chromatography, and the pure proteins were stored in buffer 25 mM HEPES pH 7.5, 250 mM NaCl, 0.5 mM TCEP and 10% glycerol.

Crystallization. For derivative **29**, crystallization experiments were performed in pre-greased 24-well plates (Crystalgen Inc, NY, USA) and reagents were purchased from commercial sources. TEV-TTBK1(14-313) protein was used in crystallization. All TTBK1 crystals were obtained using hanging drop technique at 20 °C mixing 0.5 µL of protein (9.5 mg mL⁻¹) with 0.5 µL of reservoir solution and equilibrated against 1 mL of reservoir solution. **29**-TTBK1 co-crystals were obtained preincubating the protein with the compound in 3 fold-excess molar in 27% (w/v) PEG 4000, 200mM NH₄SO₄, 100 mM Na Citrate pH5.6 and 10 mM TCEP solution. Needle-like crystals appear after one week

and grow until 50 μm in size. Crystals were transferred to a cryo solution consisting in well solution plus 20% (v/v) ethylenglycol.

For other structures, crystallization was performed using sitting drop vapor diffusion at 20 $^{\circ}\text{C}$ and the kinases at ~ 10 mg/mL that were pre-incubated with 1 mM inhibitors. For TTBK2, crystallization condition was 1.6 M Na/K phosphate pH 7.0, 5% glycerol and 0.1 M Tris pH 7.5-8.5, while for TTBK1 the condition was 26% PEG 3350, 0.2 M sodium acetate pH 7.0 and 0.1 M Tris, pH 7.5-8.5. The complexed crystals were cryo-protected with mother liquor supplemented with glycerol or ethylene glycol for TTBK2 and TTBK1, respectively.

Structure determination. Diffraction data for TTBK1-29 were collected in the XALOC beamline at the ALBA synchrotron (Barcelona, Spain). For the other crystal structures, diffraction data were collected at Swiss Light Source. The collected datasets were processed with XDS⁴¹ and AIMLESS.⁴² Structure determination was performed by molecular replacement method with PHASER⁴³ using the previously TTBK1 KD structure (PDB code 4BTM). Structure refinement was done by several cycles of computational refinement with REFMAC5⁴⁴ and manual rebuilding using Coot.⁴⁵ Crystallographic data collection and refinement statistic are summarized in Table S1.

Computational studies.

The protein-ligand docking was performed using Glide and related Schrödinger packages.⁴⁶⁻⁴⁷ The binding site was defined by the crystallographic structures obtained for TTBK1 and TTBK2 in complex with the inhibitors reported in this work (PDB codes: 7Q8V, 7Q8W, 7Q8Z, 7Q90, 7Q8Y). Before docking calculations, the protein was prepared using Maestro Protein Preparation Wizard,⁴⁸ removing ligands, metals and water molecules, adding hydrogens, ionizing residues at pH 7.5 and filling in missing side chains using Prime. Minimization of the protein structure was done with OPLS3 force field. TTBKs inhibitors were also prepared using OPLS force field to minimize

energy. The grid box was defined using the ligands co-crystallized in TTBK1 and TTBK2 as center of the boxes. The docking was performed with Glide standard precision (SP) function,⁴⁹ and the top-10 poses per docked ligand were selected and subjected to re-scoring with the Molecular mechanics generalized Born surface area (MM-GBSA) with Prime. This computational method combines molecular mechanics energy and implicit solvation models that enables to re-score the docking results and correlate the experimental activities (IC_{50}) with the predicted binding energies (ΔG_{bind}]. The binding free energies between the ligands and the receptor were calculated as previously reported.¹⁵

The crystal structures of complexes **29**-TTBK1, **42**-TTBK1 and **42**-TTBK2 as well as the best docking solutions between compound **38** and TTBK1 and TTBK2, which presents the best predicted binding free energy (MM-GBSA), were subjected to 525 ns of molecular dynamics simulations (MDs) using Desmond software⁵⁰ and the OPLS3e force field.⁵¹ To prepare the systems, the complexes were solvated with pre-equilibrated SPC water molecules in a periodic boundary condition box. Then the systems were neutralized by adding Na^+ or Cl^- counter ions to balance the net charge of the systems and NaCl at a concentration of 0.15 M was added to simulate physiological conditions. Each system was relaxed using the default Desmond relaxation protocol and then equilibrated with a spring constant force of $5.0 \text{ kcal} \times \text{mol}^{-1} \times \text{\AA}^{-2}$ applied to the TTBKs backbone atoms and the ligands for 25 ns using the NPT ensemble at constant pressure (1 atm), temperature (300 K), and number of atoms using the isothermal-isobaric ensemble and the Nosé–Hoover method with a relaxation time of 1 ps applying the MTK algorithm,⁵² with a timestep of 2 fs. Then the last frame was taken and a second non-restricted 500 ns MDs was performed using the same conditions previously described. Systems were analyzed using the *in house*, PyMol, VMD, and a modification of the KNIME workflow to profile interactions between ligands and targets along MD trajectories.

Biology

***In vitro* inhibition of TTBK1 and TTBK2 human recombinant kinases.** The inhibition experiments were performed in the MRC Phosphorylation Unit (University of Dundee). TTBK1 or TTBK2 (human recombinant enzyme) (5–20 mU diluted in 50 mM Tris pH 7.5, 0.1 mM EGTA, 0.1% β -mercaptoethanol, 1mg/mL BSA, 10mM DTT) is assayed against RRKDLHDDEEDEAMSITA in a final volume of 25.5 μ L containing 50 mM Tris pH 7.5, 0.1 mM EGTA, 0.3 mM RRKDLHDDEEDEAMSITA, 10 mM magnesium acetate and 0.005 mM [33 P- γ -ATP] (50-1000 cpm/pmol) and incubated for 30 min at room temperature. Assays are stopped by addition of 5 μ L of 0.5 M (3%) orthophosphoric acid and then harvested onto P81 Unifilter plates with a wash buffer of 50 mM orthophosphoric acid.

Kinase profiling. The kinase profiling studies were carried out by MRC Phosphorylation Unit (University of Dundee). using the appropriate protocol in any case.⁵³

Parallel Artificial Membrane Permeability Assay (PAMPA) Blood-Brain Barrier (BBB). Prediction of the blood brain barrier penetration was performed with the Parallel Artificial Membrane Permeability Assay (PAMPA).⁵⁴ Ten commercial drugs of known BBB permeability, were used as controls in each experiment to validate the analysis set; Caffeine, Enoxacin, Hydrocortisone, Desipramine, Ofloxacin, Piroxicam, Testosterone, Promazine, Verapamil and Atenolol. Controls and TTBK1 inhibitors were dissolved in 5 mL of experimental buffer (phosphate buffer saline solution at pH 7.4 (PBS): EtOH (70:30 respectively)). The donor 96-well plate (Millipore, catalog no. MAIPS4510) was filled with 180 μ L of each filtered compound solution after being coated with 4 μ L of porcine brain lipid in dodecane (20 mg mL⁻¹) (Avanti Polar Lipids, catalog no. 141101). The acceptor 96-well plate (Millipore, catalog no. 141101) was filled with 180 μ L of experimental buffer. Then the donor plate was carefully put on the acceptor plate to form a “sandwich” for 2h and 30 min at room temperature. During incubation time

compounds diffused from the donor plate through the brain lipid membrane into the acceptor plate. After incubation, the donor plate was removed and compounds concentration was determined in the acceptor and the donor plates by UV (Thermoscientific, Multiskan spectrum). Every sample was analyzed at three to five wavelengths, in 3 wells and in two independent runs. Results are given as the mean \pm standard deviation (SD) of the two runs. Commercial drugs, PBS, Ethanol and dodecane were purchased from Sigma, Acros organics, Merck, Aldrich and Fluka.

Cell lines. All components for cell culture were obtained from Invitrogen (Barcelona, Spain). Antibodies used in this study are listed in Table S5.

Neuronal cell culture. Human neuroblastoma (SH-SY5Y) cells were purchased from the European Collection of Cell Cultures (Health Protection Agency, Salisbury, UK), and were propagated in Dulbecco's Modified Eagle Medium containing L-glutamine (2 mM), 1% non-essential amino acids, 10% fetal bovine serum and 1% penicillin/streptomycin, under humidified 5% CO₂ conditions at 37 °C. On attaining semiconfluency, cells were pre-treated with TTBK1 inhibitors (5 μ M) or the commercial GSK3 β inhibitor (Tideglusib, 5 μ M) and exposed 1 hour later to ethacrynic acid (40 μ M) for 24 hours. After the incubation time, cultures were processed for cell viability assay or Western blotting analysis. Cell viability was determined by the MTT assay, as previously described.⁵⁵ Cell survival was normalized to untreated controls and is presented as a percentage.

Lymphoblasts from ALS and Control individuals. Lymphocytes were obtained from blood samples of patients or healthy individuals (Table 5) after written informed consent. Patients were diagnosed as sporadic ALS according to El Escorial criteria⁵⁶ in the Doce de Octubre Hospital (Madrid, Spain).

All study protocols were approved by the Spanish Council of Higher Research Institutional Review Board and the Doce de Octubre Hospital and are in accordance with National and European Union Guidelines. Establishment of lymphoblastoid cell lines was

performed in our laboratory as previously described by infecting peripheral blood lymphocytes with the Epstein-Barr virus.⁵⁷ Cells were grown in suspension in T flasks, in RPMI-1640 medium (Gibco, BRL) that contained 2 mM L-glutamine, 10% (v/v) fetal bovine serum (FBS) and 100 µg/mL penicillin/streptomycin and maintained in a humidified 5% CO₂ incubator at 37 °C. Lymphoblasts were seeded at an initial density of 1 x 10⁶ x mL⁻¹ in presence or absence of TTBK1 inhibitors (5, 10 µM) for 24 hours. Then, cells were harvested and processed for Western blotting analysis.

Primary rat microglia culture. Wistar Rats were house hold with free access to food and water and kept in a light-dark 12/12 h cycle. Experimental designs and procedures were in accordance to European Community and Italian laws and approved by the Ethical Committee for Animal Experimentation of the University of Bologna (Protocol No. 17-72-1212).

Flasks used for cell cultured were previously covered with poly-L-lysine (10 µg/mL) (Sigma Aldrich, St. Louis, MO, USA). Mixed cultures of glial cells were obtained from cerebral cortices of newborn rats as previously described.⁵⁸ Briefly, cerebral cortices were trypsinized and mechanically dissected after cleared from meninges. The cell suspension was washed and resuspended in Basal Medium Eagle (BME, Life Technologies Ltd, Paisley, UK) supplemented with 10% fetal bovine serum (FBS, Life Technologies), 50 mg/mL gentamicin and 2 mM L-glutamine (Sigma-Aldrich). After 6/7 days in culture, pure microglial cells were obtained through mechanical detachment, resuspended in serum-free BME and plated on 35-mm diameter dishes at a density of 1.5 x 10⁶ cells/1.5 mL medium/well. The medium was change 30 min later in order to remove non-adhering cells. Cultures were maintained in standard conditions (5% CO₂ at 37 °C) and treated the day after plated. Microglia cells were exposed to LPS (100 ng/mL) (Sigma-Aldrich) for 24 hours. Compound **29** was added to the culture 1 hour before the treatment with LPS at increasing concentrations (5 and 25 µM). Cells were collected for immunoblotting analysis.

Immunoblotting analysis. Total protein extracts were obtained by lysing the cells, collected by centrifugation, as previously described.⁵⁹ Cytosolic and nuclear fractions were obtained using the Subcellular Protein Fractionation Kit, (Cat#78840, Thermo Fisher Scientific, Madrid, Spain) following the manufacturer's instructions. α -Tubulin and Lamin B1 were used as markers for cytosolic and nuclear fractions respectively. Protein quantification was carried out using the Pierce BCA Protein Assay kit (ThermoFisher, Madrid Spain). Equal amounts of proteins were resolved by SDS–polyacrylamide gel electrophoresis. Proteins were then transferred to polyvinylidene fluoride (PVDF) membranes and immunodetected, as previously described. The primary antibodies used are listed in **Table 5**. Signals from the primary antibodies were amplified using species-specific antisera antibodies conjugated with horseradish peroxidase and detected with a chemiluminescent substrate detection system ECL (Bio-Rad, Alcobendas, Madrid, Spain). Relative band intensities were quantified using a ChemiDoc station with Quantity One 1D analysis software (Bio-Rad Laboratories, Madrid, Spain) and normalized by those of GAPDH, α -tubulin or Lamin B1.

Immunofluorescence. Cells were permeabilized for 10 min at RT with 0.25% Triton X-100 (Sigma Aldrich), rinsed with PBS and blocked with 2% BSA (Sigma Aldrich) and 0.1% casein (Sigma Aldrich) for 30 min at RT. After being fixed, cells were incubated with TDP-43 monoclonal antibody (**Table 5**) in 6% BSA for 1 h at 37 °C, rinsed with PBS and incubated with Alexa Fluor 488 anti-rabbit antibody (1:600, Jackson Immuno Research). HCS NuclearMask Deep Red (1:250, Thermo Fisher) was used to stained cell nuclei. Finally, preparations were washed with 1% BSA and 0.1% casein and mounted onto Fluoromount Mounting Medium (Sigma Aldrich). Images were acquired for ~ 60 cells per group in n = 3 independent experiments using a confocal laser scanning microscope (CLMS) Leica TCS SP5 with 63x oil immersion objective. Quantification of TDP-43 was performed using Image J software.

Pharmacokinetic Studies. The study was conducted according to the guidelines of the Institutional Animal Ethics Committee (IAEC), and approved by Sai Life Sciences (Hinjewadi, Pune, India) (no. SAIDMPK/PK-21-03-262, March 2021). Healthy male BALB/c mice (8-12 weeks old) weighing between 17 to 30 g were used in the study. Total forty-eight male mice were divided into two groups as Group 1 (n=24) and Group 2 (n=24) with 3 mice/time points design. In both cases, the formulation was based in 90% of phosphate buffer saline (PBS, pH 7.4) with a 5% of solutol HS-15 and 5% of N-methyl-2-pyrrolidone at a dose of 5 mg/kg or 10 mg/Kg for i.p. and p.o administration, respectively. Blood samples ($\approx 60 \mu\text{L}$) were collected from a set of three mice at each time point (0.08 (for i.p. only), 0.25, 0.5, 1, 2, 4, 6 (only for p.o), 8 and 24 h). In addition, along with terminal blood samples, brain samples were collected at 0.08 (for i.p only), 0.25, 0.5, 1, 2, 4, 6 (only for p.o.), 8 and 24 h post dosing from 3 mice per time point. Immediately after collection of blood, brain samples were collected from set of three animals for bioanalysis. Concentrations of compound in mouse plasma and brain samples were determined by fit-for-purpose LC–MS/MS method. Non-Compartmental-Analysis tool of Phoenix WinNonlin® (Version 8.0) was used to assess the pharmacokinetic parameters.

Animal procedures, treatment and sampling. Protocol authorized by the ethical committees of the regulatory institution and the UCM (ref. PROEX 059/16) in agreement with regulations (2010/63/EU) from European Commission was in place for all the experiments done. Wild-type and Prp-hTDP-43(A315T) transgenic littermate sibling mice were purchased from Jackson Laboratories (Bar Harbor, ME, USA) and bred in house. Mice were maintained with food and water ad libitum in a temperature-controlled atmosphere ($22 \pm 1^\circ\text{C}$) and on a cycle of 12 h light/dark. Genotyping of offspring were done as previously reported,³⁸ and four groups of male mice were randomly done (n=8). Compound **29** was dissolved in 2.9% DMSO and Tween 80-saline buffer (1:16) and administered i.p. at a dose of 5 mg/Kg daily. Control animals received vehicle injections.

Treatment started at the age of 65 days old, until animal sacrifice 30 days later. During all the treatment, physical appearance and animal weight gain were recorded. Spinal cords were rapidly collected and flash-frozen in 2-methylbutane cooled in dry ice and stored at -80 °C.

Tissue slicing. Fixed spinal cords were sliced with a cryostat at the lumbar level (L4-L6) to obtain coronal sections (20 µm thick) that were collected on gelatin-coated slides. Sections were used for procedures of Nissl-staining and immunofluorescence.

Nissl staining. Slices were used for Nissl staining using cresyl violet, as previously described, which permitted to determine the effects of each treatment on cell number. A Leica DMRB microscope (Leica, Wetzlar, Germany) and a DFC300Fx camera (Leica) were used to study and photograph the tissue, respectively. To count the number of Nissl-stained motor neurons (> 400 µm²) in the ventral horn, high-resolution photomicrographs were taken with a 10x objective under the same conditions of light, brightness, and contrast. Counting was carried out with ImageJ software (U.S. National Institutes of Health, Bethesda, Maryland, USA, <http://imagej.nih.gov/ij/>, 1997-2012). At least 6 images *per* animal were analyzed to calculate the mean of each group (n≥5). Analyses were always conducted by experimenters who were blinded to genotype and treatment conditions. In all analyses, data were transformed to the percentage over the mean obtained in the wild-type group for each parameter.

Immunofluorescence analysis. Spinal slices were used for detection and quantification of Iba-1, GFAP, or ChAT immunofluorescence. After preincubation for 1 hour with Tris-buffered saline with 0.1% Triton X-100 (pH 7.5), sections were sequentially incubated overnight at 4 °C with the following polyclonal antibodies: (i) anti-Iba-1 (Wako Chemicals, Richmond, VI, USA) used at 1:500; (ii) anti-GFAP (Dako Cytomation, Glostrup, Denmark) used at 1:200 or (iii) ChAT (Merck Millipore, MA, USA) used at 1:100. After incubation, sections were washed with Tris-buffered saline and secondary antibodies were incubated for 2 hours at 37 °C For Iba-1 and GFAP staining, anti-rabbit secondary

antibody conjugated with Alexa 488 (Invitrogen, Carlsbad, CA, USA) was used at 1:200. For ChAT staining, anti-goat secondary antibody conjugated with Alexa 546 (Invitrogen™, ThermoFisher Scientific, MA, USA). Sections were then washed and mounted with Faramount aqueous mounting medium (Dako Cytomation, Glostrup, Denmark). A DMRB microscope and a DFC300Fx camera (Leica, Wetzlar, Germany) were used for slide observation and photography. The mean density of immunolabelling was measured in the selected areas with ImageJ software (NIH, USA). At least 6 images *per* animal were analyzed to calculate the mean of each group ($n \geq 5$). Again, all data were transformed to the percentage over the mean obtained in the wild-type group for each parameter.

Statistical Analysis. Statistical analyses were performed with Graph Pad Prism 9. All the statistical data are presented as mean \pm standard error of the mean (SEM). Normality was checked with the Shapiro–Wilk test. Parametric tests were therefore used in the statistical analysis. Significant differences between groups were evaluated by using Student's t-test or by analysis of variance (ANOVA) followed by the Fisher's LSD test for multiple comparisons. A value of $p < 0.05$ was considered significant.

Supporting information

The Supporting Information is available free of charge on the ACS Publications website. Data collection, refinement statistics and crystal structures (table S1 and figure S1); MM-GBSA parameters for modelled compounds (tables S2, S3 and figure S1, S2); experimental permeability data in the PAMPA-BBB assay (table S4 and figure S4); antibodies used in WB and immunohistochemistry (table S5); viability studies for TTBK1 inhibitors (figure S5); neuroprotection of TTBK1 inhibitors in a okadaic acid cell-based assay (figure S6); images of the immunomodulatory effect of compound **29** in the spinal cord of the *in vivo* ALS model (figure S7); HPLC-MS chromatogram of lead compounds (figure S8).

Molecular Formula Strings are also included.

PDB ID of New Crystal (X-ray) Structures: Authors will release the atomic coordinates upon article publication.

Corresponding authors information:

*A.M.: e-mail ana.martinez@csic.es

ORCID

Ana Martínez: 0000-0002-2707-8110

Eva de Lago: 0000-0002-6260-3777

Valle Palomo: 0000-0002-1473-4086

Ángeles Martín-Requero: 0000-0002-3416-9-440

Carmen Gil: 0000-0002-3882-6081

David Ramírez: 0000-0003-0002-1189

Vanesa Nozal: 0000-0001-5260-5683

Loreto Martinez-Gonzalez: 0000-0003-4593-4889

Daniel Lietha: 0000-0002-6133-6486

Barbara Monti: 0000-0003-0330-482X

Stefan Knapp: 0000-0001-5995-6494

Apirat Chaikuad: 0000-0003-1120-2209

Notes: The authors declare no competing financial interest

Acknowledgements

This work was supported by Comunidad de Madrid (grant B2017/BMD-3813), and European Social Fund + (ESF+), MINECO (grant SAF2016-76693-R to A.M., RTI2018-0988885-B-I00 to E.dL. and CTQ2015-66313-R to A.M.R.), AIE (RTI2018-099318-B-I00 to D.L., co-funded by the European Regional Development Fund (FEDER), ISCiii

CIBERNED (CB18/05/00040 to A.M., C.G. and A.M.R, and CB06/05/0089 to E.dL.), MECD (FPU16/04466 to V.N.), Cost Action CA15135 “MuTaLig” (COST-STSM-CA15135-37514 to LMG), FONDECYT (grant no. 11180604 to D.R.). V.P. has received financial support through the Postdoctoral Junior Leader Fellowship Program (LCF/BQ/PR18/11640007) from “la Caixa” Banking Foundation. This work has been awarded by the SEQT (Spanish Society of Medicinal Chemistry) for young researchers in their XX edition. We thank the staff at the ALBA synchrotron facilities for their assistance during the X-ray diffraction data collection and Pilar López Navajas for help during TTBK1 protein purification.

Abbreviations used

AD, Alzheimer’s disease; ALS, amyotrophic lateral sclerosis; BBB, Blood brain barrier; CNS, central nervous system; EA, ethacrynic acid; FTD-TDP, frontotemporal dementia with TDP-43 aggregates; LATE, limbic-predominant age-related TDP-43 encephalopathy; LPS, lipopolysaccharide; MM-GBSA, molecular mechanics generalized Born surface area; iNOS, inducible nitric oxide synthase; OA, okadaic acid; PAMPA, parallel artificial membranes permeability assay; RMSD, root-mean-square deviation; TDP-43, transactive response DNA binding protein of 43 kDa; TREM2, triggering receptor expressed on myeloid cells 2; TTBK1, tau-tubulin kinase 1; TTBK2, tau-tubulin kinase 2.

References

- (1) Scotter, E. L.; Chen, H. J.; Shaw, C. E. TDP-43 proteinopathy and ALS: Insights into disease mechanisms and therapeutic targets. *Neurotherapeutics* **2015**, *12*, 352-363.
- (2) Weskamp, K.; Barmada, S. J. TDP43 and RNA instability in amyotrophic lateral sclerosis. *Brain Res* **2018**, *1693*, 67-74.
- (3) de Boer, E. M. J.; Orie, V. K.; Williams, T.; Baker, M. R.; De Oliveira, H. M.; Polvikoski, T.; Silsby, M.; Menon, P.; van den Bos, M.; Halliday, G. M.; van den Berg, L. H.; Van Den Bosch, L.; van Damme, P.; Kiernan, M. C.; van Es, M. A.; Vucic, S. TDP-43 proteinopathies: a new wave of neurodegenerative diseases. *J Neurol Neurosurg Psychiatry* **2020**, *92*, 86-95.
- (4) Suk, T. R.; Rousseaux, M. W. C. The role of TDP-43 mislocalization in amyotrophic lateral sclerosis. *Mol Neurodegener* **2020**, *15*, 45-61.
- (5) Prasad, A.; Bharathi, V.; Sivalingam, V.; Girdhar, A.; Patel, B. K. Molecular mechanisms of TDP-43 misfolding and pathology in amyotrophic lateral sclerosis. *Front Mol Neurosci* **2019**, *12*, 25.
- (6) Palomo, V.; Tosat-Bitrian, C.; Nozal, V.; Nagaraj, S.; Martin-Requero, A.; Martinez, A. TDP-43: A key therapeutic target beyond amyotrophic lateral sclerosis. *ACS Chem Neurosci* **2019**, *10*, 1183-1196.
- (7) Moujalled, D.; James, J. L.; Parker, S. J.; Lidgerwood, G. E.; Duncan, C.; Meyerowitz, J.; Nonaka, T.; Hasegawa, M.; Kanninen, K. M.; Grubman, A.; Liddell, J. R.; Crouch, P. J.; White, A. R. Kinase inhibitor screening identifies cyclin-dependent kinases and glycogen synthase kinase 3 as potential modulators of TDP-43 cytosolic accumulation during cell stress. *PLoS One* **2013**, *8*, e67433.
- (8) Kametani, F.; Nonaka, T.; Suzuki, T.; Arai, T.; Dohmae, N.; Akiyama, H.; Hasegawa, M. Identification of casein kinase-1 phosphorylation sites on TDP-43. *Biochem Biophys Res Commun* **2009**, *382*, 405-409.
- (9) Liachko, N. F.; McMillan, P. J.; Guthrie, C. R.; Bird, T. D.; Leverenz, J. B.; Kraemer, B. C. CDC7 inhibition blocks pathological TDP-43 phosphorylation and neurodegeneration. *Ann Neurol* **2013**, *74*, 39-52.
- (10) Li, W.; Reeb, A. N.; Lin, B.; Subramanian, P.; Fey, E. E.; Knoverek, C. R.; French, R. L.; Bigio, E. H.; Ayala, Y. M. Heat shock-induced phosphorylation of TAR DNA-binding protein 43 (TDP-43) by MAPK/ERK kinase regulates TDP-43 function. *J Biol Chem* **2017**, *292*, 5089-5100.
- (11) Liachko, N. F.; McMillan, P. J.; Strovas, T. J.; Loomis, E.; Greenup, L.; Murrell, J. R.; Ghetti, B.; Raskind, M. A.; Montine, T. J.; Bird, T. D.; Leverenz, J. B.; Kraemer, B. C.

The tau tubulin kinases TTBK1/2 promote accumulation of pathological TDP-43. *PLoS Genet* **2014**, *10*, e1004803.

(12) Palomo, V.; Nozal, V.; Rojas-Prats, E.; Gil, C.; Martinez, A. Protein kinase inhibitors for amyotrophic lateral sclerosis therapy. *Br J Pharmacol* **2021**, *178*, 1316-1335.

(13) Martinez-Gonzalez, L.; Gonzalo-Consuegra, C.; Gomez-Almeria, M.; Porras, G.; de Lago, E.; Martin-Requero, A.; Martinez, A. Tideglusib, a non-ATP competitive inhibitor of GSK-3 β as a drug candidate for the treatment of amyotrophic lateral sclerosis. *Int J Mol Sci* **2021**, *22*, 8975-8989.

(14) Martinez-Gonzalez, L.; Rodriguez-Cueto, C.; Cabezudo, D.; Bartolome, F.; Andres-Benito, P.; Ferrer, I.; Gil, C.; Martin-Requero, A.; Fernandez-Ruiz, J.; Martinez, A.; de Lago, E. Motor neuron preservation and decrease of in vivo TDP-43 phosphorylation by protein CK-1 δ kinase inhibitor treatment. *Sci Rep* **2020**, *10*, 4449.

(15) Rojas-Prats, E.; Martinez-Gonzalez, L.; Gonzalo-Consuegra, C.; Liachko, N. F.; Perez, C.; Ramirez, D.; Kraemer, B. C.; Martin-Requero, A.; Perez, D. I.; Gil, C.; de Lago, E.; Martinez, A. Targeting nuclear protein TDP-43 by cell division cycle kinase 7 inhibitors: A new therapeutic approach for amyotrophic lateral sclerosis. *Eur J Med Chem* **2021**, *210*, 112968.

(16) Halkina, T.; Henderson, J. L.; Lin, E. Y.; Himmelbauer, M. K.; Jones, J. H.; Nevalainen, M.; Feng, J.; King, K.; Rooney, M.; Johnson, J. L.; Marcotte, D. J.; Chodaparambil, J. V.; Kumar, P. R.; Patterson, T. A.; Murugan, P.; Schuman, E.; Wong, L.; Hesson, T.; Lamore, S.; Bao, C.; Calhoun, M.; Certo, H.; Amaral, B.; Dillon, G. M.; Gilfillan, R.; de Turiso, F. G. Discovery of potent and brain-penetrant tau tubulin kinase 1 (TTBK1) inhibitors that lower tau phosphorylation in vivo. *J Med Chem* **2021**, *64*, 6358-6380.

(17) Jackson, P. K. TTBK2 kinase: Linking primary cilia and cerebellar ataxias. *Cell* **2012**, *151*, 697-699.

(18) Cajanek, L.; Nigg, E. A. Cep164 triggers ciliogenesis by recruiting tau tubulin kinase 2 to the mother centriole. *Proc Natl Acad Sci U S A* **2014**, *111*, E2841-2850.

(19) Taylor, L. M.; McMillan, P. J.; Kraemer, B. C.; Liachko, N. F. Tau tubulin kinases in proteinopathy. *FEBS J* **2019**, *286*, 2434-2446.

(20) Sato, S.; Cerny, R. L.; Buescher, J. L.; Ikezu, T. Tau-tubulin kinase 1 (TTBK1), a neuron-specific tau kinase candidate, is involved in tau phosphorylation and aggregation. *J Neurochem* **2006**, *98*, 1573-1584.

(21) Lund, H.; Cowburn, R. F.; Gustafsson, E.; Stromberg, K.; Svensson, A.; Dahllund, L.; Malinowsky, D.; Sunnemark, D. Tau-tubulin kinase 1 expression, phosphorylation and

co-localization with phospho-Ser422 tau in the Alzheimer's disease brain. *Brain Pathol* **2013**, *23*, 378-389.

(22) Bao, C.; Bajrami, B.; Marcotte, D. J.; Chodaparambil, J. V.; Kerns, H. M.; Henderson, J.; Wei, R.; Gao, B.; Dillon, G. M. Mechanisms of regulation and diverse activities of tau-tubulin kinase (TTBK) isoforms. *Cell Mol Neurobiol* **2021**, *41*, 669-685.

(23) Nozal, V.; Martinez, A. Tau tubulin kinase 1 (TTBK1), a new player in the fight against neurodegenerative diseases. *Eur J Med Chem* **2019**, *161*, 39.

(24) Xue, Y.; Wan, P. T.; Hillertz, P.; Schweikart, F.; Zhao, Y.; Wissler, L.; Dekker, N. X-ray structural analysis of tau-tubulin kinase 1 and its interactions with small molecular inhibitors. *ChemMedChem* **2013**, *8*, 1846-1854.

(25) Kiefer, S. E.; Chang, C. J.; Kimura, S. R.; Gao, M.; Xie, D.; Zhang, Y.; Zhang, G.; Gill, M. B.; Mastalerz, H.; Thompson, L. A.; Cacace, A. M.; Sheriff, S. The structure of human tau-tubulin kinase 1 both in the apo form and in complex with an inhibitor. *Acta Crystallogr F Struct Biol Commun* **2014**, *70*, 173-181.

(26) Dillon, G. M.; Henderson, J. L.; Bao, C.; Joyce, J. A.; Calhoun, M.; Amaral, B.; King, K. W.; Bajrami, B.; Rabah, D. Acute inhibition of the CNS-specific kinase TTBK1 significantly lowers tau phosphorylation at several disease relevant sites. *PLoS One* **2020**, *15*, e0228771.

(27) Marcotte, D. J.; Spilker, K. A.; Wen, D.; Hesson, T.; Patterson, T. A.; Kumar, P. R.; Chodaparambil, J. V. The crystal structure of the catalytic domain of tau tubulin kinase 2 in complex with a small-molecule inhibitor. *Acta Crystallogr F Struct Biol Commun* **2020**, *76*, 103-108.

(28) Attwood, M. M.; Fabbro, D.; Sokolov, A. V.; Knapp, S.; Schioth, H. B. Trends in kinase drug discovery: Targets, indications and inhibitor design. *Nat Rev Drug Discov* **2021**, *20*, 839-861.

(29) Staderini, M.; Bolognesi, M. L.; Menéndez, J. C. Lewis acid-catalyzed generation of C-C and C-N bonds on π -deficient heterocyclic substrates. *Adv Synth Catal* **2015**, *357*, 185-195.

(30) Kolb, H. C.; Finn, M. G.; Sharpless, K. B. Click chemistry: Diverse chemical function from a few good reactions. *Angew Chem Int Ed Engl* **2001**, *40*, 2004-2021.

(31) Young, M. A.; Shah, N. P.; Chao, L. H.; Seeliger, M.; Milanov, Z. V.; Biggs, W. H., 3rd; Treiber, D. K.; Patel, H. K.; Zarrinkar, P. P.; Lockhart, D. J.; Sawyers, C. L.; Kuriyan, J. Structure of the kinase domain of an imatinib-resistant Abl mutant in complex with the Aurora kinase inhibitor VX-680. *Cancer Res* **2006**, *66*, 1007-1014.

(32) Schroder, M.; Bullock, A. N.; Fedorov, O.; Bracher, F.; Chaikuad, A.; Knapp, S. DFG-1 residue controls inhibitor binding mode and affinity, providing a basis for rational design of kinase inhibitor selectivity. *J Med Chem* **2020**, *63*, 10224-10234.

- (33) Cheng, A. C.; Eksterowicz, J.; Geuns-Meyer, S.; Sun, Y. Analysis of kinase inhibitor selectivity using a thermodynamics-based partition index. *J Med Chem* **2010**, *53*, 4502-4510.
- (34) Iguchi, Y.; Katsuno, M.; Takagi, S.; Ishigaki, S.; Niwa, J.; Hasegawa, M.; Tanaka, F.; Sobue, G. Oxidative stress induced by glutathione depletion reproduces pathological modifications of TDP-43 linked to TDP-43 proteinopathies. *Neurobiol Dis* **2012**, *45*, 862-870.
- (35) Boban, M.; Babic Leko, M.; Miskic, T.; Hof, P. R.; Simic, G. Human neuroblastoma SH-SY5Y cells treated with okadaic acid express phosphorylated high molecular weight tau-immunoreactive protein species. *J Neurosci Methods* **2019**, *319*, 60-68.
- (36) Haukedal, H.; Freude, K. Implications of microglia in amyotrophic lateral sclerosis and frontotemporal dementia. *J Mol Biol* **2019**, *431*, 1818-1829.
- (37) Tang, Y.; Le, W. Differential roles of M1 and M2 microglia in neurodegenerative diseases. *Mol Neurobiol* **2016**, *53*, 1181-1194.
- (38) Wegorzewska, I.; Bell, S.; Cairns, N. J.; Miller, T. M.; Baloh, R. H. TDP-43 mutant transgenic mice develop features of ALS and frontotemporal lobar degeneration. *Proc Natl Acad Sci U S A* **2009**, *106*, 18809-18814.
- (39) Posa, D.; Martinez-Gonzalez, L.; Bartolome, F.; Nagaraj, S.; Porras, G.; Martinez, A.; Martin-Requero, A. Recapitulation of pathological TDP-43 features in immortalized lymphocytes from sporadic ALS patients. *Mol Neurobiol* **2019**, *56*, 2424-2432.
- (40) Arnold, L. A.; Moyer, M. P.; Sobolov-Jaynes, S. B. Heterocyclic ring-fused pyrimidine derivatives. US 6395733 B1. **1995**.
- (41) Kabsch, W. Integration, scaling, space-group assignment and post-refinement. *Acta Crystallogr D Biol Crystallogr* **2010**, *66*, 133-144.
- (42) Evans, P. R.; Murshudov, G. N. How good are my data and what is the resolution? *Acta Crystallogr D Biol Crystallogr* **2013**, *69*, 1204-1214.
- (43) McCoy, A. J.; Grosse-Kunstleve, R. W.; Adams, P. D.; Winn, M. D.; Storoni, L. C.; Read, R. J. Phaser crystallographic software. *J Appl Crystallogr* **2007**, *40*, 658-674.
- (44) Murshudov, G. N.; Vagin, A. A.; Dodson, E. J. Refinement of macromolecular structures by the maximum-likelihood method. *Acta Crystallogr D Biol Crystallogr* **1997**, *53*, 240-255.
- (45) Emsley, P.; Cowtan, K. Coot: Model-building tools for molecular graphics. *Acta Crystallogr D Biol Crystallogr* **2004**, *60*, 2126-2132.
- (46) Halgren, T. A.; Murphy, R. B.; Friesner, R. A.; Beard, H. S.; Frye, L. L.; Pollard, W. T.; Banks, J. L. Glide: A new approach for rapid, accurate docking and scoring. 2. Enrichment factors in database screening. *J Med Chem* **2004**, *47*, 1750-1759.

- (47) Friesner, R. A.; Banks, J. L.; Murphy, R. B.; Halgren, T. A.; Klicic, J. J.; Mainz, D. T.; Repasky, M. P.; Knoll, E. H.; Shelley, M.; Perry, J. K.; Shaw, D. E.; Francis, P.; Shenkin, P. S. Glide: A new approach for rapid, accurate docking and scoring. 1. Method and assessment of docking accuracy. *J Med Chem* **2004**, *47*, 1739-1749.
- (48) Sastry, G. M.; Adzhigirey, M.; Day, T.; Annabhimoju, R.; Sherman, W. Protein and ligand preparation: Parameters, protocols, and influence on virtual screening enrichments. *J Comput Aided Mol Des* **2013**, *27*, 221-234.
- (49) Friesner, R. A.; Murphy, R. B.; Repasky, M. P.; Frye, L. L.; Greenwood, J. R.; Halgren, T. A.; Sanschagrin, P. C.; Mainz, D. T. Extra precision glide: docking and scoring incorporating a model of hydrophobic enclosure for protein-ligand complexes. *J Med Chem* **2006**, *49*, 6177-6196.
- (50) Bowers, K. J.; Chow, E.; Xu, H.; Dror, R. O.; Eastwood, M. P.; Gregersen, B. A.; Klepeis, J. L.; Kolossvary, I.; Moraes, M. A.; Sacerdoti, F. D.; Salmon, J. K.; Shan, Y.; Shaw, D. E. Scalable algorithms for molecular dynamics simulations on commodity clusters. *SC '06: Proceedings of the 2006 ACM/IEEE Conference on Supercomputing 2006*, Tampa, Florida.
- (51) Roos, K.; Wu, C.; Damm, W.; Reboul, M.; Stevenson, J. M.; Lu, C.; Dahlgren, M. K.; Mondal, S.; Chen, W.; Wang, L.; Abel, R.; Friesner, R. A.; Harder, E. D. OPLS3e: Extending force field coverage for drug-like small molecules. *J Chem Theory Comput* **2019**, *15*, 1863-1874.
- (52) Martyna, G. J.; Tobias, D. J.; Klein, M. L. Constant pressure molecular dynamics algorithms. *J Chem Phys* **1994**, *101*, 4177-4189.
- (53) Bain, J.; Plater, L.; Elliott, M.; Shpiro, N.; Hastie, C. J.; McLauchlan, H.; Klevernic, I.; Arthur, J. S.; Alessi, D. R.; Cohen, P. The selectivity of protein kinase inhibitors: a further update. *Biochem J* **2007**, *408*, 297-315.
- (54) Di, L.; Kerns, E. H.; Fan, K.; McConnell, O. J.; Carter, G. T. High throughput artificial membrane permeability assay for blood-brain barrier. *Eur J Med Chem* **2003**, *38*, 223-232.
- (55) Morgan, D. M. Tetrazolium (MTT) assay for cellular viability and activity. *Methods Mol Biol* **1998**, *79*, 179-183.
- (56) Agosta, F.; Al-Chalabi, A.; Filippi, M.; Hardiman, O.; Kaji, R.; Meininger, V.; Nakano, I.; Shaw, P.; Shefner, J.; van den Berg, L. H.; Ludolph, A. WFN Research Group on ALS/MND. The El Escorial criteria: Strengths and weaknesses. *Amyotroph Lateral Scler Frontotemporal Degener* **2015**, *16*.
- (57) Omi, N.; Tokuda, Y.; Ikeda, Y.; Ueno, M.; Mori, K.; Sotozono, C.; Kinoshita, S.; Nakano, M.; Tashiro, K. Efficient and reliable establishment of lymphoblastoid cell lines

1
2
3
4
5
6
7
8
9
10
11
12
13
14
15
16
17
18
19
20
21
22
23
24
25
26
27
28
29
30
31
32
33
34
35
36
37
38
39
40
41
42
43
44
45
46
47
48
49
50
51
52
53
54
55
56
57
58
59
60

by Epstein-Barr virus transformation from a limited amount of peripheral blood. *Sci Rep* **2017**, *7*, 43833.

(58) Polazzi, E.; Gianni, T.; Contestabile, A. Microglial cells protect cerebellar granule neurons from apoptosis: Evidence for reciprocal signaling. *Glia* **2001**, *36*, 271-280.

(59) Alquezar, C.; Salado, I. G.; de la Encarnacion, A.; Perez, D. I.; Moreno, F.; Gil, C.; de Munain, A. L.; Martinez, A.; Martin-Requero, A. Targeting TDP-43 phosphorylation by casein kinase-1delta inhibitors: a novel strategy for the treatment of frontotemporal dementia. *Mol Neurodegener* **2016**, *11*, 36-50.

